

# **Effects of magnesium-based materials on immune response mediated osteogenesis**

## **Dissertation**

zur Erlangung des akademischen Grades  
Doktor der Ingenieurwissenschaften  
(Dr.-Ing.)  
der Technischen Fakultät  
der Christian-Albrechts-Universität zu Kiel

vorgelegt von

**QIAN WANG**

Kiel 2020

Erstgutachterin: Prof. Dr. Regine Willumeit-Römer

Zweitgutachter/in: Prof. Dr. Christine Selhuber-Unkel

Termin der Disputation: 28.08.2020

# Eidesstattliche Erklärung

Hiermit erkläre ich, dass die beigefügte Dissertation, abgesehen von der Beratung durch die Betreuerin, nach Inhalt und Form meine eigene Arbeit ist.

Die Arbeit, ganz oder zum Teil, wurde nie schon einer anderen Stelle im Rahmen eines Prüfungsverfahrens vorgelegt und ist abgesehen, von den im Anhang angegebenen Veröffentlichungen, nicht anderweitig zur Veröffentlichung vorgelegt worden.

Außerdem ist die Arbeit unter Einhaltung der Regeln guter wissenschaftlicher Praxis der Deutschen Forschungsgemeinschaft entstanden.

Geesthacht, den 30.08.2020

Unterschrift

A handwritten signature in black ink, appearing to read "Gian Wang".



# Abstract

**Background:** Human mesenchymal stem cells (MSC) interact with numerous immune cells that can promote regenerative processes and inhibit inflammatory responses. It is hypothesised that the crosstalk between human umbilical cord perivascular cells (HUCPV; an alternative source of MSC) and peripheral blood mononuclear cells (PBMC)/macrophages could be influenced by degradable magnesium (Mg) and its alloy (Mg-10Gd; 10 weight % gadolinium). Moreover, the mechanisms of Mg-based material-modulated immune reactions—macrophage functions and subsequent bone formation—still need to be investigated. **Methods:** For analysis of the correlations between paracrine signalling and specific cellular behaviour during the initial host response to Mg, two *in vitro* indirect coculture systems of HUCPV and PBMC were developed in 7 days: (i) transwell (TW) and (ii) conditioned media (CM). In the subsequent 7-14 days, for analysis of the roles of Mg/Mg-10Gd on secretions of macrophages and their effects on pro-osteogenic activity, a direct coculture system of HUCPV and macrophages was established. **Results:** Cell growth was not significantly influenced by Mg (TW, CM and direct coculture system) or Mg-10Gd (direct coculture system). In the TW system, when HUCPV were cultured with degradable Mg, moderate inflammation (*i.e.*, decreased secretion of proinflammatory interleukin 1 beta (IL1 $\beta$ ), IL2, tumour necrosis factor alpha (TNF $\alpha$ ), and interferon gamma (IFN $\gamma$ ) and anti-inflammatory IL4, IL5, IL10, IL13, and 1 receptor antagonist (IL1RA) and granulocyte colony stimulating factor (G-CSF)), as well as an increased pro-healing M2 macrophage phenotype, was observed. Moreover, when PBMC were cultured with degradable Mg, the expression of migration/wound healing-related cytokines (IL8, granulocyte-macrophage colony-stimulating factor (GM-CSF), monocyte chemoattractant protein 1 (MCP-1) and macrophage inflammatory protein (MIP)-1 $\alpha/\beta$ ) increased, accompanied by an increased migration of HUCPV (cell scratch assay). In addition, an increased pro-osteogenic potential was demonstrated *via* an increase in osteoblastic markers (*e.g.*, alkaline phosphatase (ALP) activity, specific gene expression and cytokine release). In the CM system, the percentage of the M2 macrophage phenotype could only be increased by HUCPV and/or Mg. In the direct coculture system, Mg and Mg-10Gd were found to modulate osteogenic differentiation through oncostatin M (OSM) and glycoprotein 130 (gp130). Furthermore, both materials upregulated the gene expression of bone morphogenetic protein 6 (BMP6) in macrophages and of bone morphogenetic protein receptor type 1A and 2 (BMPR1A/2) and mothers against decapentaplegic homologue (Smad) 1/4/5 in cocultured MSC. In addition, both treatments could reduce the secretion of TNF $\alpha$  and IL1 $\beta$  in macrophages and cocultures, which might act synergistically in providing a pro-osteogenic microenvironment. **Conclusion:** These results collectively imply that Mg possesses osteoimmunomodulatory properties. This study also highlights the roles of material-activated macrophages in pro-osteogenic activity *via* the OSM/gp130 and Smad-related signalling pathways. Moreover, these findings provide insight into developing Mg-based bone substitute biomaterials capable of desired immune reactions (*e.g.*, tissue regenerative M2 macrophage phenotype) and therapeutic applications using interactions of immune cells and MSC for bone regeneration.

# Zusammenfassung

**Motivation:** Humane mesenchymale Stammzellen (MSC) interagieren mit zahlreichen Immunzellen, die Regenerationsprozesse fördern und Entzündungsreaktionen hemmen können. Es wird angenommen, dass die Interaktionen zwischen perivaskulären Zellen der menschlichen Nabelschnur (HUCPV; eine alternative Quelle für MSC) und mononukleären Zellen des peripheren Blutes (PBMC)/Makrophagen durch abbaubares Magnesium (Mg) und seine Legierung (Mg-10Gd; 10 Gew .-% Gadolinium) beeinflusst werden. Die Mechanismen der Wirkung von Mg basierten Materialien, die die Immunreaktion modulieren, die Makrophagenfunktionen und die anschließende Knochenbildung müssen jedoch noch aufgeklärt werden. **Methoden:** Zwei indirekte *in-vitro*-Kokultursysteme von HUCPV und PBMC wurden entwickelt, um den Zusammenhang zwischen parakrinen Signalen und spezifischem zellulärem Verhalten während der anfänglichen Reaktion (7 Tage) des potentiellen Implantatempfängers unter Mg Exposition zu untersuchen: (i) Transwell (TW) und (ii) konditionierte Medien (CM). Des weiteren wurde ein direktes Kokultursystem von HUCPV und Makrophagen etabliert, um die Rolle von Mg bzw. Mg-10Gd auf die Sekretion von Makrophagen und ihre Auswirkungen auf die proosteogene Aktivität (7-14 Tage) zu analysieren. **Ergebnisse:** Das Zellwachstum in keinem der getesteten Systeme wurde durch Mg und Mg-10Gd signifikant beeinflusst. Im transwell coculture-System, das heißt wenn HUCPV mit abbaubarem Mg kultiviert wurden, konnte eine gemäßigtere Entzündungsreaktion über die geringere Sekretion von pro-inflammatorischen Zytokinen und entzündungshemmenden Zytokinen nachgewiesen werden. Darüberhinaus wurde ein erhöhter anti-inflammatoryischer M2-Makrophagen-Phänotyp beobachtet. Wenn PBMC mit abbaubarem Mg kultiviert wurden, erhöhte sich außerdem die Expression von solchen Zytokinen, die mit der Wundheilung verbunden sind, was mit einer erhöhten Einwanderung von Stammzellen einherging. Zusätzlich wurde ein erhöhtes proosteogenes Potential durch eine gesteigerte Expression und Aktivität osteoblastischer Marker (z.B. alkalische Phosphatase (ALP)) gezeigt. Im CM-System konnte der Prozentsatz des Phänotyps der M2-Makrophagen nur durch HUCPV und/oder Mg erhöht werden. Hinsichtlich der Darstellung der zugrunde liegenden Wirkmechanismen wurde anhand des direkten Kokultursystems unter Mg Exposition eine Beteiligung der Onkostatin M (OSM) und Glykoprotein 130 (gp130) basierten Signalwege an der osteogenen Differenzierung nachgewiesen; Darüber hinaus regulierten beide Materialien die Genexpression von knochenmorphogenetischem Protein 6 (*BMP6*) in Makrophagen, von knochenmorphogenetischem Proteinrezeptor Typ 1A und 2 (*BMPR1A/2*) und den Smad-homolog Signalweg auf parakrine Weise in kokultivierten MSC. Zusätzlich reduzierten beide Materialien die Sekretion von TNF $\alpha$  und IL1 $\beta$  in Makrophagen und Kokulturen, was synergistisch für eine proosteogene Mikroumgebung sorgen könnte. **Fazit:** Diese Ergebnisse implizieren, dass Mg komplexe osteoimmunmodulatorische Eigenschaften besitzt. Diese Studie beleuchtet insbesondere die Auswirkungen auf die interzelluläre Kommunikation von Mg-aktivierten Makrophagen für die proosteogenen Entwicklung von Stammzellen. Die Wirkung wird auf einen Einfluss über den OSM/gp130- und Smad-bezogenen Signalweg beschrieben. Insbesondere durch den nachgewiesenen erhöhten Anteil der geweberegenerierenden M2 Makrophagen wird ein neuer Aspekt der therapeutischen Anwendung für die Knochenregeneration aufgezeigt.

# Contents

Abstract.....	I
Zusammenfassung .....	II
Contents.....	III
1. Introduction.....	1
2. The state of the art.....	3
2.1. Magnesium (Mg) in biology.....	3
2.2. Mg as a biomaterial .....	4
2.3. Fracture healing and interactions of MSC-immune cells.....	6
2.3.1. Bone composition.....	6
2.3.2. Fracture healing .....	7
2.3.3. Control of fracture healing .....	8
2.3.4. Models for investigating the interactions of MSC-immune cells .....	15
3. Motivation and objectives.....	18
4. Materials and methods.....	19
4.1. Material preparation and characterization .....	19
4.2. Sample sterilization, incubation, and characterization .....	19
4.3. Cell isolation and culture.....	20
4.4. Indirect <i>in vitro</i> coculture systems: transwell coculture and conditioned media system .....	22
4.5. Direct <i>in vitro</i> coculture system .....	24
4.6. Live/Dead staining and DNA contents.....	25
4.7. ALP activity .....	26
4.8. Real time semi-quantitative polymerase chain reaction (RT-qPCR).....	27
4.8.1. RNA purification .....	27
4.8.2. Reverse transcription .....	27
4.8.3. RT-qPCR .....	28
4.9. Flow cytometry analysis.....	29
4.9.1. M2 macrophages polarisation in indirect coculture (transwell coculture and conditioned media) system .....	29
4.9.2. Subpopulations of HUCPV/macrophages in cocultures in direct coculture system .....	30
4.10. Multiplex immunoassay.....	31
4.11. ELISA.....	33
4.12. Wound healing assay.....	35
4.13. Neutralization experiment .....	36
4.14. Statistical analysis .....	37
5. Results .....	38
5.1. Interactions between PBMC and HUCPV in an indirect coculture (transwell coculture and conditioned media) system .....	38
5.1.1. Mg content, pH, and osmolality characterisation .....	38

5.1.2.	Cell viability and proliferation .....	39
5.1.3.	Cytokine release in the transwell coculture system .....	43
5.1.4.	M2 macrophages polarisation.....	49
5.1.5.	Migratory ability of HUCPV.....	51
5.1.6.	Osteogenic potential of HUCPV .....	53
5.2.	Interactions between macrophages and HUCPV in a direct coculture system .....	56
5.2.1.	Mg concentration, pH, osmolality, and corrosion rate characterisation.....	56
5.2.2.	Cell viability and proliferation .....	57
5.2.3.	Subpopulations of HUCPV cell and macrophage cocultures .....	58
5.2.4.	Mg and Mg-10Gd stimulated the pro-osteogenic activity of HUCPV .....	59
5.2.5.	Possible signalling factors (OSM/IL6/BMP6/TNF $\alpha$ /IL1 $\beta$ ) involved in the pre-osteogenic activity of HUCPV .....	60
6.	Discussion .....	66
6.1.	HUCPV and immune cell growth correlates with Mg contents as well as physiological osmolality and pH.....	67
6.2.	Interactions between PBMC/macrophages and HUCPV in indirect coculture (transwell coculture and conditioned media) system .....	69
6.2.1.	Inflammation .....	70
6.2.2.	Migration/wound healing .....	73
6.2.3.	Osteogenic potential of HUCPV .....	74
6.3.	Mechanisms of macrophage-mediated osteogenic activity of HUCPV in direct coculture systems.....	74
6.3.1.	OSM and gp130 dependency .....	76
6.3.2.	Stimulatory roles of BMP/Smad signals .....	76
6.3.3.	Inhibitory roles of TNF $\alpha$ and IL1 $\beta$ .....	77
7.	Outlook.....	78
7.1.	Possible strategies for bone substitute materials.....	78
7.1.1.	Modification by incorporation of Ca, Strontium (Sr), and Zn .....	78
7.1.2.	Functionalization with inflammatory mediators (IL4, IL10 and OSM) and growth factors (TGF $\beta$ 1, BMP and VEGF).....	79
7.1.3.	Combinations with anti-inflammatory drugs.....	80
7.2.	Therapeutic potential of utilising MSC (HUCPV)-macrophages for bone formation ..	80
8.	Summary and conclusion.....	82
	Reference.....	83
	Acknowledgements.....	112
	Appendix .....	113
	Supplementary data .....	113
	Symbols and abbreviations.....	118
	List of figures and tables.....	121
	Curriculum Vitae.....	124
	List of publications and conferences .....	125

# 1. Introduction

Fracture is the most common major organ trauma in humans, and approximately 10% cannot be properly cured [1]. The incidence of fractures increases dramatically from all causes at many skeletal sites [2]. Furthermore, the correlation between the incidence of fracture and various diseases, including chronic kidney disease [3, 4], coeliac disease [5], chronic liver disease [6], is a growing concern. Therefore, improvement of fracture healing is important for clinical practice.

Fixation biomaterials have emerged as a classical treatment to recover mobility and support healing after fractures. As proposed by D.F. Williams, “A biomaterial is a substance that has been engineered to take a form which, alone or as part of a complex system, is used to direct, by control of interactions with components of the living system, the course of any therapeutic or diagnostic procedure, in human or veterinary medicine” [7]. Desirable biomaterials are nontoxic and show good strength, biocompatibility and self-assembly. In recent decades, biomaterials have become more biocompatible, and demand has increased. Among the biomaterials, titanium (Ti) and its alloys are preferred as orthopaedic materials [8, 9]. However, in addition to the high expense, Ti and its alloys can cause implant failure and allergies to metal debris [10]. Recent studies on orthopaedic materials have concentrated on materials dissolving in physiological environments (body fluid) while stimulating bone regeneration. For example, magnesium (Mg) and its alloys have been used as bioabsorbable materials for medical implants and show promising degradation behaviour [11], exhibiting an appropriate inflammatory response [12, 13] while improving tissue healing and bone regeneration [14].

After implantation into fracture sites (Fig. 1), a sequence of events occurs at the surface of the biomaterials.

- 1) A layer of proteins from the surrounding microenvironment is adsorbed onto the material surface, forming a surface matrix and conditioning all further steps. Surface-modified biomaterials are continuously developed to influence protein absorption [15, 16] and subsequent bone formation [17, 18].
- 2) An immune response, such as neutrophil activation, occurs on fracture sites, followed by macrophage activation, foreign body giant cell (FBGC) production and formation of granulation tissue.
- 3) These cells release chemoattractants and cytokines to recruit tissue-repairing cells, such as fibroblasts and mesenchymal stem cells (MSC), to injury sites to deposit collagen matrix and form a fibrous encapsulation.

The implant-induced immune reactions could also contribute to the cellular interaction and differentiation of bone-forming cells (e.g., MSC, osteoblasts and osteoclasts). Regarding the complexity of processes 2) and 3), more studies about the mechanism of the immune response following biologically Mg-based biomaterial implantation are still required. Hence, the current research examines the effects of immune cells (peripheral blood mononuclear cells

(PBMC)/macrophages) and MSC, which are two vital factors participating in the immune response of fracture healing.

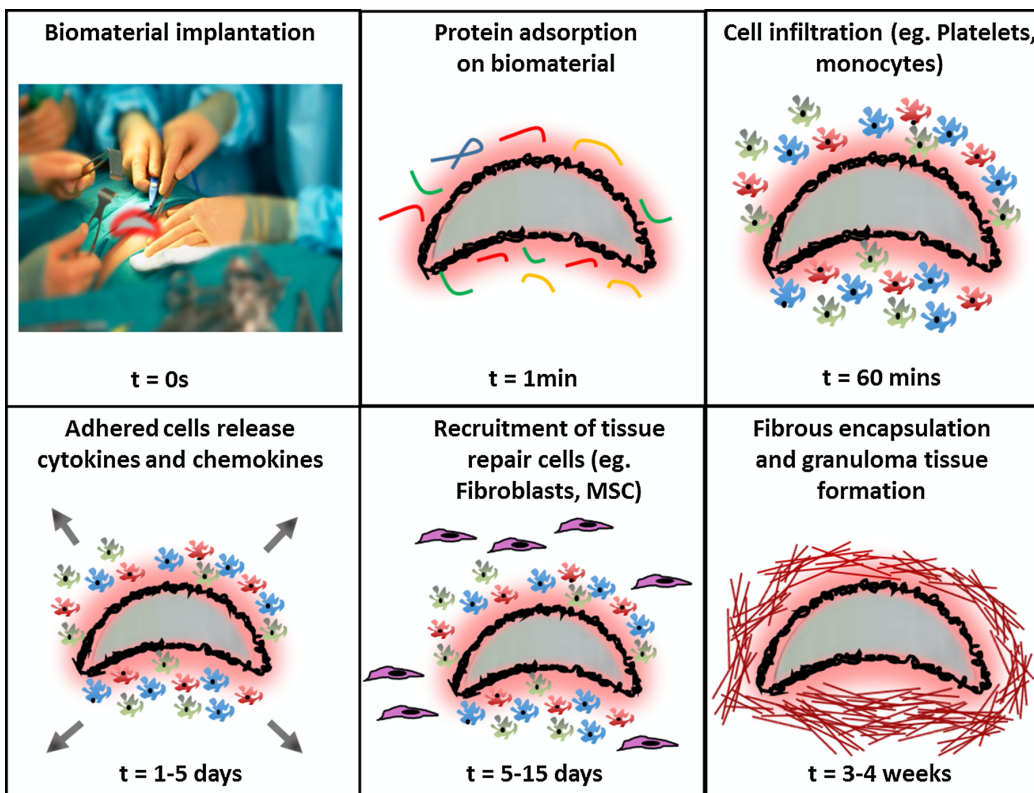


Fig. 1 Biological responses following biomaterial implantation. Adapted from [19]. Reused by permission from Elsevier Publishers, Ltd.: Materials Today.

First, the effects of pure Mg on indirect interactions (cell-cell noncontact) of PBMC/macrophages and mesenchymal stem cells (MSC) were evaluated. Parameters such as released cytokine levels, macrophage polarization, migratory ability and osteoblastogenesis potential of MSC were measured. Second, the effects of Mg or Mg-10Gd (Gd; gadolinium, 10 weight %) on direct communication (cell-cell contact) between MSC and macrophages involved in osteogenic activity were also investigated. The possible signalling factors, such as immunoregulatory factors (oncostatin M (OSM) and interleukin 6 (IL6)), growth factors (bone morphogenetic protein (BMP)) and proinflammatory cytokines (tumour necrosis factor alpha (TNF $\alpha$ ) and interleukin 1 beta (IL1 $\beta$ )) were analysed. The underlying signalling pathways, such as OSM/IL6-gp130 (glycoprotein 130) and BMP/Smad (mothers against decapentaplegic homologue), mediating the osteogenic activity of MSC when interacting with macrophages and/or Mg-based biomaterials were investigated.

## 2. The state of the art

### 2.1. Magnesium (Mg) in biology

Mg is the fourth most abundant mineral in the body. An adult body contains approximately 22 to 26 g of Mg, with 60% found in bone (one-third on the surface of hydroxyapatite), 20% in muscle, and the rest in soft tissue [20]. Mg ions act as cofactors or complexes with more than 300 enzymes and proteins that regulate several and various biochemical reactions or metabolic processes, such as deoxyribonucleic acid (DNA), ribonucleic acid (RNA) and protein synthesis [21]. Importantly, Mg ions can also bind to adenosine triphosphate (ATP) to form the Mg-ATP complex [22]. This complex acts as an energy source and plays a role in intracellular energy production and regulation of neuromuscular activity in the body [23, 24]. In addition, Mg is often referred to as a calcium (Ca) antagonist due to, for example, its role in muscle contraction/relaxation. This in muscle contraction/relaxation has been proven to inhibit Ca influx via the blockage of Ca channels [25] and the N-methyl-d-aspartate (NMDA) receptor [26].

Mg has been shown to play multiple and important roles in the immune system. Mg has been associated with various clinical symptoms, including inflammation [27, 28] and cardiovascular pathologies [29, 30]. Magnesium deficiency is a mechanism associated with increased inflammation and oxidative pathology [31, 32]. As shown in Table 1, Mg regulates the immune reaction because it can, for instance, reduce the harm caused by reactive oxygen species (ROS) [33]. *In vitro* studies also demonstrated a direct role of MgSO<sub>4</sub> in decreasing the production of proinflammatory cytokines [34], as well as mediating anti-inflammatory effects by activating the phosphatidylinositol 3-kinase (PI3K)/protein kinase B (Akt) pathway [35]. A mechanism of action study from B Rochelson *et al.* showed that Mg ions could also reduce nuclear factor kappa-light-chain-enhancer of activated B cell (NFκB) nuclear translocation and protect cytoplasmic nuclear factor of kappa light polypeptide gene enhancer in B-cell inhibitor, alpha (IκBα; an NFκB inhibitor) from degradation in lipopolysaccharide (LPS)-treated human umbilical vein endothelial cells (HUVECs) [36]. In contrast, Mg supplementation or Mg-rich conditions are known to exert an anti-inflammatory action. For instance, in rats, increasing Mg concentrations decreased the inflammatory response, while reducing extracellular Mg resulted in macrophage activation and secretion of inflammatory molecules [31]. *In vivo* investigation of the macrophage response to Mg ions was also carried out and indicated that Mg salts could inhibit inflammation and further suppress thrombus formation [37]. L-type Ca channels were shown to be involved in magnesium supplementation, reducing the production of proinflammatory cytokines, which increase due to NFκB [38].

In addition, an increasing number of studies have been conducted on the roles of Mg in bone metabolic activity (Table 1). Numerous reports over recent years have demonstrated that Mg ions can stimulate osteogenic differentiation of MSC and bone regeneration *in vitro* [39, 40]. Furthermore, Mg appears to influence the activities of osteoblasts and osteoclasts [41]. Mg deficiency is a major contributing factor in patients with established osteoporosis, with low vitamin D and parathyroid hormone (PTH) levels [42]. Another population-based study showed

that Mg therapy could contribute to preventing fractures and lead to a clear increase in bone density in menopausal women [43].

Table 1 The roles of Mg and its deficiency/supplementation in biology.

<b>Effect</b>	<b>Mechanism</b>	<b>Model</b>	<b>Reference</b>
<b>Cellular/molecular biology</b>	Cofactor of or complex with more than 300 enzymes and proteins	Human	[21]
	Intracellular energy production by Mg-ATP complex	Human	[22-24]
	Muscle contraction/relaxation by influencing Ca influx and NMDA receptor	Human	[25, 26, 44]
<b>Mg deficiency/supplementation and inflammation</b>	L-type Ca channels and cytosolic Ca activation	Human	[27, 28, 31, 32, 34]
	Cardiovascular pathologies through inflammatory/pro-oxidant events	Rodent	[29, 30]
	Reactive oxygen species (ROS)	Rodent	[33]
	Proinflammatory cytokines	Human	[34]
	(PI3K)/protein kinase B (Akt) pathway	Rodent	[35]
	NF $\kappa$ B signalling	HUVECs	[36]
<b>Mg deficiency/supplementation and bone metabolic activity</b>	MSC differentiation	Human cells	[39]
	Inhibition of pathways of macrophages and osteoclastic activities	Rodent cell lines	[40]
	Osteoblast and osteoclast	Rodent cell lines	[40, 41]
	Osteoporosis, vitamin D and PTH	Human	[42]
	Bone density	Human	[43]

## 2.2. Mg as a biomaterial

The use of Mg and its alloys in cardiovascular and orthopaedic applications is not a new concept. In the past hundreds of years, Mg and its alloys were reported to be more or less effective.

As shown in Table 2, the history of bioresorbable and biodegradable Mg and its alloys as implants in cardiovascular applications started in the year of 1878, when Huse proposed that Mg wire could end the bleeding in vessels [45]. In 1900, Payr designed a tubular, thin-walled Mg cylinders as connectors for vessels [46]. Engineered as rings [47], clips and staples [48], as well as wires [49], Mg and its alloys, were considered attractive implants for the closure of

tissue vessels and deep wound. Mg wires were used in a rabbit model by Seelig *et al.* in 1924; They confirmed Mg was a suitable biomaterials for suture and ligature [50]. In the early years of the 2000s, the properties and influences on coronary arteries of two materials, AE21 (containing about 2 % aluminium and 1 % rare earth elements) and WE43 (containing about 4 % yttrium, 3 % neodymium and less than 1 % zirconium), have been assessed [51-53]. In 2005, Zartner *et al.* described the first successful implantation of Mg stent into the left pulmonary artery of a preterm baby, highlighting advantage of the resorbable property of Mg-based biomaterials (especially in growing paediatric patients) [54]. Afterwards, several generations of a successful absorbable metal stents (AMS) were produced from Mg-based alloys, such as AMS, AMS INSIGHT, PROGRESS-AMS and BIOCOLVE-1 DREAMS (products from BIOTRONIK AG, Berlin, Germany). The clinical use has shown high biocompatibilities (no blood or vessel toxicity to implanted stents) [55-61]. Especially, the Mg stents could degrade safely in 4 months and present good coronary angiography result [54, 55, 59].

Table 2 The history of Mg and its alloys in cardiovascular applications. Summarised by previous works [44, 62-64].

Year	Mg/its alloys	Application	Model	Reference
1878	Mg wire	Stop bleeding vessels	Human	[45]
1900	Tubular, thin-walled Mg cylinders	Connectors for vessel anastomosis	Human and animals	[44]
1910	Mg rings	Extravascular sutures of vessels	Dogs	[47]
1917	Mg and its alloys as clips and staples	Closing tissue vessels, such as brain	Dogs	[48]
1924	Mg wires	Suture and ligature	Rabbits	[50]
1951	Mg and Mg-Al wires	Double-coiled wires in aortas	Dogs	[49]
2003	AE21 stents	Cardiovascular implant	Domestic pigs	[51]
2006-2007	WE43 stents	Coronary arteries implant	Pigs	[52, 53]
2008-2009	AMS	Coronary arteries implant	Pigs	[65, 66]
	AMS			[55-57]
	AMS INSIGHT			[58]
2005-2013	PROGRESS-AMS BIOCOLVE-1 DREAMS	Blood vessels implants	Human	[59, 60] [61]

In accordance with the importance of Mg in bone structural development, Mg is frequently explored as one of the most promising orthopaedic implants . Bioresorbable Mg-based implants have mechanical properties similar to those of bone and could thus reduce implantation failure from stress shielding [16]. As shown in Table 3, early in the 1900s, Lambotte, Verbrugge and McBride reported machined Mg and its alloys in plates, sheets, screws and nails for transfixion

and/or bone tissue fracture support, resulting in human osteosynthesis activity [44, 67, 68]. As mentioned in [62], in 1940 and 1948, Mg and its alloys were further placed in fracture sites, and bone synthesis and formation were measured. Since then, more than 20 different alloys of bare metal (BM) Mg implants have already been tested in bone tissues and animal models [64]. Then, a Mg alloy, MgYREZr (Mg-yttrium-rare earth-zirconium alloy), was reported to achieve good compatibility and osteoconductivity without acute or chronic toxicity [69], leading to the approval of the MAGNEZIX® screw (Syntellix AG, Hannover, Germany) in medical applications in Europe [70].

Table 3 The history of Mg and its alloys in orthopaedic applications.

Year	Mg/its alloys	Application	Model	Reference
1909-1937	Mg plates, sheets and screws	Bone synthesis	Human	[44]
1938	Mg alloys as screws and nails	Transfixion in the fracture	Human and dogs	[67, 68]
1940	Mg sheets	Bone synthesis in fractures	Human and rabbits	[62]
1948	Mg-Cd alloy as plates and screws	Formation of callus bone	Human	[62]
~2014	Mg alloys	Bone synthesis in fractures	Animals	[64]
2014-2017	MgYREZr as screws	Transfixion in the fracture	Rabbits and human	[69, 71]
2014	MAGNEZIX® screw	Bone synthesis in fractures	Human	[70]

## 2.3. Fracture healing and interactions of MSC-immune cells

### 2.3.1. Bone composition

Bone is the hardest connective tissue in the body and consists of 50% water [72]. During bone growth, bone relies on the blood supply as a fundamental source of energy equivalents and hormones to regulate the growth process. The basic composition of bone is cells and related matrix (Fig. 2).

There are four main types of cells in bone tissues: osteogenic cells (stem cells), osteoblasts, osteoclasts and osteocytes. Osteoclasts are derived from haematopoietic progenitors (e.g., monocytes and macrophages) in the bone marrow. They are formed by fusion of precursor cells and are thus multinucleated. The three other types of cells are derived from the mesenchymal lineage. Human MSC are multipotent stem cells and form heterogeneous populations that can be found in different organs and tissues [73]. MSC can differentiate into several specific cell types and produce cytokines and soluble factors. Moreover, MSC can migrate to the damage sites and show potent anti-inflammatory and immunomodulatory effects via released mediators [73, 74]. Osteoblasts are derived from osteoprogenitor cells and synthesize bone (*i.e.*, collagen

matrix and calcium salts). Osteocytes are mature bone cells (formed from osteoblasts) entrapped in the matrix and involved in the maintenance of bone. Osteoclasts degrade the bone matrix and resorb bone tissue. Osteoblasts and osteoclasts form and degrade bone tissues and regulate bone turnover.

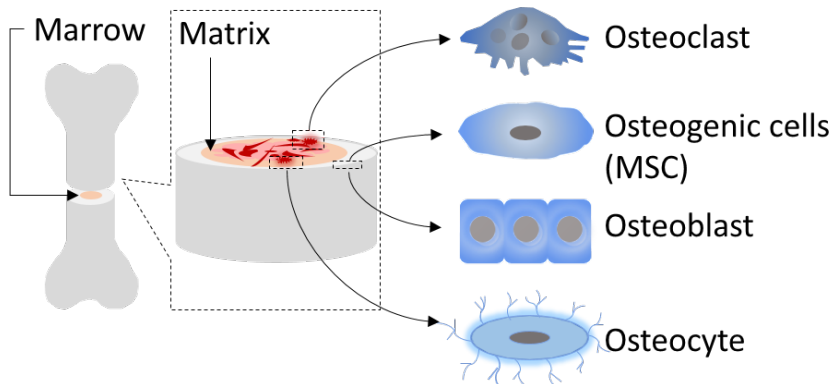


Fig. 2 The basic composition of bone. Osteoclasts, osteogenic cells, osteoblasts and osteocytes exhibit different functions and are found in different locations in bone. Osteogenic cells can be found in the deep layers of the periosteum and the bone marrow. Osteoblasts are located in growing parts of the bone (including the periosteum and endosteum). Osteoblasts trapped in the matrix that they secrete are called osteocytes. Osteoclasts are on the bone surfaces and at sites of old or injured bone.

### 2.3.2. Fracture healing

Fracture healing involves three main stages: inflammation, tissue repair, and remodelling phases, as indicated in Fig. 3.

The three main phases in fracture healing are as follows:

- 1) Inflammation (0-5 days). Haematoma formation with inflammatory reactions (polymorphonuclear leukocytes (PMNs, also called granular leukocyte, granulocytes), monocytes/macrophages, T cells, B cells). PMNs consist of neutrophils (50%-70%), eosinophils (2-4%) and basophils (0.5-1%) [84]. Neutrophils have a relatively short life and can only circulate for days [85]. Normally, monocytes live for several days, but macrophages can survive up to months [86].
- 2) Tissue repair (5-21 days). Close to the fracture lines, granulation tissue (new connective tissue and microscopic blood vessels) will form. Chondrocytes, arising from mesenchymal stem cells, form extracellular matrix until all granulation and fibrous tissues are replaced by cartilage [75]. Then, the chondrocytes undergo mineralization. With soft callus development, the initial woven bone is formed. This process is synthesized by mature osteoblasts. Osteogenic factors, such as BMP, are responsible for the differentiation of osteoprogenitors to mature osteoblasts.

3) Remodelling: (21+ days) The woven bone is replaced by cortical bone, and the medullary cavity is repaired [64]. Osteoclasts, which are the main cell type participating in the resorption of mineralized bone, are derived from the differentiation and fusion of myeloid/monocyte lineage precursors [76]. The period of the remodelling phase is dominated by transformational cycles of osteoblast and osteoclast behaviour.

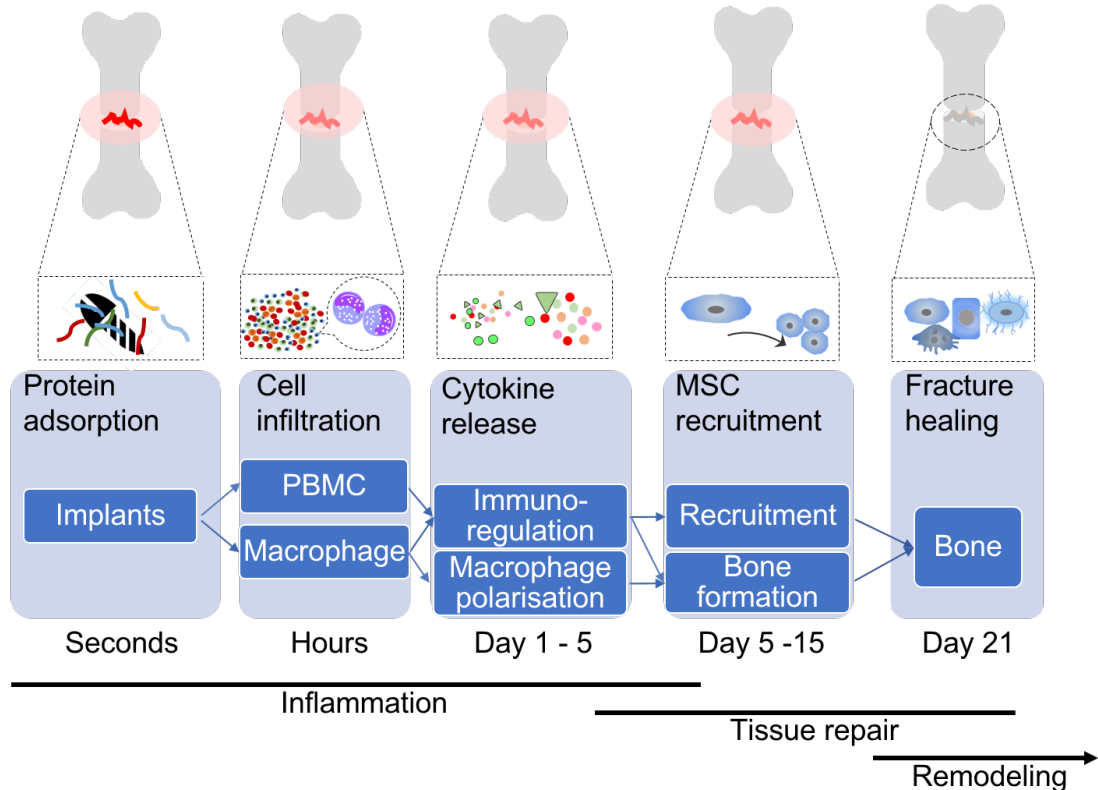


Fig. 3 Fracture healing. The biological stage of fracture healing is revealed in three main phases: inflammation, tissue repair and remodelling. The phases of inflammation are indicated in three events: protein adsorption, cell infiltration and cytokine release. The following phases of tissue repair and remodelling are indicated in two main events: MSC recruitment and differentiation, as well as turnover of osteoblasts and osteoclasts.

### 2.3.3. Control of fracture healing

Normally, fracture healing is governed by the nature and extent of the wound, the stability of the implants (fracture fixation), and the regulation of biological processes, including the immune reactions and developmental processes associated with the bone [1]. In brief, successful fracture healing involves the following control elements: 1) immune reactions, 2) bone formation and 3) the implants.

#### 1) Immune reactions

A fracture leads to the activation of the immune response. Activated platelets, macrophages and other inflammatory cells (granulocytes, lymphocytes and monocytes) infiltrate fractured sites, release cytokines and chemokines, and regulate the inflammation phase in fracture healing [77].

Neutrophils and macrophages, acting as the main cells in the first natural immunological defence response to xenogenic materials (e.g., implants), have drawn the most attention because of their multiple functions in bone healing [19, 78]. It has been suggested that macrophages can recognize foreign implants *via* the Toll-like receptor (TLR) pathway, which stimulates an initial innate host response and could lead to material rejection [79]. In addition, macrophages, as secretory cells, modulate the function of other cell types and innate/adaptive immunity by releasing a range of cytokines, chemokines and growth factors. These factors include TNF $\alpha$ , IL1/6, macrophage colony stimulating factor (M-CSF), BMP, transforming growth factor beta 1 (TGF $\beta$ 1), platelet-derived growth factor (PDGF), vascular endothelial growth factor (VEGF) and fibroblast growth factor (FGF) [75, 80-83]. Moreover, secretion could be regulated by some bioactive agents of implant materials (released ions, particles, etc.).

Macrophage polarization also plays a vital role in fracture healing [84, 85]. Based on the microenvironment (space) and its evolution (time), macrophages can exhibit various phenotypes and functions, e.g., macrophage polarization plasticity. Thus, macrophages present various phenotypes [86]. From a historical and simplified perspective, the macrophage phenotype has been divided into 2 groups: M1 (classically activated macrophages) and M2 (alternatively activated macrophages). Monocytes and activated macrophages could be polarized into an antimicrobial M1 type (proinflammatory macrophages) with the cytokine release of TNF $\alpha$  and interferon gamma (IFNy). Additionally, a tissue regenerative M2 phenotype (anti-inflammatory macrophages) shows the secretion of IL10 and interleukin 1 receptor antagonist (IL1ra) [87, 88]. Normally, M1 induces chemokines such as IL8 and monocyte chemotactic protein 1 (MCP-1), and M2 induces chemokines such as osteopontin (OPN) [89]. The alternatively activated M2 has been shown to contain 3 subpopulations (e.g., M2a, M2b and M2c). Each of them has its own unique inducer, product and function [90].

These macrophages and their fused or polarized morphologic variants always remain at the material-tissue interface *in vivo*. This cell-cell fusion also contributes to the degradation of biomaterials *via* their phagocytosis and release of mediators [91, 92]. Over time, macrophages and neutrophils release lysosomes (digestive enzymes) and work with other phagocytic cells to clear degraded cells and debris (e.g., particles from implants) [93]. Adaptive immune cells, including T cells, B cells and natural killer (NK) cells, also play a role as indispensable modulators in bone healing [79]. Taken together, macrophages, cytokines and other released substances influence tissue healing and remodelling and can thus affect the mechanical properties and performance of biomaterials [79, 94, 95].

In recent years, it has become clear that MSC modulate the majority of immune cells [96-98], especially macrophage functions [84, 85, 99]. Fracture rehabilitation is significantly increased *in vivo* by skewing macrophage differentiation towards an anti-inflammatory phenotype (type 2 macrophages: M2) [100]. Emerging results indicate that MSC (mediated by IL6 and lactate) can induce activated monocytes to polarize into an M2 phenotype [101-105]. Another study indicated that MSC could recruit M2 depending on NF $\kappa$ B and signal transducer and activator of transcription 3 pathway (STAT3) [106]. Accordingly, *in vitro* results have shown that MSC can regulate the immune response by influencing the activation and proliferation of B cells [107],

suppressing NK cell proliferation [108] and T cell/dendritic cell maturation [109], and inducing regulatory T cells (Treg) [110, 111]. In animal models, MSC also induce strong immunosuppressive effects or promote immunosuppression of effector T cells [112] and the T-cell-mediated immune response [113, 114].

## 2) Bone formation

The entire maturation process of osteoblasts, *i.e.*, osteoblastogenesis, can be divided into proliferation, matrix maturation, mineralization, and apoptosis. Osteoprogenitor cells (MSC) start differentiating into preosteoblasts and begin to express adhesion and extracellular matrix (ECM; mostly synthesis). With the increase in the levels of alkaline phosphatase (ALP) activity, preosteoblasts further differentiate into mature osteoblasts. Then, the ECM components produced by osteoblasts mature and soon begin to mineralize in specialized sites. In the final stage, only a small proportion of cells survive as osteocytes (Fig. 4) [115].

Each phase of osteoblastogenesis can be followed by specific markers. High ALP activity and upregulated specific pro-osteogenic genes are indicators of osteogenic differentiation of MSC populations. These specific markers, *e.g.*, COL1, type 1 collagen, are considered the main component of bone formation and can be found in most connective tissues, including cartilage, bone, tendon, and skin [116]. Osteocalcin (OC) is a regulator of osteogenesis that can be induced after MSC differentiation into osteoblast-like cells [117]. OPN, as a player in osteogenesis, also drives chemotaxis of immune cells (neutrophils, macrophages and mast cells) [118].

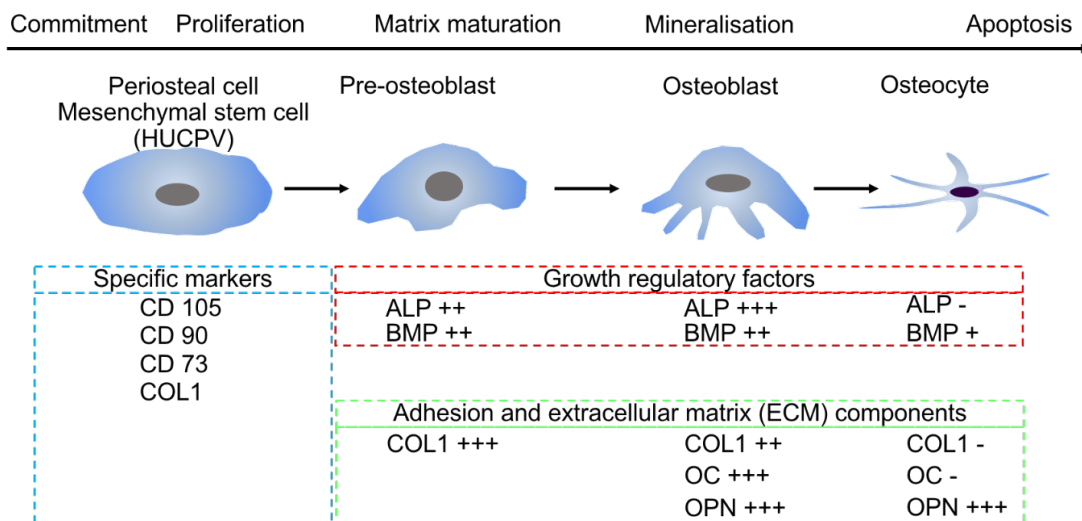


Fig. 4 Specific markers in different stages of osteogenic differentiation of MSC. Summarized by the former report [119].

After any bone tissue fracture or subsequent biomaterial implantation, the immune response is accompanied by bone tissue repair processes. Thus, immune cells, especially macrophages, play important roles in the cellular response of tissue repair [120, 121] by mediating cell recruitment, proliferation, and differentiation or by influencing different cells, *e.g.*, fibroblasts [122], osteoblasts [100, 123], and endothelial cells [124].

Specifically, macrophages can attract MSC to migrate quickly to damage sites by secreting factors, such as MCP-1, macrophage inflammatory protein (MIP-1a), and IL8 [125, 126]. In addition, the roles of immunoregulatory cytokines have been extensively studied when interacting with MSC, especially in bone tissue repair. W Zhao *et al.* (2012) confirmed that injected MSC interact with monocytes during treatment of liver fibrosis and macrophages and result in a high concentration of IL10 and decreased levels of TNF $\alpha$  and IL6 [127]. In coculture of macrophages with MSC, some studies found a decreased level of proinflammatory cytokines (TNF $\alpha$  and IFNy) as well as an increased concentration of anti-inflammatory cytokines (IL4 and IL10) [128, 129]. Nevertheless, the involvement of TNF $\alpha$  in bone formation is still controversial, as the recruitment of MSC could be antagonized by this inflammatory factor [125, 126, 130]. However, TNF $\alpha$  was confirmed to elevate ALP activity and mineralization of MSC in a dose-dependent manner by activating the NF $\kappa$ B pathway [131, 132]. Another proinflammatory cytokine, IL1 $\beta$ , could regulate bone repair by inhibiting osteoblast maturation and stimulating osteoclast activity [133-135]. In addition, TNF $\alpha$ , IL1 $\beta$ , and IFNy were reported to suppress osteoblast differentiation and inhibit collagen synthesis [136-138].

Physiological bone formation is orchestrated by bone repair-related growth factors, including TGF $\beta$ 1 [80] and BMP [139]. BMPs, a group of signalling molecules identified as members of the TGF $\beta$  superfamily, are multifunctional chemokines (Fig. 5) [140]. BMP2 and BMP6 are vital differentiation factors that promote cartilage ossification through cytokines as well as migration and differentiation of MSC, thereby inducing bone regeneration in the treatment of fractures [141-143].

BMP molecules regulate osteoblast differentiation through the classical BMP/Smad pathway. Smads are basically divided into three classes according to their function: BMP receptor-regulated Smads (Smad 1/5/8), co-Smads (Smad 4), and inhibitory Smads (Smad 6/7) [144]. Typically, BMP initially activates BMP receptors of target cells, namely, a type 1 and type 2 BMP receptor (BMPR1 and BMPR2). Then, the activated BMP signals can be transferred via specific phosphorylating Smads (Smad 1/5/8). Ultimately, the Smads interact with Smad 4 to form a complex that will be subsequently translocated into the cell nucleus to modulate the key osteoblast transcription factors and related gene expression of osteogenic differentiation factors [145]. For instance, runt-related transcription factor 2 (RUNX2), which is also known as core-binding factor subunit alpha-1 (CBF-alpha-1), is regulated. RUNX2, as a master switch for inducing osteoblast differentiation [119], directly promotes the transcription of downstream target genes, including COL1, OC and OPN [146, 147].

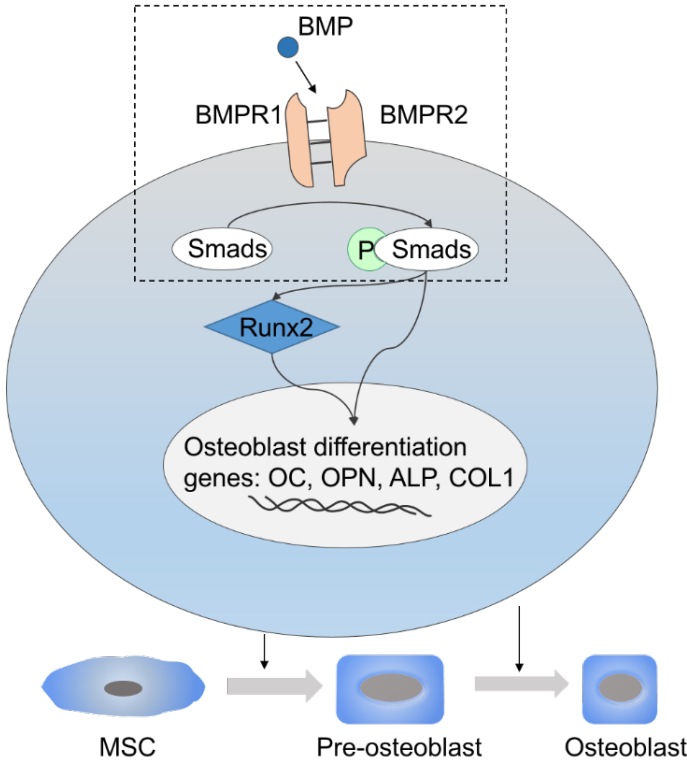


Fig. 5 BMP signalling pathway. The present graph is summarized from previous reports [141, 148].

The regulatory factor IL6/OSM is another important player in immune cell-mediated osteogenesis [149, 150]. The IL6 family is a group of cytokines, including IL6, IL11, ciliary neurotrophic factor (CNTF), leukaemia inhibitory factor (LIF), OSM, cardiotrophin 1 (CT1), cardiotrophin-like cytokine (CLC), and IL27 [151]. These factors are grouped because they share a coreceptor (gp130). The gp130 protein is commonly expressed in most tissues and is responsible for signal transduction into cells by activating related cytoplasmic tyrosine kinases (such as JAK; Janus kinase) and leading to the phosphorylation of various transcription factors, particularly STAT3 [152-154].

IL6 is a proinflammatory cytokine that is normally expressed and/or stimulated in damaged tissue or stress [155, 156]. There are two types of IL6-mediated signals: classical IL6 signals and IL6 receptor (sIL6R) signals [157]. IL6 is essential for callus mineralization and maturation in a mouse model [158]. IL6 together with sIL6R stimulates osteogenic differentiation of MSC by activating STAT3 [159].

As shown in Fig. 6, IL6 binds and signals through its own unique receptor (IL6R) on the plasma membrane [154]. The complex of IL6/IL6R interacts with gp130 (coreceptor for the IL6 family) and results in an activated complex (IL6, IL6R and two molecules of gp130). Consequently, both signalling pathways contribute to the activation of JAK proteins, which are responsible for the phosphorylation of STAT recruitment, especially STAT3 [160].

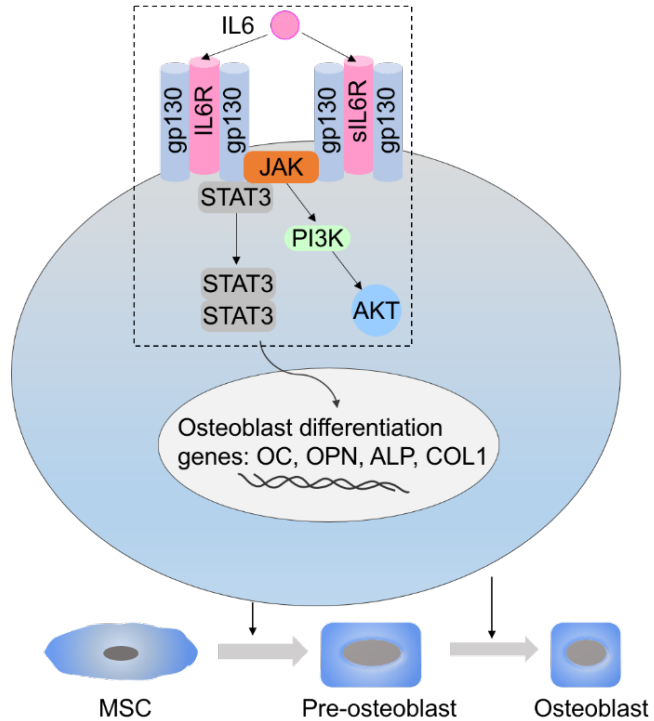


Fig. 6 IL6 signalling pathway. The present graph is summarized in a previous report [160].

OSM is mainly released by immune cells, epithelial tissue cells, and stromal cells during the regulation of immune reactions [161-163]. OSM produced by monocytes/macrophages has been reported to promote the osteogenesis of human MSC [164] by activating STAT3 signalling in MSC (Fig. 7) [165]. OSM interacts with its receptors (OSMR/gp130). Then, the complex (OSM, OSMR, and gp130) results in JAK activation and the phosphorylation of STAT3 recruitment (Fig. 7).

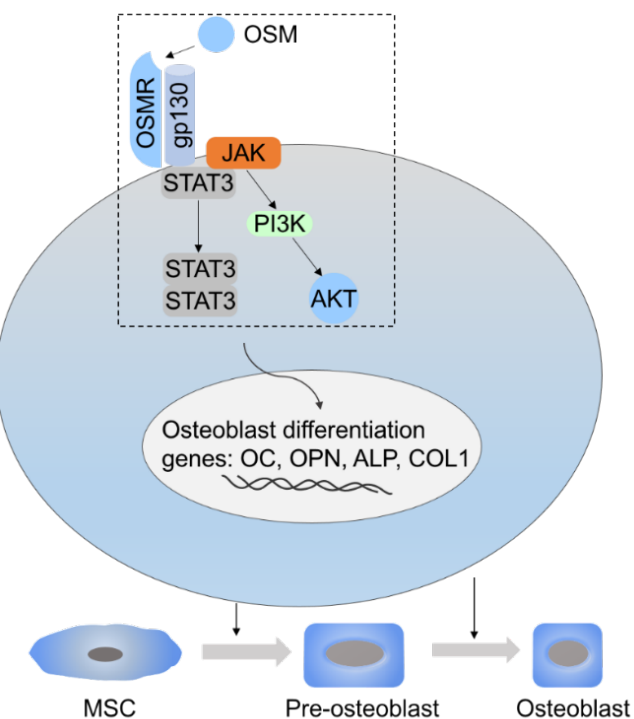


Fig. 7 OSM signalling pathway. The present figure is produced based on previous work [166].

Studies have examined the correlations of OSM/OSMR/gp130, STAT3 signals and ALP activity. For instance, the stimulation of pro-osteogenic activity by activated macrophages can be blocked with neutralizing antibodies to OSM, the OSM receptor subunits gp130 and OSMR, or the downstream transcription factor STAT3 [166]. Thus, neutralized OSM was related to the reduced ALP level *in vitro* [165]. Moreover, OSM knockout in mice led to decreased new bone formation [167].

### 3) The implants

The immune reactions induced by the interaction that exists between the implants and biological systems contribute to both the success and failure of biomaterial implantation [168, 169]. On the one hand, as a favourable host response, immune cells can secrete cytokines to stimulate bone tissue repair in addition to their inflammatory roles. On the other hand, macrophages act as key factors of excessive inflammation [170-172]. An excessive immune reaction may create continuous inflammation and the formation of granuloma and fibrous tissue around the implants. Thus, bone-forming cells cannot attach to the surface of implants to form new bone tissue, which will lead to implant loosening.

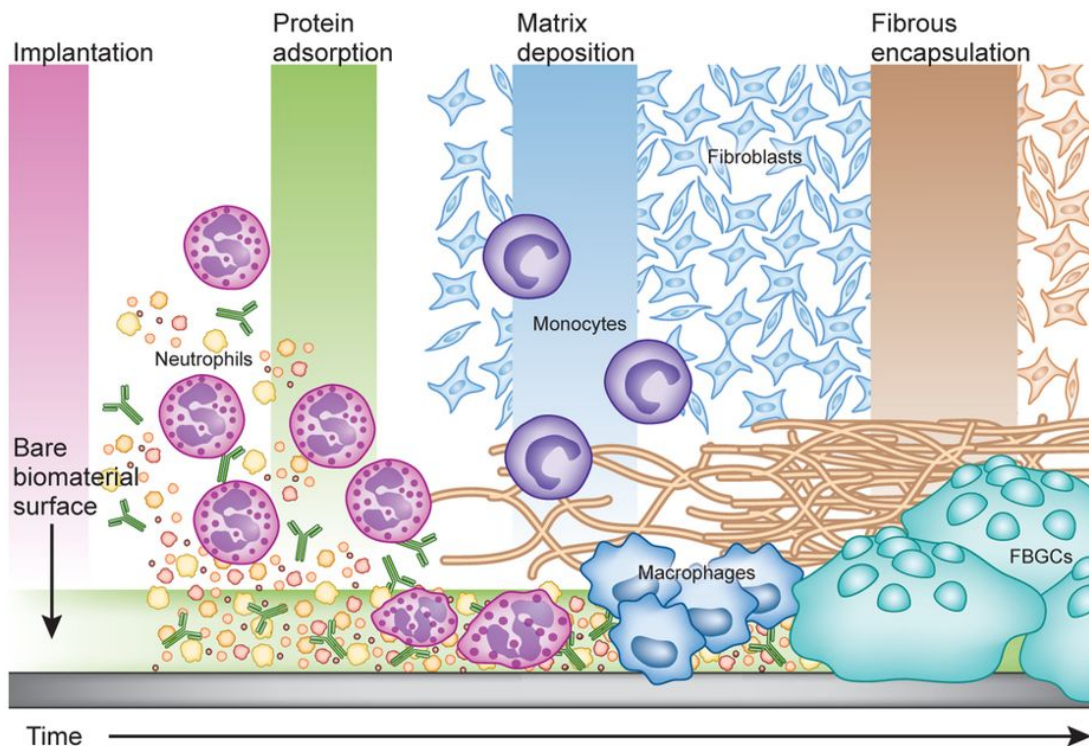


Fig. 8 An excessive immune reaction resulting in encapsulation of an implant. Adapted from [173]. Reused with permission from Springer Nature Publishers, Ltd.: Nature Biotechnology.

The excessive immune reactions of macrophages primarily respond to microenvironmental cues and the consequent events that occur due to biomaterial implantation. As shown in Fig. 8, macrophages react to implants by secreting molecules that attract fibroblasts. Fibroblasts subsequently generate excessive collagen. Their presence is associated with the formation of foreign body giant cells *via* fusion of monocyte-derived macrophages. Over time, a fibrous capsule is formed around the implants, completely separating the implants from the cellular components of the foreign body reaction (FBR) [95].

In general, inflammation and formation of granulation tissue are common in wound healing and biomaterial implantation, while FBR is unique to implantation. The FBR to implants comprises foreign body giant cells and the components of granulation tissue (fibroblasts, macrophages, and capillaries) [174]. This inappropriate immune response of capsule formation, dominated by FBR, is suggested to be altered by biomaterials [79], which is determined by the match of implants and fractured tissue, as well as the interaction of implant shape and tethering forces [175].

Consequently, the host response starts immediately upon implantation of any material and lasts throughout tissue remodelling. The host's response to implants will be a key factor in determining the success or failure of any surgical or regenerative strategy. Strategies to influence or control macrophage polarization with positive effects on fracture (tissue) remodelling may lead to improved outcomes in biomaterials [176]. As a promising biomaterial, biodegradable Mg-based materials have attracted extensive interest. For instance, *in vitro* and *in vivo* studies demonstrated a direct role of Mg ions or their salts in suppressing inflammation [34, 35, 37]. In a mouse model, the anti-inflammatory effect of Mg oxide nanoparticles was reported [177]. Similarly, Mg alloys exhibited anti-inflammatory properties [13].

Implants can provide support for MSC adhesion and growth. Furthermore, the implants can affect MSC recruitment and osteogenic differentiation at fractured sites. Numerous reports in recent years have demonstrated that Mg ions can stimulate osteogenic differentiation of MSC and bone regeneration *in vitro* [39, 40]. Additionally, it has been shown that Mg-based alloys can promote bone formation *in vivo* [178, 179]. Magnesium–calcium phosphate cement (MCPC) has been reported to enhance the osteogenic capacity of MSC by decreasing TNF $\alpha$  and upregulating TGF $\beta$ 1 [80].

Thus, osteoimmunomodulation (convergence of osteoimmunology and immunomodulation) could be an important feature of implants to stimulate tissue repair and eliminate fibrous encapsulation. When orthopaedic implants are designed, both biological and engineering methods can be applied to modify biomaterials and their degradable components. Various methods have been proposed to manufacture implants that release anti-inflammatory [180], pro-osteogenic [181, 182], and proangiogenic [183] drugs or mediators to reduce foreign body reactions. In some reports, the implant surface was modified to modulate the cellular response (e.g., inflammation and bone/cartilage formation) [184, 185].

#### **2.3.4. Models for investigating the interactions of MSC-immune cells**

The choice of *in vitro* models, such as indirect and direct contact cocultures, for studying the interactions of MSC-immune cells depends on the stage of the natural cell niche that needs to be mimicked or studied [186].

At the initial stages of immune reactions (Fig. 3), immune cells and MSC are in an indirect cell-cell interaction stage (cell infiltration, recruitment, and cytokine exchange). Given these specific cellular and molecular interactions (Fig. 9), two different indirect *in vitro* coculture systems were established to explore various events: transwell coculture (TW) and conditioned media (CM) systems. In addition, MSC can regulate the immune response in a paracrine manner [187, 188];

thus, a transwell coculture and conditioned media system should be applied. With higher complexity, a transwell coculture system involves two-way communication. By employing an indirect *in vitro* transwell coculture system, MSC and PBMC/macrophages grow separately while sharing the same microenvironment and soluble factors. Thus, the synergistic contribution of each cell type can be investigated. The conditioned media system is a one-way communication system, offering a simplified *in vivo* model while being more complex than a monoculture. Conditioned media has been used to investigate the single effect of MSC or PBMC/macrophage secretory cytokines on opposite cell types [189, 190].

In the subsequent fracture healing stage, immune cells and MSC will be in a direct cell-cell interaction. Thus, a direct-contact coculture system was also established to represent the physical interactions after MSC and PBMC/macrophages attached to the biomaterial surface (Fig. 3). A limitation of such direct cell-cell coculture is that it is not possible to distinguish the contribution of MSC or PBMC/macrophages in cytokine production.

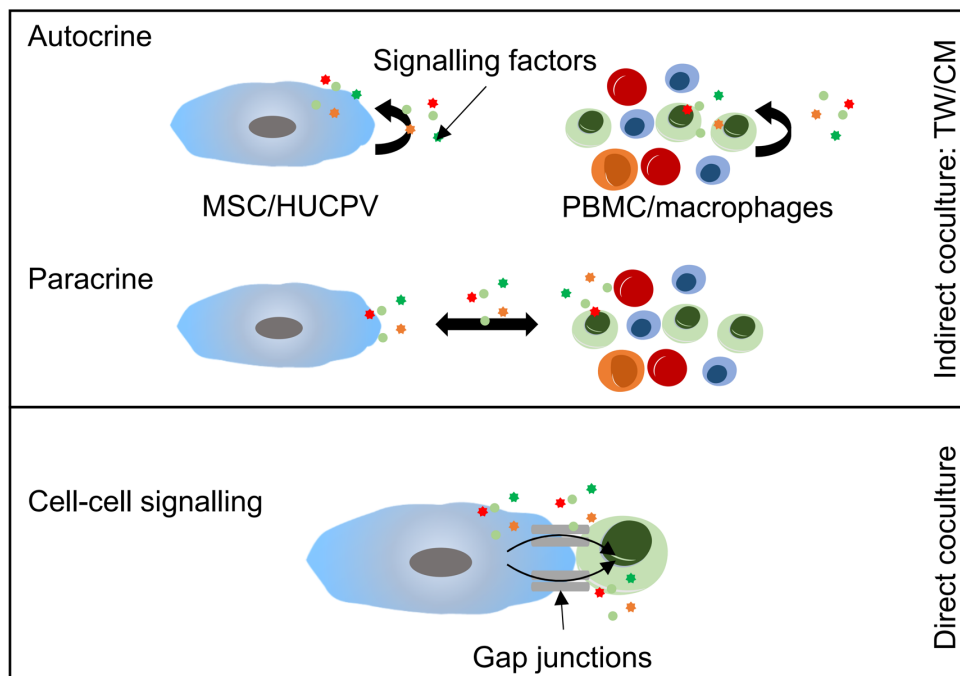


Fig. 9 Forms of chemical signalling and models for investigating the interactions of MSC (HUCPV)-immune cells (PBMC/macrophages).

To investigate the osteoimmunomodulation of Mg-based materials, researchers used three factors in current *in vitro* models: bone-forming cells (MSC), immune cells, and Mg biomaterials. As a source of MSC, human umbilical cord perivascular cells (HUCPV) were selected as osteoprogenitor cells for these three *in vitro* systems. HUCPV exhibit a high proliferation rate and differentiation potential into an osteogenic phenotype, as well as low immunogenicity. For analysis of the initial stage of immune reactions, PBMC were applied as infiltrated immune cells in indirect coculture systems (conditioned media system and transwell coculture). PBMC, comprising monocytes (10%~20%), various lymphocytes (T cells, B cells, and NK cells; 70%~90%), and dendritic cells (only 1%~2%), were isolated from human leukocyte-enriched blood samples. Subsequently, as one of the first key players during immune reactions,

macrophages were obtained or differentiated from CD14-positive monocytes isolated from PBMC.

Pure Mg was chosen to avoid the complexity due to alloying elements. Gd, as a possible alloy element, can ameliorate material properties such as decreasing the degradation rate and improving mechanical properties [191]. Gd salts also show other interesting properties, such as modulation of inflammation [192, 193]. Furthermore, Mg-10Gd maintains its cytocompatibility and can even enhance osteoblast mineralization [194]. Therefore, pure Mg and Mg-10Gd were chosen to investigate the interactions between cells and biomaterials (third model). The advantages and disadvantages of each *in vitro* system are summarized in Table 4 based on the previous results [195-197]:

Table 4 Summary of different coculture systems.

<b>Names</b>	<b>Advantages</b>	<b>Disadvantages</b>
<b>Conditioned media (CM)</b>	<ul style="list-style-type: none"> <li>● Easy to handle, low cost and could be frozen for replicate experiments</li> <li>● Conditioned media system could be applied for more expanded range, <i>i.e.</i>, cells from different species</li> <li>● Migration/wound healing assay</li> </ul>	<ul style="list-style-type: none"> <li>● The variation of the medium composition, such as serum components and glucose</li> </ul>
<b>Transwell coculture (TW)</b>	<ul style="list-style-type: none"> <li>● The initial stage of biomaterial/immune response-mediated osteogenesis could be mimicked, allowing communications with no cell-cell contact</li> <li>● Changes in gene and protein expression could be investigated in a cell type-specific manner</li> <li>● Migration/wound healing assay</li> </ul>	<ul style="list-style-type: none"> <li>● Variation due from difficult operation</li> <li>● High cost</li> </ul>
<b>Direct coculture</b>	<ul style="list-style-type: none"> <li>● Represents the <i>in vivo</i> cell-cell contact</li> <li>● Several signalling pathways could only be regulated in cell-cell contact</li> </ul>	<ul style="list-style-type: none"> <li>● Limited discrimination of the influence from particular cell types</li> </ul>

### 3. Motivation and objectives

Osteoimmunomodulation is a vital and necessary process in fracture healing. Elucidation of this process can lead to better clinical therapy for chronic disease in relation to bone dynamic balance, in which immune cells are influenced by implants. For an expanded understanding of the roles of the material-modulated immune response in osteogenesis, two indirect *in vitro* systems (transwell coculture and conditioned media) and one direct coculture system were applied using PBMC/macrophages and bone-forming HUCPV.

In the early stage (indirect coculture; within 7 days) of inflammation, PBMC were typically seeded on the top of the chamber and HUCPV in the lower compartment, avoiding cell-cell contact but allowing monocytes to differentiate into macrophages, while HUCPV could differentiate into osteoblast-like cells (transwell coculture system). Thus, cell proliferation, microscopic characteristics, gene expression, etc. could be monitored for each cell. Regarding the conditioned media system, HUCPV-conditioned media was utilized to examine the direct M2 differentiation potential, and PBMC-conditioned media was employed to investigate the induction of HUCPV towards a pro-calcification phenotype. Moreover, in the later stage (direct coculture; 7-14 days) of inflammation, a mixture of macrophages and HUCPV were coseeded on pure Mg and Mg-10Gd. Cell growth and cell subpopulations were followed. ALP activity and genes expression, known as indicators of osteogenic differentiation, were studied. Furthermore, the underlying specific signalling factors (IL6/OSM signals, BMP signals, etc.) and subsequent cascades creating a pro-osteogenic circumstance for bone regeneration were explored. The hypothesis of the present study is schematized in Fig. 10.

In the early stage (indirect coculture; within 7 days) of inflammation:

- Mg (+/-HUCPV) could induce anti-inflammatory properties, such as lower pro- or higher anti-inflammatory levels of released cytokines, as well as a favourable M2 profile;
- Mg (+/-PBMC) could enhance the motility of HUCPV;
- Mg (+/-PBMC) could stimulate the osteogenic potential of HUCPV.

In the later stage (direct coculture; 7-14 days) of inflammation:

- Mechanisms of materials (+/-macrophages) induced osteogenic differentiation: OSM/IL6; BMP6; TNF $\alpha$ /IL1 $\beta$ .

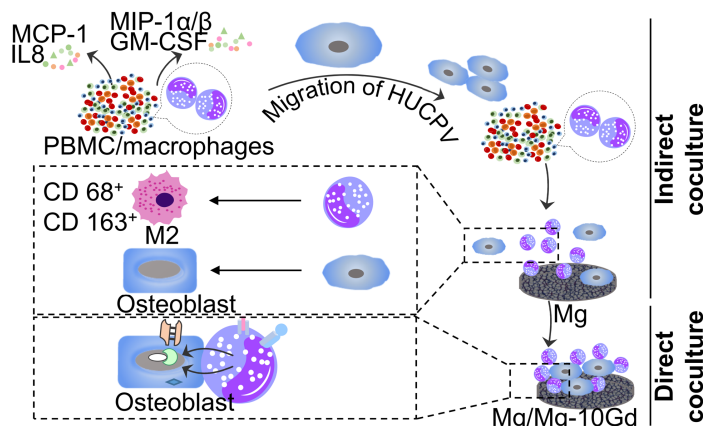


Fig. 10 Hypothesis in the present study (indirect and direct coculture system).

## 4. Materials and methods

### 4.1. Material preparation and characterization

High-purity Mg (99.93 %) and Mg-based alloys Mg-10Gd (9.44 % Gd, 90.51 % Mg) were supplied by Helmholtz-Zentrum Geesthacht, Germany. High-purity Mg (99.93 %) was prepared by permanent mould gravity casting. The produced ingots were processed by a heat T4 treatment, extruded into rods of 10 mm in diameter, and finally Mg discs were cut (1.5 mm thickness). Each disc weight about 0.2 g. Mg-10Gd was manufactured in constant mould gravity casting, a T4 treatment was performed on the produced ingots, extruded into rods, and finally cut as discs with 10 mm in diameter and 1.5 mm in thickness. The composition of Mg and Mg-10Gd were measured by X-ray fluorescence spectrometry according to weight percentage (Bruker AXS S4 Explorer, Bruker AXS GmbH, Germany), as shown in Table 5.

Table 5 Compositions of Mg and Mg-10Gd.

<b>Biomaterials</b>	<b>Composition wt.%</b>						
	Mg %	Gd %	Fe %	Cu %	Ni %	Al %	Be %
<b>Mg</b>	99.93	-	0.0011	0.00024	<0.0002	0.018	0.000046
<b>Mg-10Gd</b>	90.51	9.44	0.041	0.0020	<0.0038	-	0.000204

### 4.2. Sample sterilization, incubation, and characterization

All samples were treated *via* sonication for 20 min in 100 % n-hexane, 100 % acetone, 100 % ethanol, as well as sterilization in 70 % ethanol (Merck, Darmstadt, Germany). Afterwards, the dry discs were pre-incubated for 24 hours in specific culture medium before seeding cells.

To evaluate the corrosion behaviour of Mg and Mg-10Gd discs, the corrosion rates (CR; mm/y) were determined by the mass loss method and calculated using the following equation [198]:

$$CR = \frac{\Delta m \cdot k}{A \cdot t \cdot \rho}$$

The collected samples were washed in double distilled water. Samples were drying for 24 hours at 37 °C. Then weight the samples with corrosion layer ( $m_0$ ). The corrosion products were subsequently removed by chronic acid. Then dried the samples and weight them again ( $m_t$ ). The  $\Delta m$  (g;  $m_0 - m_t$ ) represents the mass loss; k is constant ( $8.79 \times 10^4$ ); A represents the surface area ( $\text{cm}^2$ ); t means the culture time and  $\rho$  stands for the density of discs ( $\text{g}/\text{cm}^3$ ).

Osmolality and pH of all the samples were measured with a cryoscopic osmometer (Gonotec 030-D cryoscopic osmometer; Gonotec, Berlin, Germany) and a pH Meter (ArgusX Sentron pH meter; Sentron Europe BV, Roden, the Netherlands), respectively. Mg concentration (mM) in each cell culture supernatant was measured by atomic absorption spectroscopy (AAS) analysis (Agilent 240/280 Series AA; Agilent Technologies, Waldbronn, Germany).

### 4.3. Cell isolation and culture

HUCPV were isolated from perivascular site (Wharton's jelly) of umbilical cords. The isolation process was approved by Ethik-Kommission der Ärztekammer Hamburg (PV4058). The isolation can be divided in the following steps:

- 1) Wash the umbilical cord with cold PBS to remove the blood.
- 2) Dissect the umbilical cord to obtain the arteries.
- 3) Ligate both ends of the arteries with sterilized surgical thread.
- 4) Culture the ligated arteries in T175 flask (Fisher Scientific, Roskilde, Germany) with α minimum essential medium (α-MEM; Fisher Scientific GmbH, Schwerte, Germany) supplemented with 15 % (v/v) foetal bovine serum for human mesenchymal stem cell (SC-FBS; Biological Industries, Beit-Haemek, Israel) and 1 % (v/v) Penicillin/Streptomycin (P/S; Life Sciences, Karlsruhe, Germany) under physiological condition (5 % CO<sub>2</sub>, 20 % O<sub>2</sub>, 95 % relative humidity, 37 °C).
- 5) Cells proliferation were seen until no more than 70 % confluence to avoid the possible differentiation. Isolated HUCPV were expanded until they reached 5-8<sup>th</sup> passage.

Human leukocytes-enriched blood samples were provided by University Hospital Hamburg-Eppendorf (UKE; Hamburg, Germany). Then PBMC were isolated (Fig. 11) as follows:

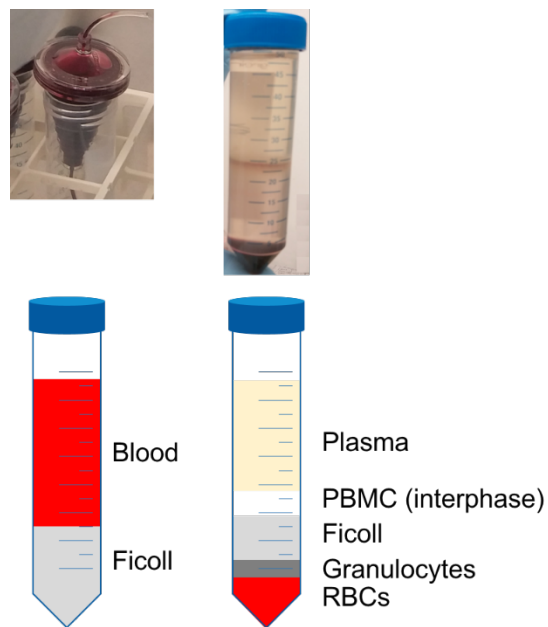


Fig. 11 PBMC isolation. PBMC: peripheral blood mononuclear cells; RBCs: red blood cells.

- 1) Transfer 10 mL leukocyte-enrichment blood into a sterilized 50 mL tube.
- 2) Fill up the tube with 40 mL ice-cold phosphate-buffered saline (PBS; Thermo-Fisher Scientific GmbH, Langenselbold, Germany) and mix thoroughly.
- 3) Overlay carefully 25 mL PBS-diluted blood with 25 mL Ficoll Paque 400 (GE Healthcare, Chicago, Illinois, USA), avoiding the mixture of two layers.
- 4) Centrifuge at 350 g for 30 min without brake at room temperature.

- 5) A visible white layer was accumulated at the interface between the PBS and Ficoll Paque 400. Then, collect the white ring (mononuclear hematopoietic precursors).
- 6) Wash them with ice-cold PBS twice and the centrifuge at 300 g for 10 min (with brake).
- 7) Seed  $5 \times 10^5$  cells/well fresh-isolated PBMC immediately into inserts in indirect coculture, or use for the subsequent isolation CD 14 positive monocytes.

The pooled human serum was used in the indirect coculture system instead of FBS to avoid variation of serum components, glucose and other possible activating factors in the cell culture medium. During the isolation of PBMC, the human serum was collected after step 4) via a centrifugation of 300 g for 10 min. The collected serum was filtered through a 0.45 µm sterile filter (Thermo-Fisher Scientific™, Langenselbold, Germany), pooled, and frozen at -20 °C for further use. Afterwards, α-MEM medium supplemented with 10 % human serum (v/v) and 1% P/S was used as culture medium in further indirect coculture system (transwell coculture and conditioned media system).

To acquire macrophages for the direct coculture system, high purity monocytes were isolated and then differentiated into macrophages. CD 14 is a specific monocytes/macrophages antigen on the surface of myeloid lineage [199]. This positive selection of CD 14 positive monocytes will not activate the cells. The anti-human CD 14 M-pluriBead® (pluriSelect, Leipzig, Germany) and M-pluriBead® Maxi Reagent Kit (pluriSelect, Leipzig, Germany) was used to get high purity monocytes in three steps - samples preparation, incubation, washing and detachment as follows (Fig. 12):

- 1) Prepare a single cell suspension with the fresh isolated PBMC in 500 µL dilution buffer and 500 µL washing buffer.
- 2) Pre-filter the PBMC with S-pluriStrainer to remove aggregates.
- 3) Add the samples and pluriBead suspension into a sterilized 15 mL tube and incubate them up to 30 min using a tube roller (Sunlab, Hamburg, Germany) at 10-15 rpm and 7.5° angel.
- 4) Pour samples onto the pluristrainer, and wash the unbounded cells into a sterilized 50 mL tube with at least 25 mL washing buffer. Meanwhile, the bead-bounded cells still remain on the strainer. At each wash step, the wash buffer was used in a circular way at 2 steps of 1 mL wash buffer.
- 5) Incubate the bead-bounded cells with detachment buffer for 10 min at room temperature. The bounded cells were detached from the pluriBeads.
- 6) The (CD 14 positive) target cells were released with serum-free RPMI 1640 medium (Sigma-Aldrich, Munich, Germany) and flowed into fresh tubes.

The isolated monocytes were characterized for their expression of FITC-conjugated CD 14 (555397; BD Pharmingen™, Heidelberg, Germany) and analysed with a Bio-Rad S3e™ Cell Sorter (Bio-Rad Laboratories, Munich, Germany). The CD 14 positive of isolated monocytes was always above 95 %.

To activate the differentiation of macrophages, the isolated monocytes were expanded as  $3 \times 10^6$  cells in 2 mL differentiation medium per well, in a 12-well plate, for 7 days under physiological

conditions. The differentiation medium was composed of RPMI 1640 medium, 2 mM L-glutamine (Sigma-Aldrich, Munich, Germany), 10 mM HEPES (Lonza, Köln, Germany), 10 µg/mL gentamycin (Sigma-Aldrich, Munich, Germany), 10 % (v/v) heat-inactivated FBS (Biochrom, Berlin, Germany) and 12.5 ng/mL macrophage colony-stimulating factor (M-CSF; Sigma-Aldrich, Munich, Germany).

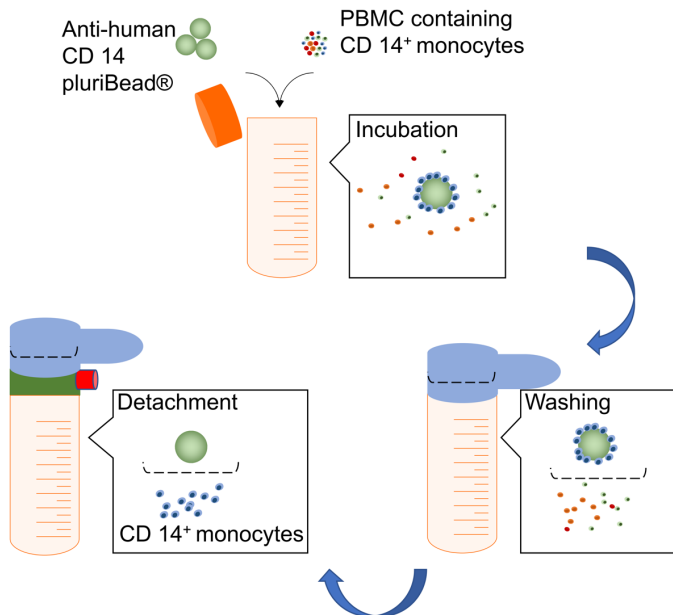


Fig. 12 The isolation of CD 14<sup>+</sup> monocytes from PBMC.

#### 4.4. Indirect *in vitro* coculture systems: transwell coculture and conditioned media system

To study the influence of degradable Mg on the interaction between bone-forming cells and immune cells, an *in vitro* transwell coculture (Alvetex™ Strata, Glasgow, United Kingdom) and conditioned media system were applied.

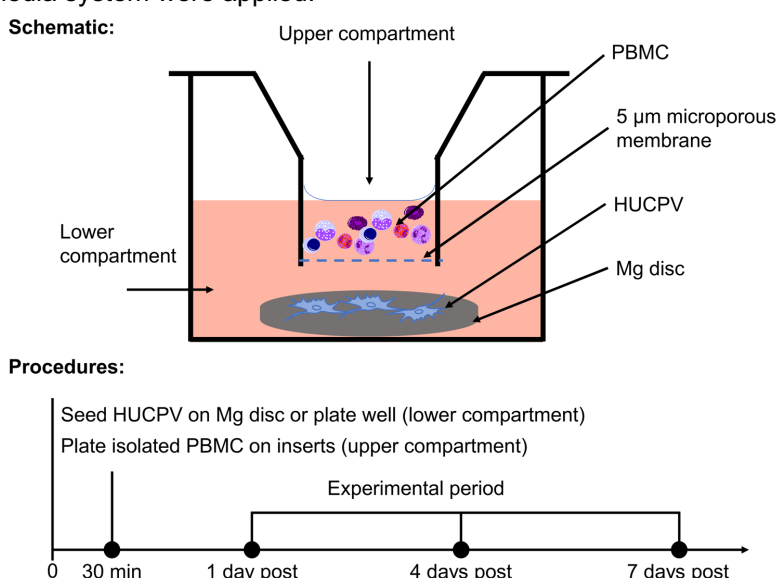
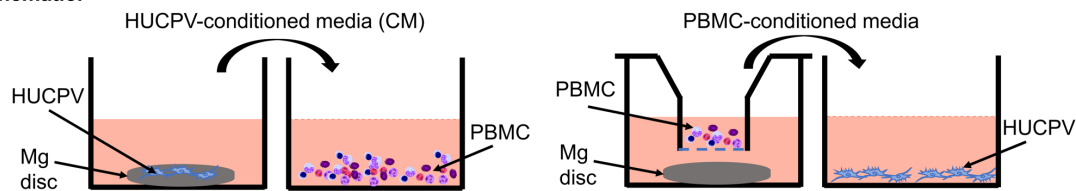


Fig. 13 Indirect *in vitro* coculture systems: transwell coculture of HUCPV and PBMC.

For transwell (Fig. 13), the wells in lower compartment were coated with 1 % (v/v) agarose (Sigma-Aldrich, Darmstadt, Germany) to avoid HUCPV adherence on the plate surface rather than Mg surface. HUCPV and PBMC, as a 1:2.5 ratio, were seeded on Mg surface in lower compartment and on inserts (5  $\mu$ m pore size) in upper compartment of 12-wells plate, respectively (Fig. 13). As shown in Table 6, the groups of HUCPV, PBMC or their transwell coculture on Mg disc were nominated as H+Mg, P+Mg, or H+P+Mg. The medium was changed every 3 days. Samples were collected at day 1, 4 and 7 and stored at -80 °C until further analysis. Cell growth, gene expression, ALP activity and cytokine levels were investigated.

**Schematic:**



**Procedures:**

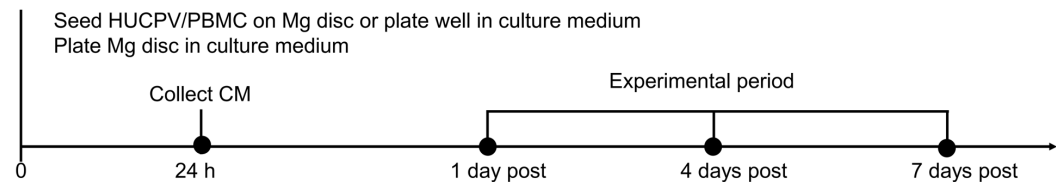


Fig. 14 Indirect *in vitro* coculture systems: HUCPV/PBMC-conditioned media.

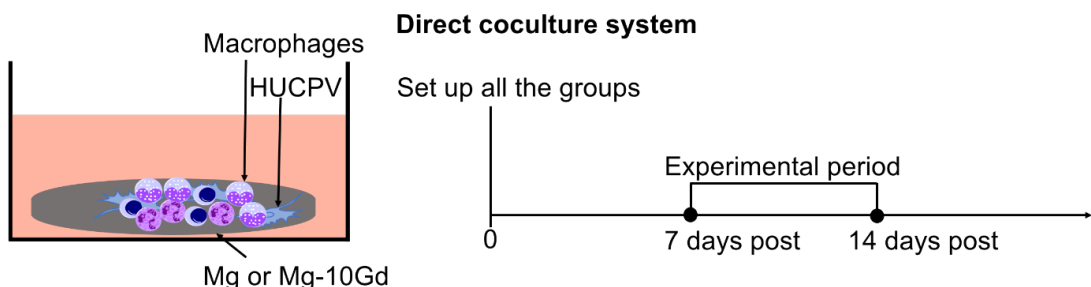
For the conditioned media system (Fig. 14), to generate conditioned media, HUCPV or PBMC alone were cultured as  $2 \times 10^5$  or  $5 \times 10^5$  cells, respectively, per Mg disc or inserts. After 30 min adherence, HUCPV-seeded Mg discs or PBMC-seeded inserts were transferred into 12-wells plate with 2 mL culture medium for 24 hours. These conditioned media were termed as H+Mg CM or P+Mg CM (Table 6). After 24 hours, conditioned media (H+Mg CM and P+Mg CM) were harvested and centrifuged at 10000 g for 2 min. All the conditioned media were diluted with culture medium (1:1) and frozen at -80 °C until use. Cell growth and specific gene profiles, as well as ALP levels were also analysed.

For both transwell coculture and conditioned media system, cell culture medium was set as blank control (termed as Blank). Mg disc incubated with cell culture medium but without any cell was used as no-cell controls (Mg or Mg CM). In transwell coculture without Mg discs, monoculture of HUCPV or PBMC and cocultured HUCPV and PBMC was applied as cell control (H, P or H+P). Without Mg disc, HUCPV or PBMC in conditioned media system were regarded as controls termed as H/P CM.

Table 6 Experimental conditions of the indirect *in vitro* coculture systems.

Name	No.	Abbreviation	Experimental conditions
<b>Transwell coculture system</b>	1	Blank	Cell culture medium
	2	Mg	Only Mg disc
	3	H	HUCPV alone
	4	H+Mg	HUCPV on Mg disc
	5	P	PBMC alone
	6	P+Mg	PBMC (upper compartment) with Mg disc (lower compartment)
	7	H+P	Coculture of HUCPV and PBMC
	8	H+P+Mg	Coculture of HUCPV on Mg disc (lower compartment) with PBMC (upper compartment)
<b>Conditioned media system</b>	1	Blank	Cell culture medium
	2	Mg CM	Only Mg disc
	3	H/P CM	HUCPV/PBMC alone
	4	H/P+Mg CM	HUCPV/PBMC with Mg disc

#### 4.5. Direct *in vitro* coculture system

Fig. 15 Direct *in vitro* coculture systems.

As shown in Fig. 15 and Table 7, HUCPV alone, differentiated macrophages alone, and a mixture of HUCPV and macrophages were respectively seeded on the preincubated Mg and Mg-10Gd in 24-well plates. HUCPV alone (H+Mg/Mg-10Gd) and differentiated macrophages alone (M+Mg/Mg-10Gd) were seeded on discs as a cell number of  $2.5 \times 10^4$  and  $2.5 \times 10^5$  per well, respectively. In coculture, the  $2.5 \times 10^4$  of HUCPV and  $2.5 \times 10^5$  of macrophages were seeded together in each well of 24-well plates (H+M+Mg/Mg-10Gd). Cells culture medium without discs and cells were regarded as the blank control (Blank in Table 7). The groups only included material discs were termed as material controls (Mg/Mg-10Gd). HUCPV, macrophage, or their mixture directly cultured on wells (without discs), were used as cell controls (H, M or H+M). Differentiated macrophages were detached using buffer containing ice-cold PBS, 2 mM EDTA (Sigma-Aldrich, Munich, Germany) and 2 % FBS. The culture medium for direct coculture system was  $\alpha$ -MEM supplemented with 15 % FBS and 1 % P/S. Medium was changed every 3 days.

After 4, 7 and 14 days, the supernatant in each treatment were collected, centrifuged and frozen at -80 °C for ALP tests and cytokines analysis. Cells viability and proliferation as well as gene expression were investigated.

Table 7 Direct *in vitro* coculture system.

Name	No.	Abbreviation	Experimental conditions
<b>Direct coculture</b>	1	Blank	Cell culture medium
	2	H	HUCPV on blank wells
	3	H+Mg/Mg-10Gd	HUCPV seeded on materials surface
	4	M	Macrophages on blank wells
	5	M+Mg/Mg-10Gd	Macrophages seeded on materials surface
	6	H+M	Coculturing of HUCPV and macrophages on blank wells
	7	H+M+Mg/Mg-10Gd	Coculturing of HUCPV and macrophages on materials surface

#### 4.6. Live/Dead staining and DNA contents

Cellular membrane of alive cell is intact but incomplete in dead cells. The ubiquitous intracellular esterase activity is also another feature of alive cells. When staining at the same time, green fluorescent Calcein AM indicates intracellular esterase activity, and red fluorescent Ethidiumhomodimer-1 indicates loss of plasma membrane (Ethidiumhomodimer-1 could dye deoxyribonucleic acid only in cells with incomplete membrane). Therefore, the two highly fluorescent dyes of Live/Dead staining (LIVE/DEAD Viability/Cytotoxicity Kit for mammalian cells, Thermo–Fisher Scientific GmbH, Langenselbold, Germany) could differentially label alive (green) and dead cells (red).

The staining steps are:

- 1) Wash cells with Mg discs gently with serum-free α-MEM medium.
- 2) Prepare the staining solution and avoid direct light in case of Calcein AM hydrolysis. The staining solution included 5 mL cell specific media without FBS, 1.6 mM Calcein AM, and 2.0 mM Ethidiumhomodimer-1.
- 3) Incubate cells with staining solution for 20 min in dark at room temperature.
- 4) Finally, replace the staining solution with serum-free α-MEM medium.
- 5) Visualize the cells viability and morphology using an inverted microscope (Eclipse Ti, Nikon GmbH, Düsseldorf, Germany) immediately.

To investigate proliferative cells on disc surface, the deoxyribonucleic acid (DNA) content was measured. In addition, DNA contents were used to normalize the variation induced by cell proliferation in other experiments. Chemicals and solutions involved in DNA measurement were prepared as shown in Table 8.

The DNA isolation and quantification can be performed by following the steps below:

- 1) Digest the cells with 200 µL lysis buffer per well and incubated for 5 min at 37 °C.
- 2) Collect the lysate and incubate for 1 hour at 98 °C and 1000 rpm using a thermomixer (Eppendorf thermomixer comfort, Hamburg, Germany).
- 3) Reduce the lysate to 15 °C at 700 rpm using the thermomixer. In these steps, buffer without cells was also prepared as blank control for measurement.
- 4) Add the same volume of neutralization buffer and centrifuge at 13000 rpm for 1 min.
- 5) Dilute lysate samples as 1:5 (v/v) in DNA dilution buffer.
- 6) Transfer 100 µL diluted sample to wells in a flat bottom 96-well-plate.
- 7) Pipette 50 µL of DNA working solution and 50 µL of bisbenzimidole (1:500 in working solution) into wells and incubate for 15 min in the dark.
- 8) To obtain the standard curve, dilute gDNA into concentrations of 3, 1.5, 0.75, 0.375, 0.188, 0.094, and 0.047 µg/mL, separately.
- 9) Ultimately, measure fluorescence (excitation: 355 nm, emission: 460 nm) with a VICTOR3 multilabel microtiter plate reader (Perkin Elmer, Massachusetts, USA).
- 10) Calculate the DNA content by plotting DNA content versus relative fluorescence in the standard curve. The linear equation is  $y = ax + b$  ( $y$ : relative fluorescence unit (RFU);  $a$ : the slope;  $x$ : DNA concentration;  $b$ : the intercept).

Table 8 Chemicals of DNA assay.

<b>Buffer name</b>	<b>Compositions</b>	<b>Supplier</b>
<b>Lysis buffer</b>	25.0 mM NaOH, 0.2 mM EDTA, pH 6.0	
<b>Neutralization buffer</b>	40.0 mM Tris/HCl, Adjust pH to 5.5 with HCl	
<b>DNA dilution buffer</b>	2.5 M NaCl in 19.0 mM sodium citrate, pH 7.0	Sigma-Aldrich Chemie GmbH (Munich, Germany)
<b>DNA working buffer</b>	2.0 M NaCl in 15.0 mM sodium citrate, pH 7.0	
<b>DNA standard</b>	Calf thymus DNA	
<b>Bisbenzimidole working solution</b>	2.0 µg/mL bisbenzimidole in DNA working buffer	

#### 4.7. ALP activity

The QuantiChrom™ alkaline phosphatase assay (BioAssay Systems, Hayward, CA, USA) utilizes p-nitrophenyl phosphate (pNPP) that can be hydrolysed by ALP into a yellow coloured product- p-Nitrophenol. Therefore, the ALP activity can be quantified:

- 1) Pipette the sample supernatant (50 µL) into each well of a clear bottom 96-well-plate.
- 2) Prepare the total working solution for a whole 96-well assay by mixing 200 µL supplied Assay Buffer, 5 µL Mg acetate (5 mM) and 2 µL pNPP liquid substrate (10 mM).
- 3) Pipette quickly the working solution (150 µL) into sample wells.

- 4) Use the same amount (200 µL) of distilled water and calibrator solution as controls.
- 5) Read the optical density (OD) with 405 nm wavelength at the beginning (t0) and after 4 min incubation (t4) using a microplate reader (Sunrise™ Tecan, Männedorf, Switzerland).
- 6) Calculate ALP activity (IU/L=µmol/(L\*min)) with following equation and normalize with the DNA content of HUCPV under according conditions:

$$\frac{(OD_{sample\ t4} - OD_{sample\ t0}) * Reaction\ volume * 35.3}{(OD_{calibrator} - OD_{water}) * Sample\ volume}$$

## 4.8. Real time semi-quantitative polymerase chain reaction (RT-qPCR)

### 4.8.1. RNA purification

The total cellular RNA was extracted by RNeasy Mini Kit (Qiagen, Hilden, Germany).

- 1) Lysis the samples with RNeasy lysis buffer (buffer RLT) and harvest with QIA shredder. In which, buffer RLT contains a high level of guanidine isothiocyanate, which supports the binding of RNA to the silica membrane.
- 2) Mix the lysate with 70 % (v/v) ethanol and place into a spin column so that the RNA can bind to the membrane of column.
- 3) Wash them twice with buffer RW1 (contains a guanidine salt and ethanol, and is used for washing of membrane-bound RNA) and RPE (remove traces of salts, which are still on the column due to buffers RW1 used earlier in the procedure).
- 4) After centrifugation, obtain the total RNA samples in 30 µL RNase-free water.
- 5) Pipette a 1 µL sample onto a measurement pedestal of Nanodrop 2000c (Thermo-Fisher Scientific GmbH, Langenselbold, Germany). The RNA content was measured by the absorbance at 260 nm. Also, the purity of RNA samples was ensured by the ratio of the absorbance at 260 to that at 280 nm (A260/280; the ratio for pure RNA is around 2.0).

### 4.8.2. Reverse transcription

Complementary DNA (cDNA) was produced by reaction mixture using Omniscript or Sensiscript Reverse Transcriptase Kit depending on the amount of total template RNA (Qiagen, Hilden, Germany).

- 1) Prepare the master mix. For each reaction, total volume of 8 µL master mix contained 2 µL 10x buffer, 2 µL dNTP Mix (a solution containing sodium salts of dATP, dCTP, dGTP and dTTP), 2 µL Oligo-dT primer, 1 µL RNase inhibitor, and 1 µL Omniscript/Sensiscript Reverse Transcriptase. Oligo-dT primer is a better choice for cDNA synthesis, because of their specificity for mRNA, and also because it allows to study different targets from the same cDNA pool.
- 2) Add template RNA and RNase-free water (total volume: 12 µL) into individual 8 µL master mix. The final volume for each tube is 20 µL.

- 3) Incubate the reaction mixture at 37 °C for 1 hour.

#### 4.8.3. RT-qPCR

Primers (Table 9) were designed *via* Primer 3 (version 4.0.0) or found in the RTPrimerDB databased. The primers were purchased from Eurofins MWG Operon (Ebersberg, Germany). The cDNA was quantified with specific primers, RT-qPCR, and SsoFast™ EvaGreen® Supermix (Bio-Rad Laboratories GmbH, Munich, Germany) using CFX96 Touch™ real-time PCR (software: version 3.1; Bio-Rad Laboratories GmbH, Munich, Germany). Beta 2 microglobulin (*B2M*), glyceraldehyde3-phosphate dehydrogenase (*GAPDH*) and ribosomal protein L10 (*RPL10*) were selected as reference (endogenous) genes. No template control (NTC, no cDNA) was performed to exclude reaction contamination and primer dimerization. The relative fold of gene expression was calculated by 2 (-Delta CT) method ( $\Delta\Delta Ct$ ).

- 1) Dilute the cDNA product with RNase-free water as 1:40.
- 2) Dilute the targeted primers into 20 µM with double distilled water (ddH<sub>2</sub>O).
- 3) For each sample, mix the 1 µL diluted cDNA with 16.5 µL SsoFast™ EvaGreen® Supermix, 1.65 µL Forward/Reverse Primer, and 12.8 µL ddH<sub>2</sub>O.
- 4) Pipette 10 µL sample into triplicate in 96-well plate and cover it with seal film (MSB 101; Bio-Rad Laboratories, Munich, Germany).
- 5) In a CFX96 Touch™ real-time PCR detection system, a thermal cycling was performed (Table 10).

Table 9 Primers sequences.

Full name	Abbreviation	Sequences
<b>Alkaline phosphatase</b>	ALP	Forward: 5'-CACCCACGTCGATTGCATCT-3' Reverse: 5'-TAGCCACGTTGGTGTGAGC-3'
<b>Collagen type I alpha 1</b>	COL1A1	Forward: 5'-AAGACATCCCACCAATCACC-3' Reverse: 5'-GCAGTTCTGGTCTCGTCAC-3'
<b>Osteocalcin</b>	OC	Forward: 5'-ATGAGAGCCCTCACACTCCT-3' Reverse: 5'-TGGACACAAAGGCTGCAC-3'
<b>Osteopontin</b>	OPN	Forward: 5'-CTCCATTGACTCGAACGACTC-3' Reverse: 5'-CAGGTCTGCGAAACTTCTTAGAT-3'
<b>B2 microglobulin</b>	B2M	Forward: 5'-TGCTGTCTCCATGTTGATGTATCT-3' Reverse: 5'-TCTCTGCTCCCCACCTCTAAGT-3'
<b>Glyceraldehyde3-phosphate dehydrogenase</b>	GAPDH	Forwards: 5'-GTCGGAGTCAACGGATTG-3' Reverse: 5'-TGGGTGGAATCATATTGGAA-3'
<b>Ribosomal protein L10</b>	RPL10	Forwards: 5'-AGTGGATGAGTTCCGCTT-3' Reverse: 5'-ATATGGAAGCCATTTGCC-3'
<b>Bone morphogenetic protein 6</b>	BMP6	Forward: 5'-AGCGACACCACAAAGAGTTCA-3' Reverse: 5'-GCTGATGCTCCTGTAAGACTTGA-3'

Table 9 (Continued)

Full name	Abbreviation	Sequences
<b>Bone morphogenetic protein receptor type 1a</b>	BMPR1A	Forward: 5'-ACTGCCCTGTTGTCATAG-3' Reverse: 5'-AATGAGCAAAACCAGCCATC-3'
<b>Bone morphogenetic protein receptor type 2</b>	BMPR2	Forward: 5'-CTGCCCTGTTACTGCCATTATT-3' Reverse: 5'-GGCAGCAGTATAACAGATAGGTG-3'
<b>Mothers against decapentaplegic homolog 1</b>	Smad1	Forward: 5'-GTATGAGCTTGTTAAGGGC-3' Reverse: 5'-TAAGAACTTATCCAGCCACTGG-3'
<b>Mothers against decapentaplegic homolog 4</b>	Smad4	Forward: 5'-CTCCAGCTATCAGTCTGTCAG-3' Reverse: 5'-CCCGGTGTAAGTGAATTCAAT-3'
<b>Mothers against decapentaplegic homolog 5</b>	Smad5	Forward: 5'-TCATCATGGCTTCATCCCACC-3' Reverse: 5'-GCTCCCCAACCTTGACAAA-3'

Table 10 Protocol of the thermal cycling.

Step	Duration	Temperature	Cycle
<b>Initial duration</b>	3 min	95 °C	1
<b>Denaturation</b>	20 sec	95 °C	40
<b>Primer-annealing</b>	20 sec	60 °C	40
<b>Elongation</b>	30 sec	75 °C	40
<b>Denaturation</b>	30 sec	95 °C	1
<b>Melting curve</b>	5 sec	65-95 °C	0.5 °C/step

## 4.9. Flow cytometry analysis

### 4.9.1. M2 macrophages polarisation in indirect coculture (transwell coculture and conditioned media) system

To study the effects of Mg and/or HUCPV on the monocytes/macrophages variation, the ratios of M2 in PBMC (cluster of differentiation (CD) 68<sup>+</sup>) were measured with flow cytometry. Intracellular antigen CD 68 [200] (FITC, 130-096-964; Miltenyi Biotec GmbH, Bergisch Gladbach, Germany), a transmembrane glycoprotein, heavily glycosylated in its extracellular domain, with a molecular weight of 110 kD, is a pan marker for monocyte lineage - macrophages, so it was used to identify the activated macrophages from PBMC. Meanwhile, antibody anti-human CD 163-PE (560933; BD Biosciences, Heidelberg, Germany), a scavenger receptor for haptoglobin–haemoglobin complexes, was selected as specific marker

for M2 population [201]. Thus the proportion of M2-macrophages in PBMC (M2/CD 68<sup>+</sup>) was represented by the percentage of double positive (CD 68 and CD 163) in all single positive (CD 68) events: (CD 68<sup>+</sup> CD 163<sup>+</sup>)/CD 68<sup>+</sup> cells (%).

Single staining of CD 68-FITC and CD 163-PE were used for the further results compensation [202]. Propidium iodide (PI) solution (ReadiDrop™; Bio-Rad Laboratories, Munich, Germany) was used to exclude dead cells from each analysis. Isotype controls were corresponding mouse IgG2b (130099119; Miltenyi Biotec GmbH, Bergisch Gladbach, Germany) and IgG1 (559320; Thermo-Fisher Scientific GmbH, Langenselbold, Germany). Samples without antibodies staining were applied as blank controls.

The detailed procedures are as follows:

- 1) Wash the cell pellet two times with ice-cold PBS and centrifuge at 1000 rpm for 5 min.
- 2) Resuspend the cells as 1×10<sup>6</sup> cells per tube in 1 mL ice-cold PBS containing 1 % bovine serum albumin (BSA, albumin fraction≥98 % (v/v); Carl Roth, Karlsruhe, Germany).
- 3) Dilute Anti-human CD 163-PE as a ratio of 1:10 in ice-cold PBS.
- 4) Incubate cells with 20 µL CD 163 solution, on ice in the dark with gentle shaking, for 1 hour.
- 5) Wash cells twice with ice-cold PBS.
- 6) Fix them with 3.7 % (v/v) formaldehyde (Sigma-Aldrich, Darmstadt, Germany) and permeabilize with 0.7 % (v/v) Tween 20 (Sigma-Aldrich, Darmstadt, Germany).
- 7) Wash cells with ice-cold PBS twice.
- 8) Dilute Anti-human CD 68-FITC as 1:10 in PBS.
- 9) Stain the cells with intracellular anti-human CD 68-FITC at room temperature in the dark with gentle shaking for 30 min.
- 10) Finally, wash samples again and resuspend them in PBS with 1 % BSA.
- 11) With help of flow cytometer (S3e; Bio-Rad Laboratories, Munich, Germany), investigate the immunophenotyping of CD 68 and/or CD 163. The corresponding fluorescence intensity of different conditions and their propidium iodide (PI) staining were detected *via* the collection of 5000 to 10000 events per assay.

#### **4.9.2. Subpopulations of HUCPV/macrophages in cocultures in direct coculture system**

To measure the subpopulation of HUCPV and macrophages in cocultures upon the stimulation of Mg biomaterials (Mg and Mg-10Gd), the collected cells were investigated with flow cytometry. HUCPV were stained with specific surface antigen-CD 90 [203] (A15761; Thermo-Fisher Scientific GmbH, Langenselbold, Germany). CD 90 (Thy-1) is a small membrane glycophasphatidylinositol (GPI) anchored protein.

Propidium iodide (PI) drop solution (Bio-Rad Laboratories, Munich, Germany) was used to exclude dead cells from each analysis. Isotype controls were corresponding mouse IgG1

(559320; Thermo-Fisher Scientific GmbH, Langenselbold, Germany). Samples without antibodies staining were applied as blank controls.

The procedure is as follows:

- 1) Wash the collected cell pellet two times with ice-cold PBS and centrifuge at 1000 rpm for 5 min.
- 2) Resuspend the cells as  $1 \times 10^6$  cells per tube in 1 mL ice-cold PBS containing 1 % bovine serum albumin.
- 3) Dilute Anti-human CD 90-FITC as a ratio of 1:10 in ice-cold PBS.
- 4) Incubate cells with 20  $\mu$ L CD 90 solution, on ice in the dark with gentle shaking, for 1 hour.
- 5) Wash samples and resuspend them in PBS with 1 % BSA.
- 6) With help of flow cytometer, investigate the immunophenotyping of CD 90. The corresponding fluorescence intensity of different conditions and their propidium iodide (PI) staining were detected via the collection of 5000 to 10000 events per assay.

#### **4.10. Multiplex immunoassay**

Normal enzyme-linked immunosorbent (ELISA) assays could detect only individual molecules in each well or each plate. The vital pros of ELISA are easy to use, high flexibility and low cost. Different from this, multiplex immunoassay is a beads-based multiplex immunoassay. Firstly, each identifiable bead with a distinct colour bead or spectral address, that allows for the simultaneous detection of multiple molecules in a single well (only with 12.5  $\mu$ L serum or 50  $\mu$ L cell culture supernatant) or plate. Besides, in this technology, one antibody to a specific analyte is attached to a set of beads of the same colour, while another antibody to the analyte is attached to a fluorescent reporter dye. The detector comprising two lasers that excite the beads and fluorescent reporter. The fluorescence data could be detect efficiently by identifying the specific target and measuring the number of specific molecules connect the coupled beads. The instructive scheme of multiplex immunoassay is introduced in the Fig. 16.

To investigate the secretory production from HUCPV and/or PBMC under the stimulation of Mg in transwell coculture system, a panel of selected human inflammatory factors (Bio-Plex Pro™ Human Cytokine 27-plex Assay; Bio-Rad Laboratories, Munich, Germany) was applied in our experiments. The principle of this beads-based assay is similar to those of sandwich enzyme-linked immunosorbent (ELISA) assays but allows simultaneous detection of multiple analytes in a single well or reaction. The beads, with a distinct colour or spectral address, are coupled covalently to capture (*i.e.*, specific) antibodies. These coupled beads directly react to the multiple targeted or desired molecules in samples. After several washing steps to remove the unbound protein, a biotinylated detection antibody is pipetted into each well to form a sandwich complex. The final detection complex is consisted of this sandwich complex and streptavidin-phycerythrin (PE; PE acts as a fluorescent indicator) conjugate. The cytokines measured in this assay are presented in Table 11.

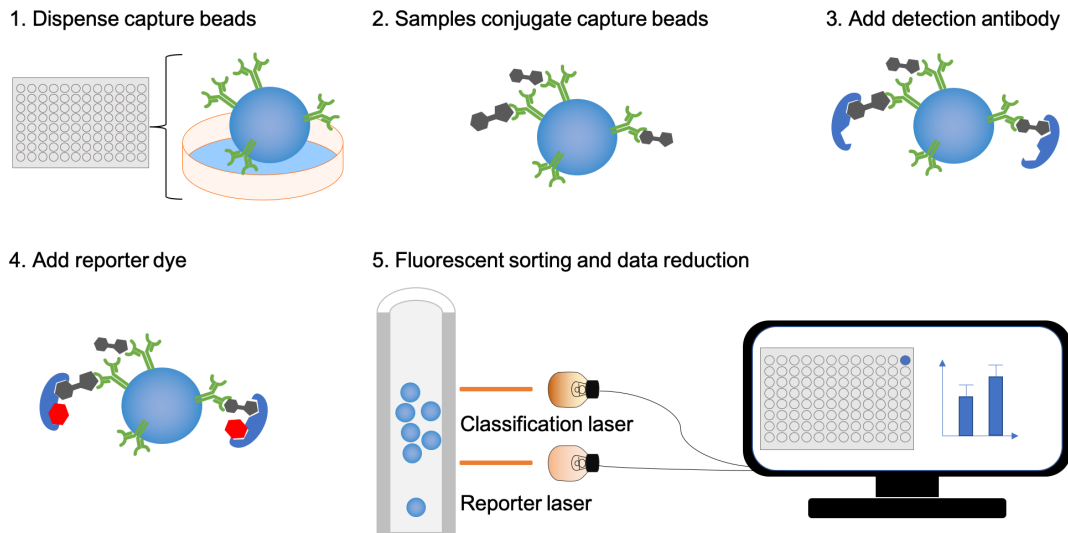


Fig. 16 The scheme of multiplex immunoassay.

The procedure is as follows:

- 1) Soak the 96-well plate by ddH<sub>2</sub>O, in which 50 µL beads was added into each well.
- 2) After 30 min incubation under room temperature, wash the plate twice with 100 µL supplied washing buffer using an automatic plate washer (Bio-Rad Laboratories, Munich, Germany).
- 3) Add 50 µL standards, blanks and samples into wells.
- 4) Incubate at room temperature with shaking at 850 rpm for 30 min (Eppendorf thermomixer comfort, Hamburg, Germany).
- 5) After washing three times, pipette 25 µL 1× detection antibody into each well.
- 6) Incubate with shaking at 850 rpm for 30 min at room temperature.
- 7) Wash the bounded samples three times.
- 8) Pipette 50 µL 1× streptavidin-phycoerythrin (PE) into each well.
- 9) Incubated with shaking at 850 rpm for 10 min at room temperature.
- 10) Wash the plate three times.
- 11) Finally, resuspend the mixture in each well with 125 µL assay buffer and shake at 850 rpm for 30 sec.
- 12) Read the fluorescence and analyse using Bio-Plex™ 200 system supplemented with Bio-Plex Manager™ (Bio-Rad Laboratories, Munich, Germany).

The plate was covered with a dark sealing tape during each shaking step. All the incubation procedures were performed in dark and direct light was avoided.

Table 11 Cytokines and functions investigated by multiplex immunoassay.

Function	Full name	Abbreviation
Pro-inflammatory	Interleukin 1 beta	IL1 $\beta$
	Interleukin 2	IL2
	Tumour necrosis factor alpha	TNF $\alpha$
	Interferon gamma	IFN $\gamma$
Anti-inflammatory	Interleukin 10	IL10
	Interleukin 4	IL4
	Interleukin 5	IL5
	Interleukin 13	IL13
Migration/Wound healing	Interleukin 1 receptor antagonist	IL1RA
	Granulocyte-colony stimulating factor	G-CSF
	Interleukin-8	IL8
	Granulocyte-macrophage colony-stimulating factor	GM-CSF
Angiogenesis	Monocyte chemoattractant protein 1	MCP-1
	Macrophage inflammatory proteins 1 alpha	MIP-1 $\alpha$
	Macrophage inflammatory proteins 1 beta	MIP-1 $\beta$
	Basic fibroblast growth factor	bFGF
Others	Vascular endothelial growth factor	VEGF
	Interleukin 6	IL6
	Interleukin 7	IL7
	Interleukin 9	IL9
	Interleukin 12	IL12
	Interleukin 15	IL15
	Interleukin 17	IL17
	Interferon gamma-induced protein 10	IP10
	Platelet-derived growth factor-BB	PDGF-BB
	Regulated upon activation, normal T cell expressed and presumably secreted	RANTES
	A chemoattractant cytokine (chemokine) selective for eosinophils	Eotaxin

#### 4.11. ELISA

To investigate specific cytokines, the protein production of TNF $\alpha$ , IL1 $\beta$ , OSM and IL6 were detected with ELISA (R&D Systems, Abingdon, UK) as following procedures (Fig. 17). Capture antibody was lyophilized with epitopes and response to the specific antigen of targets. Detection antibody, designed as biotinylated antibody, connected with the capture antibody and streptavidin-horseradish peroxidase (HRP). Streptavidin-HRP has a high affinity for biotin and is extensively used in molecular biology. Biotinylated secondary antibodies were used for amplifying targeted signals. As multiple biotin molecules can conjugate to one secondary antibody, the biotinylated secondary antibodies allow detection of proteins expressed at low levels. The materials used for this procedure are listed in Table 12.

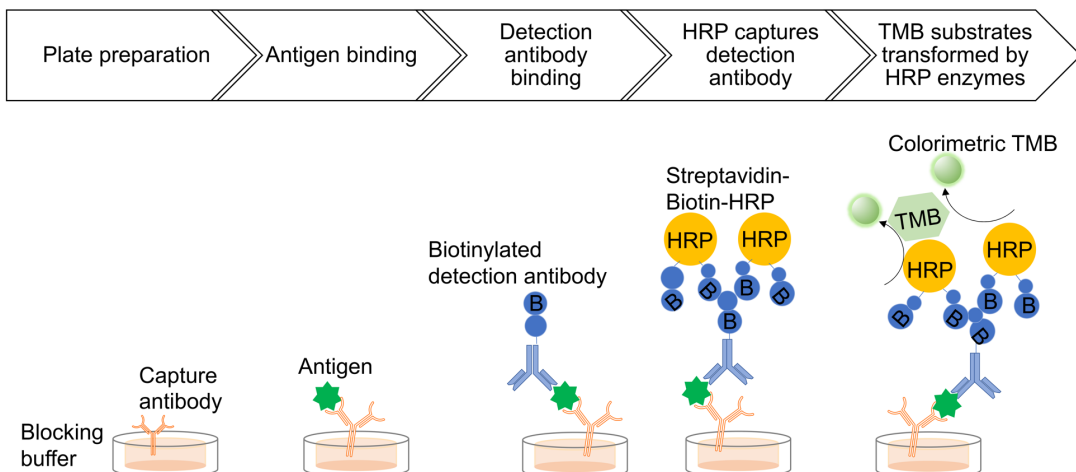


Fig. 17 Procedures of ELISA.

The procedure is as follows:

- 1) Dilute capture antibody in PBS to the working concentration.
- 2) Coat the 96-well plates with 50 µL capture antibody, cover with sealers, and incubate at room temperature overnight.
- 3) Rinse the plates twice with wash buffer using automatic plate washer.
- 4) Pipette 150 µL 1× reagent buffer into each well and incubate at room temperature for 1 hour to block the plates.
- 5) Rinse the plates twice with wash buffer using the auto washer.
- 6) Add 50 µL of standards, unknown samples and blank controls into according wells and incubate for 1 hour at room temperature.
- 7) Rinse the plates twice with wash buffer using the auto washer.
- 8) Add detection antibody (diluted with 1× reagent buffer) as 50 µL per well and incubate for 1 hour at room temperature.
- 9) Rinse the plates twice with wash buffer using the auto washer.
- 10) Dilute the Streptavidin-HRP with reagent buffer into working solution, add as 50 µL per wells and incubate in the dark for 20 min.
- 11) Rinse the plates twice with wash buffer using the auto washer.
- 12) Add 50 µL of substrate solution to each well and incubate in the dark for another 20 min.
- 13) Terminate the reaction with 25 µL of stop solution in each well.
- 14) Gently tap the plate to mix solution thoroughly.
- 15) Detect the optical density (OD) of each well immediately using a Sunrise™ microplate reader at 450 nm wavelength (540 nm as reference).

Table 12 Materials and kits for ELISA.

Content	Name	Supplier
<b>Human TNF<math>\alpha</math> DuoSet® ELISA</b>	TNF $\alpha$ kit	
<b>Human IL1<math>\beta</math> DuoSet® ELISA</b>	IL1 $\beta$ kit	
<b>Human OSM DuoSet® ELISA</b>	OSM kit	
<b>Human IL6 DuoSet® ELISA</b>	IL6 kit	
<b>Stabilised hydrogen peroxide (H<sub>2</sub>O<sub>2</sub>), stabilised with tetramethylbenzidine (TMB)</b>	Substrate solution	R&D Systems, Abingdon, UK
<b>Plate sealer</b>	Sealers	
<b>Comprehensive collection of reagents and plates</b>	Reagent buffer	
<b>2 N sulfuric acid (H<sub>2</sub>SO<sub>4</sub>)</b>	Stop solution	
<b>Gibco™ phosphate-buffered saline buffer</b>	PBS	
<b>Nalgene syringe filter, sterile, SFCA membrane, 0.2 <math>\mu</math>m</b>	0.2 $\mu$ m filter	Thermo - Fisher Scientific GmbH, Langenselbold, Germany
<b>0.05 % (v/v) Tween® 20 in PBS, pH 7.3 adjusted with 20 % (v/v) hydrochloric acid (HCl)</b>	Wash buffer	Germany
<b>ELISA plate, high binding, flat base</b>	ELISA plate	Sarstedt, Nümbrecht, Germany
<b>Polyethylene glycol sorbitan monolaurate</b>	Tween® 20	Sigma-Aldrich, Germany
<b>Bio-Plex Pro™ wash station</b>	Autowasher	Bio-Rad Laboratories, Munich, Germany
<b>Sunrise™ microplate reader</b>	Plate reader	Tecan, Männedorf, Switzerland

#### 4.12. Wound healing assay

To investigate the motility of HUCPV stimulated by Mg-discs or - conditioned media, a scratch assay was employed (Fig. 18). Normally, *in vitro* “wound” was created by a straight line scratch across the HUCPV monoculture. Measurements are usually limited for 24 hours to study the migration, as well as reduce the contribution of cell proliferation on gap filling [204].

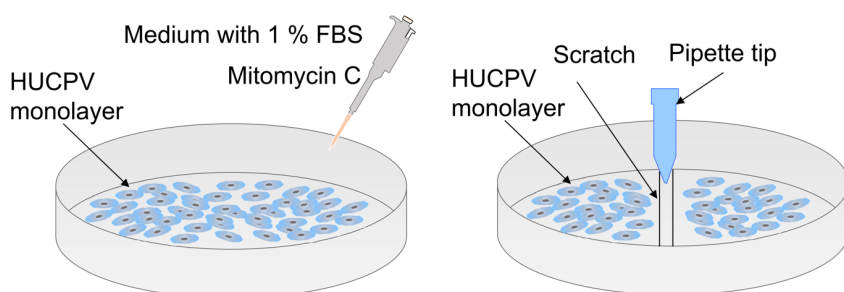


Fig. 18 The wound healing assay of HUCPV.

The procedure is as follows:

- 1) Seed HUCPV as  $1 \times 10^5$  cells per well of the 12-well plates in  $\alpha$ -MEM culture medium until the cell reach 80 % confluence.
- 2) Replace the medium with low serum (1 % FBS) to starve cells for overnight under physiological conditions in an incubator.
- 3) Treat the cell with 0.01 mg/mL mitomycin C for 2 hours [205] (Sigma-Aldrich, Munich, Germany) in each well.

The starvation and mitomycin C solution were used to synchronize cell cycle and avoid unnecessary cellular proliferation [204]. In addition, mitomycin C inhibits DNA synthesis [204], but it has no effect on RNA, protein synthesis, cytokine levels and gene profiles etc. [206].

- 4) Use a standard 1 mL pipette to produce the scratch (no cell area) in the middle of each well.
- 5) After scratching, take photographs immediately (T0) with an inverted microscope under bright light (Eclipse Ti, Nikon GmbH, Düsseldorf, Germany).
- 6) Afterwards, incubate the scratches with control medium ( $\alpha$ -MEM with 10 % plasma), corresponding Mg disc from transwell coculture or conditioned media treatments for another 24 hours.
- 7) Visualize the scratches in the same area of each well (T24).
- 8) Analyse the relative cell migration distance automatically with the difference between T0 and T24 via NIS-Elements Imaging Software (Nikon, Minato, Japan).

#### **4.13. Neutralization experiment**

Mg materials have been proved to stimulate the secretion of soluble factors of macrophage. Thus, the osteogenic differentiation of HUCPV could response to such Mg-modulated macrophage and soluble factors.

Human anti-OSM is an inhibitor for OSM protein. OSM receptor is composed of gp130/OSMR (Fig. 7). IL6 could connect to receptor complex IL6R/gp130 and sIL6R/gp130 (Fig. 6). Therefore, anti-OSM was chosen for blocking OSM antigen while an anti gp130 was selected as co-blocking antibody for both OSM and IL6. A neutralization experiment was performed to investigate effects of OSM and gp130 neutralization.

HUCPV and macrophages were cultured as mixture in culture medium with 0.2  $\mu$ g/mL human anti-OSM (MAB295; R&D Systems, Abingdon, UK), 0.2  $\mu$ g/mL human anti-gp130 (MAB228; R&D Systems, Abingdon, UK) or both antibodies. According monoclonal mouse IgG1 (555748; BD BioScience, Germany) and IgG2a (555573; BD BioScience, Germany) were applied as isotype controls. Cocultures without blocking antibodies were selected as controls.

#### 4.14. Statistical analysis

Overall, for all *in vitro* systems (transwell coculture, conditioned media and direct contact system), data was acquired from at least biological duplicate of three independent experiments came from at least two donors of HUCPV, PBMC or macrophages, resulting in samples size  $n \geq 12$ . The data are presented as mean  $\pm$  standard deviation (SD). The statistical significance between two conditions was analysed by t-test. The statistical significance between multiple comparisons was analysed by one-way ANOVA or one-way ANOVA on ranks using the SigmaPlot 13.0 (Systat Software Inc, USA). The following post hoc multiple comparisons were based on Turkey when equal variance was assumed or Dunn's when equal variance was not assumed ( $\alpha=0.05$ , \* $P \leq 0.05$ , \*\* $P \leq 0.01$ , and \*\*\* $P \leq 0.001$ ). For RT-qPCR, the regulation threshold (expression fold-change) and p-values (a measure of the evidence against the null hypothesis according to the statistical test) were set to 1.5 and 0.05, respectively. To detect differential expression, a t-test ( $P \leq 0.05$ ) was employed and directly calculated using CFX Manager Software (Bio Rad, Munich, Germany; version 3.0).

## 5. Results

### 5.1. Interactions between PBMC and HUCPV in an indirect coculture (transwell coculture and conditioned media) system

#### 5.1.1. Mg content, pH, and osmolality characterisation

The experimental conditions, Mg concentration and the pH and osmolality of the supernatants at each time point were analysed. Because of the degradation of Mg over time, the Mg concentration, pH and osmolality characterisation under different conditions of transwell coculture were determined at days 1, 4, and 7 (Table 13). The conditioned media were prepared *via* dilution of the collected conditioned media. The specimen characterisations of the diluted conditioned media are shown in Table 14.

Table 13 The Mg concentration under different conditions in the transwell coculture system. The blank group at day 0 was also characterised (Mg concentration: 0.71 mM; pH: 7.60; osmolality: 0.31 Osmol/kg). The transwell coculture data were obtained from biological duplicates of three independent experiments, resulting in a sample size of n=6. H: HUCPV; P: PBMC.

Timepoints	Conditions	Mg (mM)	pH	Osmolality (Osmol/kg)
Day 1	Mg	7.66±0.074	8.27±0.004	0.33±0.013
	H	0.68±0.007	8.10±0.012	0.31±0.007
	H+Mg	5.74±0.001	8.15±0.041	0.25±0.006
	P	0.54±0.002	8.05±0.009	0.31±0.007
	P+Mg	4.71±0.011	8.23±0.022	0.32±0.009
	H+P	0.64±0.001	8.27±0.004	0.31±0.003
	H+P+Mg	6.87±0.043	8.27±0.051	0.26±0.008
Day 4	Mg	11.75±0.079	8.20±0.013	0.36±0.023
	H	0.63±0.005	8.05±0.029	0.33±0.013
	H+Mg	18.03±0.070	8.27±0.030	0.28±0.015
	P	0.64±0.004	8.10±0.023	0.32±0.009
	P+Mg	15.62±0.064	8.31±0.066	0.35±0.029
	H+P	0.70±0.003	8.20±0.013	0.32±0.005
	H+P+Mg	17.91±0.083	8.32±0.039	0.27±0.015
Day 7	Mg	8.36±0.044	8.30±0.054	0.34±0.003
	H	0.60±0.002	8.10±0.013	0.32±0.017
	H+Mg	13.81±0.206	8.24±0.009	0.33±0.012
	P	0.78±0.004	8.14±0.015	0.33±0.008
	P+Mg	8.19±0.057	8.23±0.036	0.34±0.009
	H+P	0.69±0.003	8.25±0.132	0.34±0.017
	H+P+Mg	14.86±0.107	8.26±0.058	0.32±0.010

In the transwell coculture system, the Mg concentration under conditions without an Mg disc showed a similar range (0.54 to 0.78 mM) compared to the blank (0.71 mM). With Mg disc

treatment in the transwell coculture system, the Mg concentration in the cell-seeded conditions (*i.e.*, H+Mg, P+Mg and H+P+Mg) ranged from 4.71 to 6.87, 15.62 to 18.03, and 8.19 to 14.86 mM, respectively, at various time points.

As shown in Table 13, according to the pH values in all experimental conditions of the transwell coculture system, Mg and/or cells were exposed to a pH range from 8.05 to 8.32. The pH value under each condition was clearly higher compared to the culture medium (blank group at day 0; pH: 7.60).

Consistently, under different conditions in the transwell coculture system, the osmolality of the supernatants ranged from 0.25 to 0.36 Osmol/kg (osmolality in the blank group: 0.31 Osmol/kg).

**Table 14** The Mg concentration, pH and osmolality under different conditions in the conditioned media system. The blank group at day 0 was also characterised (Mg concentration: 0.71 mM; pH: 7.60; osmolality: 0.31 Osmol/kg). The data in transwell coculture were obtained from biological triplet tests, resulting in a sample size of n=3. H: HUCPV; P: PBMC.

Conditions	Mg (mM)	pH	Osmolality (Osmol/kg)
<b>Mg-CM</b>	3.82±0.226	8.13±0.004	0.33±0.011
<b>H-CM</b>	0.69±0.035	8.13±0.012	0.27±0.017
<b>P-CM</b>	0.63±0.035	8.10±0.010	0.30±0.007
<b>(H+Mg)-CM</b>	3.51±0.250	8.47±0.040	0.30±0.009
<b>(P+Mg)-CM</b>	3.12±0.025	8.15±0.020	0.31±0.006

All the conditioned media were diluted with culture medium (1:1; v/v), and thus, under conditions with Mg in this system, the Mg concentration was kept at approximately 3-4 mM. The Mg concentration under conditions without an Mg disc had a similar range (0.63 to 0.69 mM) compared to the blank (0.71 mM) in conditioned media system. Without Mg discs, the Mg concentration was 0.63 and 0.69 mM.

In the conditioned media system, the pH value normally ranged from 8.10 to 8.50. The pH value in the conditioned media system was also elevated compared to the culture medium with a pH value of 7.60.

The osmolality under each condition was approximately 0.30 Osmol/kg, similar to the culture medium (osmolality: 0.31 Osmol/kg).

### 5.1.2. Cell viability and proliferation

To evaluate the effects of the Mg disc on cell viability and proliferation, live/dead staining and the DNA content of HUCPV and PBMC were investigated in the transwell coculture (Fig. 19) and conditioned media (Fig. 20) systems. After staining, the bright green cells represent live cells, whereas red fluorescent ones indicate dead cells with incomplete membranes. The DNA content directly correlates with cell number and could reflect the cell content in monoculture and cocultures upon stimulation by the Mg discs.

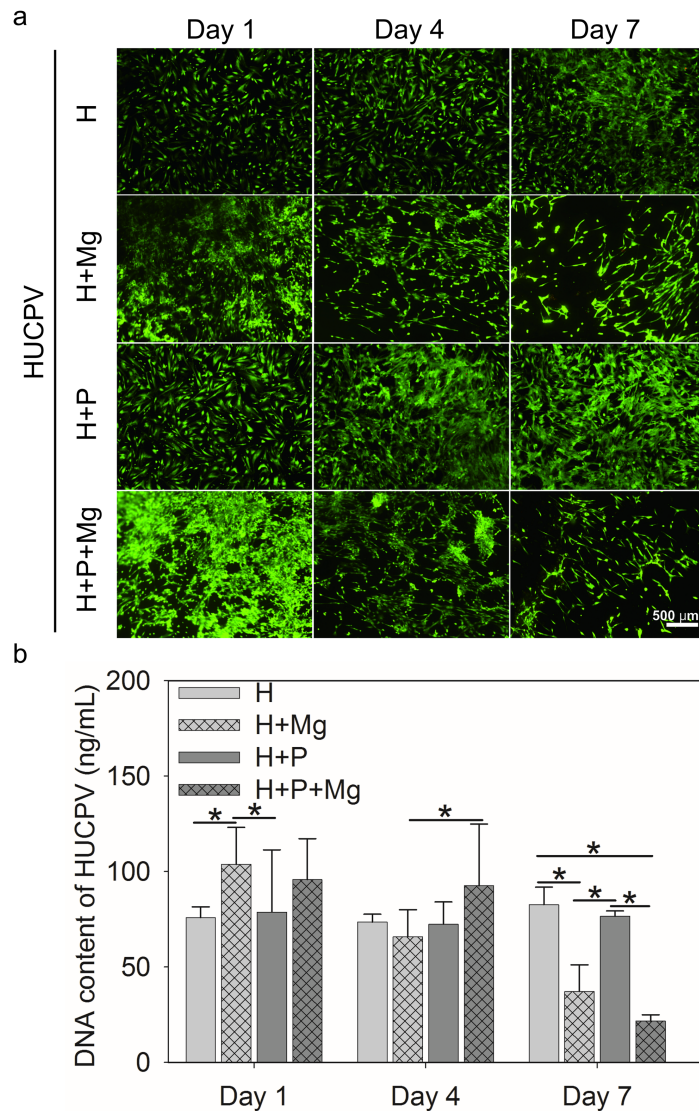


Fig. 19 Cell viability and proliferation of HUCPV in the transwell coculture system. (a) Live/dead staining of HUCPV. The green and red spots represent live and dead cells, respectively. (b) The DNA content of HUCPV. The scale bar represents 500  $\mu$ m. The bars represent the mean  $\pm$  SD ( $n \geq 12$ ). The asterisks indicate significant differences between the two conditions (ANOVA;  $\alpha=0.05$ ,  $*P \leq 0.05$ ). H: HUCPV; P: PBMC.

In the transwell coculture system, adherent HUCPV could be found under all experimental conditions up to 7 days of culture (Fig. 19a, green). For HUCPV cell growth, on day 1, the Mg disc increased the HUCPV cell number (Fig. 19a) and DNA content (Fig. 19b) compared to the HUCPV cell monoculture. During the subsequent culture period, the PBMC stimulated HUCPV cell growth under H+Mg vs. H+P+Mg (day 4) and H+Mg vs. H+P conditions (day 7), rather than the Mg discs. However, decreased DNA content was observed at day 7 compared to the control groups. The HUCPV cell monocultures in the control wells as well as the HUCPV-PBMC cocultures with and without Mg discs showed no obvious changes in the number of dead cells (red) and alive cells (green). Again, similar observations were observed for the corresponding DNA contents.

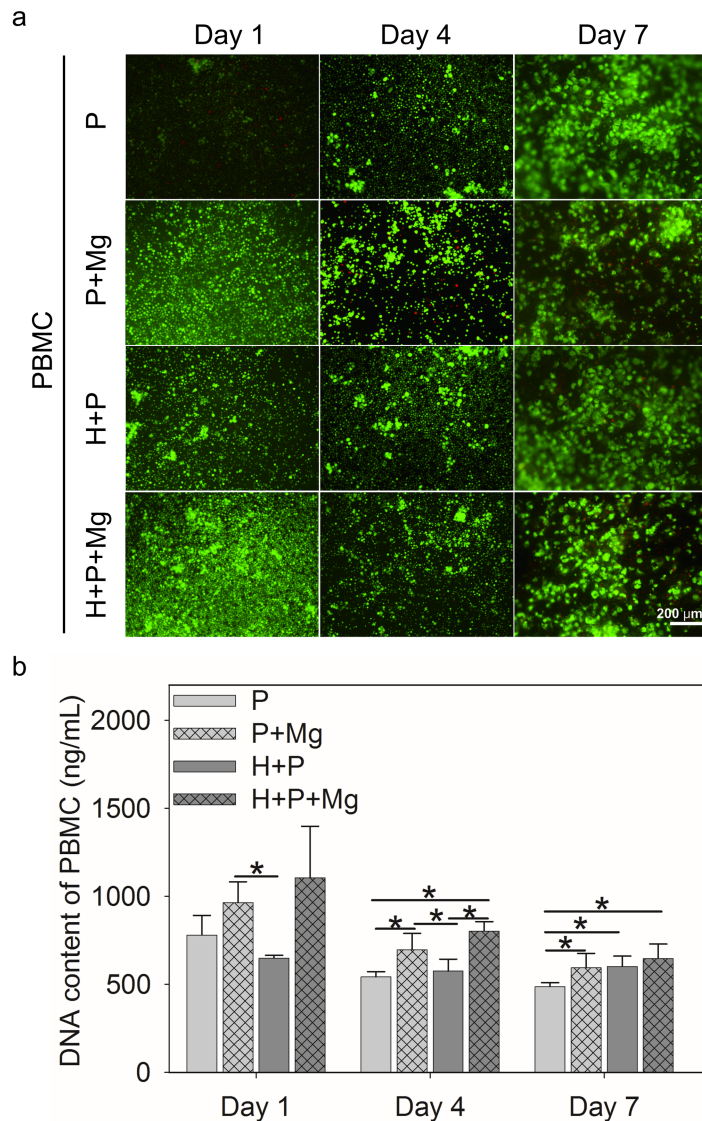


Fig. 20 Cell viability and proliferation of PBMC in the transwell coculture system. (a) Live/dead staining of PBMC. The green and red spots represent live and dead cells, respectively. (b) The DNA content of PBMC. The scale bar represents 200 μm. The bars represent the mean ± SD ( $n \geq 12$ ). The asterisks indicate significant differences between the two conditions (ANOVA;  $\alpha=0.05$ ,  $*P \leq 0.05$ ). H: HUCPV; P: PBMC.

PBMC growth in the transwell coculture system is summarised in Fig. 20. Under the presence of the Mg disc, PBMC proliferation (Fig. 20a, green) was observed, but the number of dead PBMC did not significantly increase. As suggested by the DNA results, the number of PBMC was elevated on days 4 and 7 in the presence of Mg, H or both (Fig. 20b). PBMC exposed to Mg proliferated much faster than those cultured with HUCPV at days 1 and 4.

In the conditioned media system, the HUCPV grew well on plastic during the entire culture period. Almost no obvious dead cells (red colour) were observed (Fig. 21a). For HUCPV cell differentiation, conditioned media from treatments with Mg, PBMC, or both did not markedly affect the DNA content at days 1, 4 and 7 (Fig. 21b).

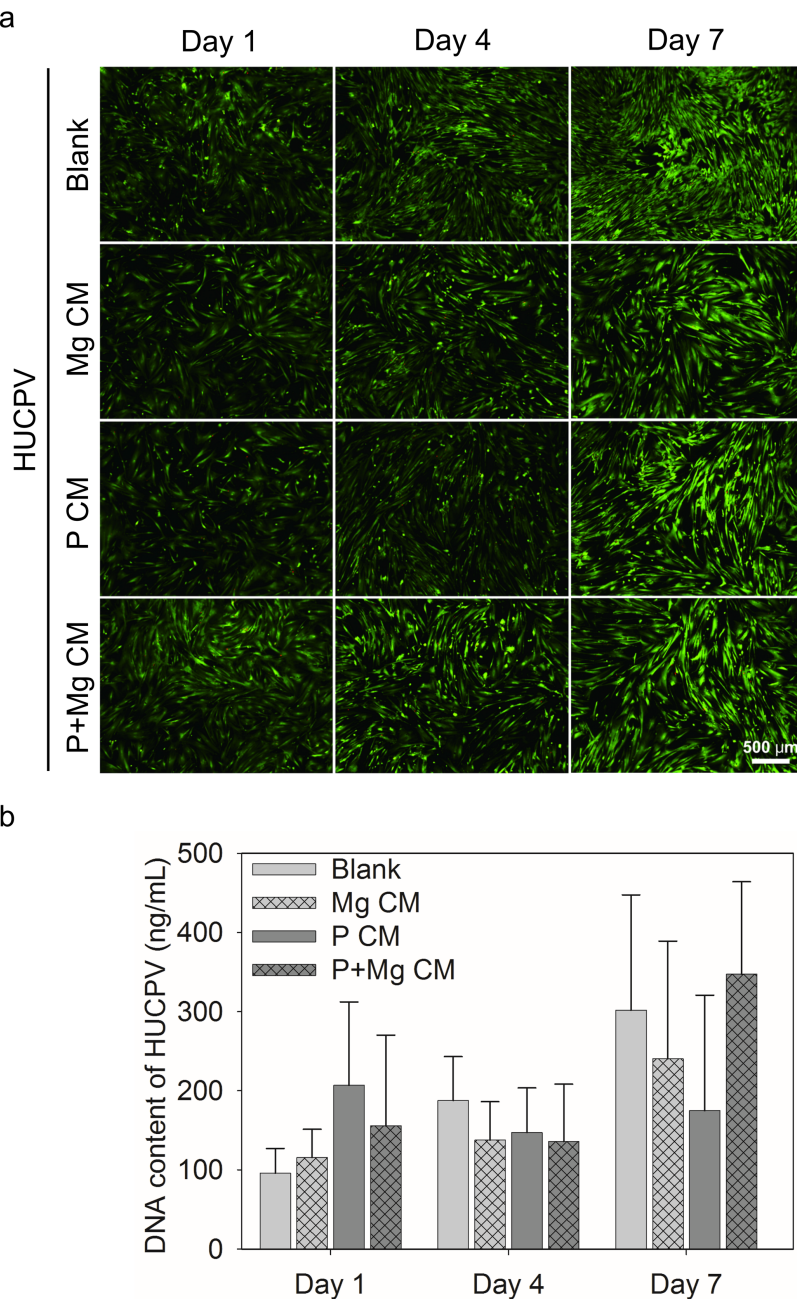


Fig. 21 Cell viability and proliferation of HUCPV in the conditioned media system. (a) Live/dead staining of HUCPV. The green and red spots represent live and dead cells, respectively. (b) The DNA content of HUCPV. The scale bar represents 500 µm. The bars represent the mean  $\pm$  SD ( $n \geq 12$ ). The asterisks represent significant differences between the two conditions (ANOVA;  $\alpha=0.05$ ). H: HUCPV; P: PBMC; CM: conditioned media.

In the conditioned media system, PBMC growth up to 7 days is shown in Fig. 22. A large number of live cells (green) and a few dead cells (red) were observed (Fig. 22a). As shown in Fig. 22b, no significant differences in the proliferation of PBMC were observed among the Ctr (blank) and conditioned media following treatment with Mg, HUCPV, or both.

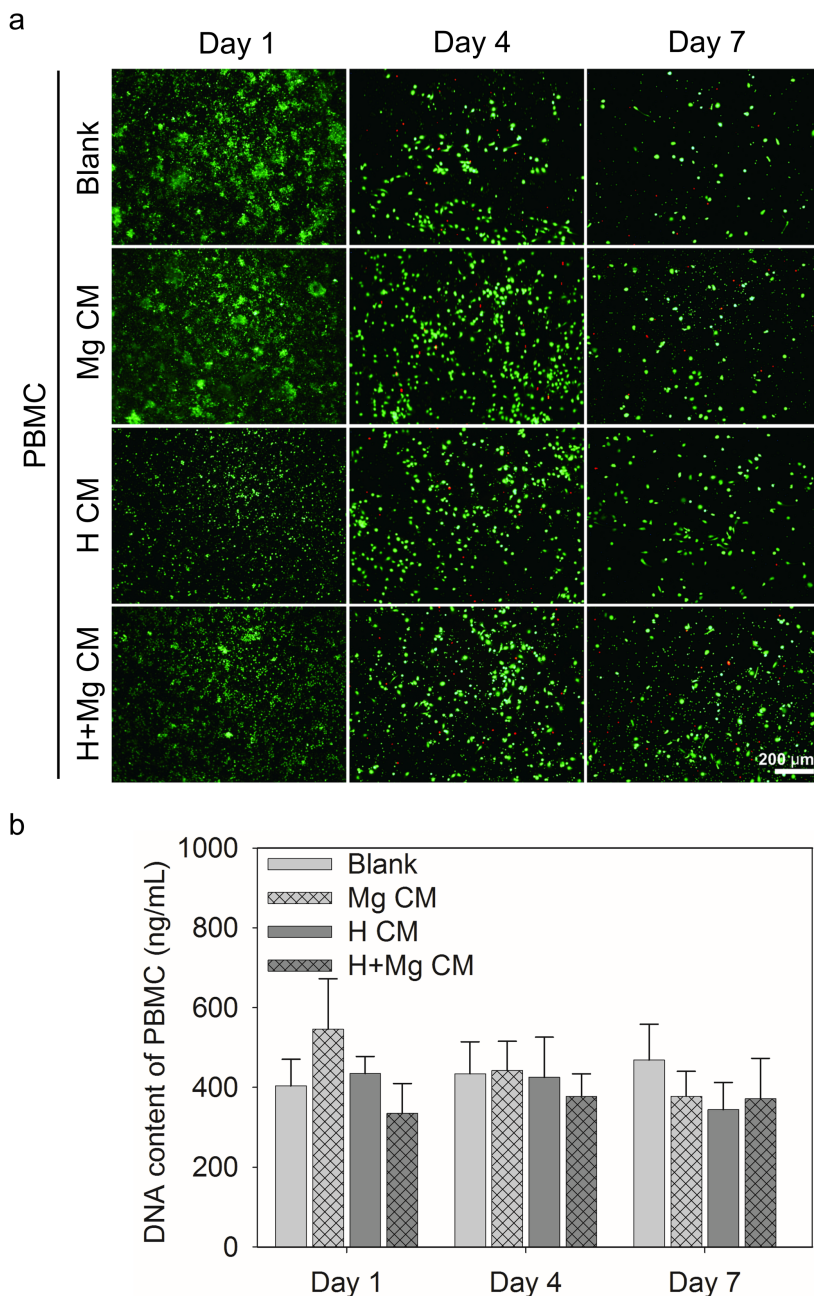


Fig. 22 Cell viability and proliferation of PBMC in the conditioned media system. (a) Live/dead staining of PBMC. The green and red spots represent live and dead cells, respectively. (b) The DNA content of PBMC. The scale bar represents 200  $\mu$ m. The bars represent the mean  $\pm$  SD ( $n \geq 12$ ). The asterisks represent significant differences between the two conditions (ANOVA;  $\alpha=0.05$ ). H: HUCPV; P: PBMC; CM: conditioned media.

### 5.1.3. Cytokine release in the transwell coculture system

The inductive or suppressive roles of MSC in inflammation can be mediated by Mg or immune cells (PBMC, macrophages, etc.). Additionally, migration-related factors contribute to the recruitment of cells to damaged sites to participate in wound healing.

To determine the influence of the Mg biomaterial on the cell-cell communication mediated by soluble factors, cytokine release in the supernatant of all treatment conditions in the transwell coculture system was measured *via* a multiplex assay. A panel of targets (Table 11) was utilised to investigate selected inflammatory cytokines at the protein level.

These cytokines can be classified into several functional groups:

- (a) pro-inflammatory: IL1 $\beta$ , IL2, TNF $\alpha$  and IFN $\gamma$ ;
- (b) anti-inflammatory: IL4, IL5, IL13, G-CSF, IL10 and IL1RA (immunomodulation: IL10 and IL1RA);
- (c) migration/wound healing: GM-CSF, IL8, MCP-1 and MIP-1 $\alpha/\beta$ .

The data were calculated as the cytokine level (pg/mL) normalised by total DNA content ( $\mu$ g/mL) (Table 15). After comparing the cytokine levels between the conditions with and without Mg (+Mg vs. -Mg, respectively), the cytokine production fold change was quantified and summarised in Fig. 23. The results of the other cytokines are summarised in Table S1.

As shown in Fig. 23, decreased levels of pro-inflammatory proteins (IL2, TNF $\alpha$ , IL1 $\beta$ , and IFN $\gamma$ ) and increased production of anti-inflammatory (IL13 and G-CSF) cytokines were observed in HUCPV in contact with Mg. Thus, Mg may induce HUCPV into an anti-inflammatory state.

Initially, the PBMC were activated when cultured with Mg (day 1), expressing high levels of all the above cytokines; however, when the PBMC were cocultured with HUCPV, a downregulation of the pro-inflammatory factors IL2, TNF $\alpha$ , and IFN $\gamma$  (fold change -5 to -10) at day 4, as well as an increase in the anti-inflammatory factors IL13 and G-CSF (fold change 5 to 10) at day 7 were observed (Fig. 23). A similar increase in IL4/5 following Mg exposure was also observed in the PBMC. A clear decrease in IL4/5 caused by Mg appeared in the cocultures. Moderate inflammation was observed when the HUCPV mediated Mg-induced cytokine production in the PBMC.

Taken together, these results indicate that when exposed to Mg, HUCPV can create an anti-inflammatory microenvironment. Furthermore, HUCPV play a role in the suppression of Mg-induced inflammatory cytokine production in PBMC. This immune-modulation of HUCPV on PBMC/macrophage behaviour is dominated by the immunomodulatory characteristics of HUCPV [207, 208].

To elucidate the influence of Mg (+/-PBMC) on MSC migration into the injury *in vitro*, a multiplex assay of migration/wound healing-related cytokines (IL8, GM-CSF, MCP-1 and MIP-1 $\alpha/\beta$ ) was performed and showed an increase regardless of cell type (HUCPV, PBMC, and HUCPV cocultured with PBMC) exposed to Mg compared to the control group without Mg (Table 15).

Also, as summarised in Fig. 23, PBMC exhibited a more robust production of GM-CSF, IL8, MCP-1 and MIP-1 $\alpha/\beta$  after Mg exposure. On both days 1 and 7, PBMC exhibited a higher production of GM-CSF, IL8, MCP-1 and MIP-1 $\alpha/\beta$  after Mg exposure. These cytokines promote stem cells (HUCPV) to migrate into the injury site and are further involved in tissue repair processes [125, 209, 210].

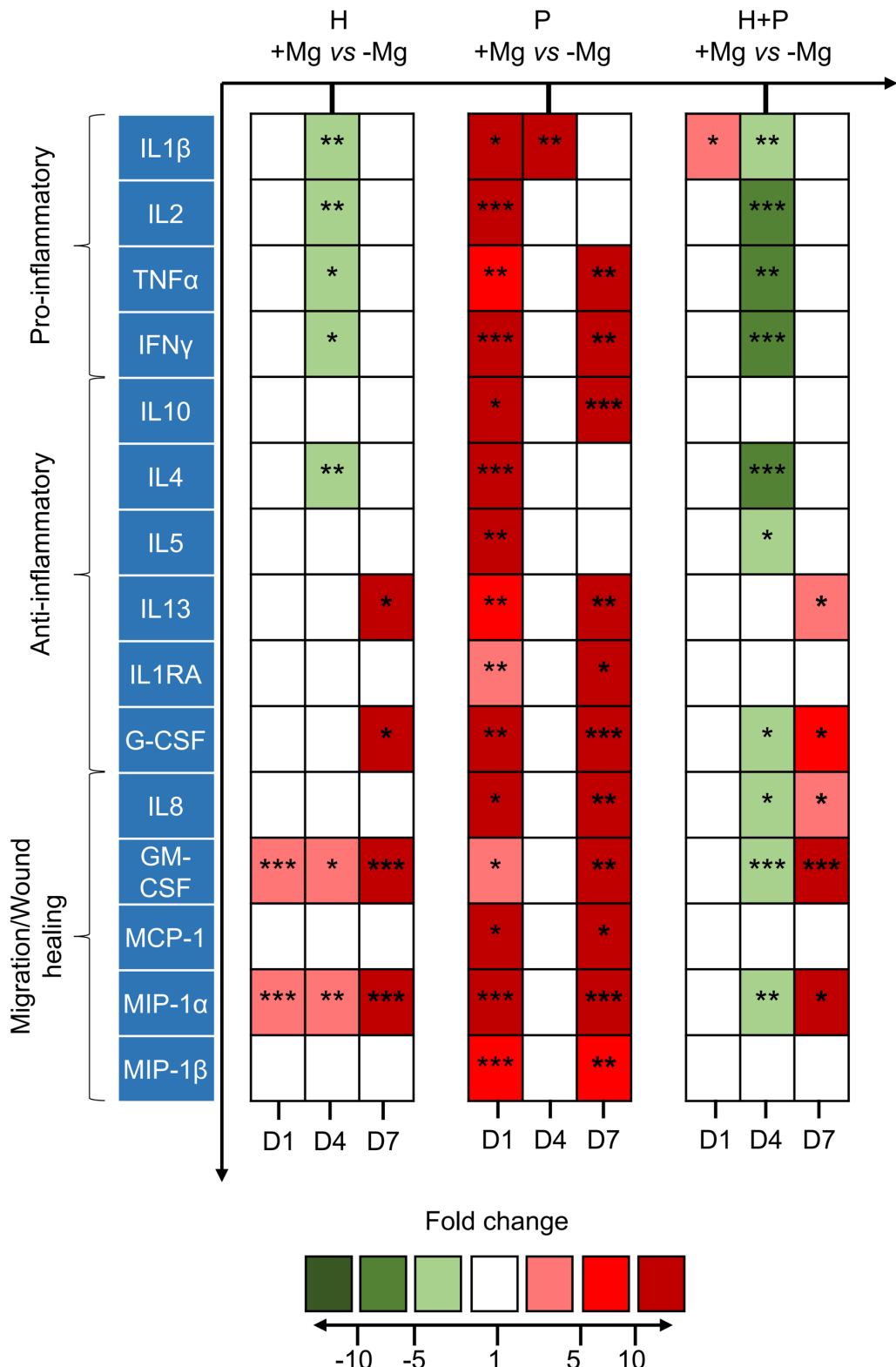


Fig. 23 The cytokine levels in the supernatant of HUCPV, PBMC and HUCPV-PBMC coculture in the presence and absence of Mg discs. The colour scale represents the fold change between the conditions with Mg discs and controls without Mg discs. The bars represent the mean  $\pm$  SD ( $n\geq 12$ ). The asterisks indicate significant differences between the two conditions (ANOVA;  $\alpha=0.05$ ,  $*P\leq 0.05$ ,  $**P\leq 0.01$  and  $***P\leq 0.001$ ).

Table 15 The levels of secreted cytokines (normalised by the total DNA content) in the supernatants in the transwell coculture system at days 1, 4 and 7. The cytokine level (pg/mL)/total DNA content (µg/mL) data were obtained from biological duplicates of three independent experiments from at least two donors of HUCPV (H) and PBMC (P), resulting in n≥12 (samples size). <<OOR represents “out of calibration range” in the multiplex immunoassay. H: HUCPV; P: PBMC.

Day 1	H		H+Mg		P		P+Mg		H+P		H+P+Mg	
	Mean	SD	Mean	SD	Mean	SD	Mean	SD	Mean	SD	Mean	SD
<b>IL1β</b>	112.49	93.16	223.95	161.37	0.20	0.28	72.51	111.20	9.69	7.04	21.73	17.47
<b>IL1RA</b>	947.80	1430.40	765.65	1132.95	777.33	1057.00	3848.48	2933.03	109.87	118.62	99.22	110.68
<b>IL2</b>	231.45	294.98	199.52	160.04	1.31	1.57	34.53	19.99	11.26	11.57	13.13	16.01
<b>IL4</b>	31.14	42.56	35.85	31.16	0.02	0.08	3.94	1.92	2.11	2.51	1.97	2.53
<b>IL5</b>	99.23	80.07	141.13	110.44	1.49	2.21	30.26	29.13	10.00	9.08	10.44	9.41
<b>IL8</b>	377362.64	280342.73	267521.13	107729.67	1741.93	1631.52	47130.23	51341.62	39223.65	41908.95	14809.99	10617.96
<b>IL10</b>	29.61	42.46	53.16	59.89	1.24	0.96	23.00	32.76	1.71	1.77	1.99	2.38
<b>IL13</b>	21.22	25.82	31.18	33.82	0.80	0.47	4.04	3.23	1.58	1.36	1.90	2.09
<b>G-CSF</b>	30993.58	35849.00	84752.56	98183.36	72.53	64.12	947.55	885.22	2186.26	2264.59	3095.06	3700.32
<b>GM-CSF</b>	316.50	198.73	725.10	143.18	2.16	3.16	6.15	5.33	26.27	9.85	31.01	14.88
<b>IFNγ</b>	4340.81	1208.24	4247.98	1275.01	24.08	25.01	536.04	361.30	350.01	170.52	236.57	104.79
<b>MCP-1</b>	21550.82	12997.84	35332.07	28468.99	47.90	42.77	2231.23	2994.36	2010.24	1463.37	1092.65	907.82
<b>MIP-1α</b>	37.53	31.17	164.24	95.86	6.85	4.29	482.59	184.57	13.18	15.83	6.90	2.72
<b>MIP-1β</b>	7.30	21.77	20.00	32.06	152.16	130.21	1294.07	872.15	42.35	68.62	5.44	11.97
<b>TNFα</b>	513.90	681.32	563.58	448.44	78.81	69.79	666.35	483.70	82.23	105.76	38.56	33.41

Table 15 (Continued)

Day 4	H		H+Mg		P		P+Mg		H+P		H+P+Mg	
	Mean	SD	Mean	SD	Mean	SD	Mean	SD	Mean	SD	Mean	SD
<b>IL1<math>\beta</math></b>	96.69	71.43	33.79	25.57	0.02	0.05	0.68	0.66	10.38	5.36	3.45	5.08
<b>IL1RA</b>	913.39	1352.38	168.16	459.73	80.42	120.46	208.02	466.65	108.88	122.97	57.27	86.42
<b>IL2</b>	233.61	163.50	72.04	69.98	0.34	0.51	2.78	7.30	24.58	11.47	5.13	7.64
<b>IL4</b>	42.35	32.55	6.28	9.25	1.00	1.00	1.22	1.59	4.15	2.37	0.45	1.00
<b>IL5</b>	164.09	146.90	169.44	129.93	1.53	2.57	2.64	6.80	21.46	16.10	6.96	6.27
<b>IL8</b>	211981.36	135043.24	237123.19	167788.42	1861.42	1013.84	2720.32	3274.06	55702.31	47065.31	26375.91	29809.00
<b>IL10</b>	18.95	15.56	12.26	17.53	0.88	1.33	1.19	1.67	1.71	1.42	1.53	2.41
<b>IL13</b>	16.40	18.08	11.02	15.21	3.90	4.07	1.65	3.29	0.74	0.36	1.58	2.49
<b>G-CSF</b>	28714.25	31884.81	15395.39	13375.97	26.40	36.34	77.57	161.22	2747.49	2520.88	808.71	1052.47
<b>GM-CSF</b>	311.98	94.96	758.82	370.33	1.00	1.00	1.23	1.94	43.26	7.43	22.12	1.21
<b>IFNy</b>	6859.57	3344.98	4650.89	2610.78	28.77	28.87	141.48	245.51	872.04	410.38	174.12	94.25
<b>MCP-1</b>	36659.69	35074.10	63510.42	25720.57	141.84	113.43	1109.69	2294.08	14320.78	25555.60	998.01	628.45
<b>MIP-1<math>\alpha</math></b>	51.23	23.35	160.10	86.18	2.07	2.46	23.68	41.61	10.84	4.65	5.13	3.74
<b>MIP-1<math>\beta</math></b>	0.59	2.04	1.00	1.00	1231433	1113326	79.49	154.28	7.31	12.31	5.35	14.57
<b>TNF<math>\alpha</math></b>	625.46	647.61	182.00	207.48	63.22	50.41	29.59	74.00	69.10	52.62	13.19	18.87

Table 15 (Continued)

Day 7	H		H+Mg		P		P+Mg		H+P		H+P+Mg	
	Mean	SD	Mean	SD	Mean	SD	Mean	SD	Mean	SD	Mean	SD
<b>IL1β</b>	8.55	4.75	13.79	17.48	1.00	1.00	3.09	2.52	1.50	1.03	2.07	1.71
<b>IL1RA</b>	300.48	452.66	534.35	885.08	37.36	68.26	11183.67	13328.93	1402.46	2365.35	1129.93	1333.00
<b>IL2</b>	22.56	27.57	17.81	26.97	1.00	1.00	39.23	25.56	8.22	7.17	16.06	11.46
<b>IL4</b>	4.09	4.98	3.48	8.18	1.00	1.00	2.65	2.29	1.24	1.43	2.95	3.03
<b>IL5</b>	49.18	49.79	86.82	66.37	1.00	1.00	15.68	13.07	6.07	7.37	12.32	9.60
<b>IL8</b>	56307.17	66937.96	414156.35	673431.15	273.86	120.30	4438.35	3813.26	9569.56	17090.65	27651.52	16596.98
<b>IL10</b>	4.05	6.30	36.51	55.47	0.52	0.96	8.12	3.04	1.53	2.24	6.71	6.76
<b>IL13</b>	1.89	2.79	36.58	43.99	6.98	11.07	208.22	209.99	1.76	2.51	6.00	6.08
<b>G-CSF</b>	1245.99	1826.57	21097.46	24074.23	26.77	30.31	312.63	122.46	281.35	372.88	2509.50	2588.40
<b>GM-CSF</b>	1.01	2.36	422.68	201.64	0.43	1.02	10.45	10.28	2.42	2.69	44.42	19.77
<b>IFNγ</b>	3186.65	2225.59	3741.77	1864.68	3.93	6.02	671.28	544.40	389.18	292.42	420.36	182.78
<b>MCP-1</b>	14679.79	12693.32	19707.66	10905.45	54.22	43.39	9216.65	13361.23	1508.12	1431.63	2799.74	2472.91
<b>MIP-1α</b>	9.16	8.41	158.78	26.42	3.64	2.35	47.98	23.61	5.31	4.72	74.32	88.26
<b>MIP-1β</b>	1.00	1.00	1.00	1.00	23.14	28.06	117.80	79.45	24.28	32.87	83.09	92.49
<b>TNFα</b>	215.86	260.97	198.09	315.88	1.61	3.66	334.06	307.07	50.92	36.07	104.60	81.09

### 5.1.4. M2 macrophages polarisation

PBMC are a cluster of immune cells that include granulocytes (neutrophils, basophils, and eosinophils), monocytes, and many lymphocytes (T cells, B cells, and NK cells). The subpopulation of each cell cluster in the isolated PBMC that were used in this study is shown in Fig. 24.

During flow cytometric analysis, the cells pass through the beam and scatter light, which is then detected as forward scatter (FSC) and side scatter (SSC). FSC is related to cell size, and SSC provides information about the internal complexity (*i.e.*, granularity) of a cell. In this way, one can often distinguish cell populations based solely on differences in cell size. Larger, more granular granulocytes produce a large population with high FSC and SSC. Monocytes are large cells, but not so granular, so they produce a separate population with high FSC but low SSC. Smaller, but non-granular lymphocytes produce a population with low FSC and low SSC. Therefore, these cells can be divided into different populations based solely on their FSC and SSC.

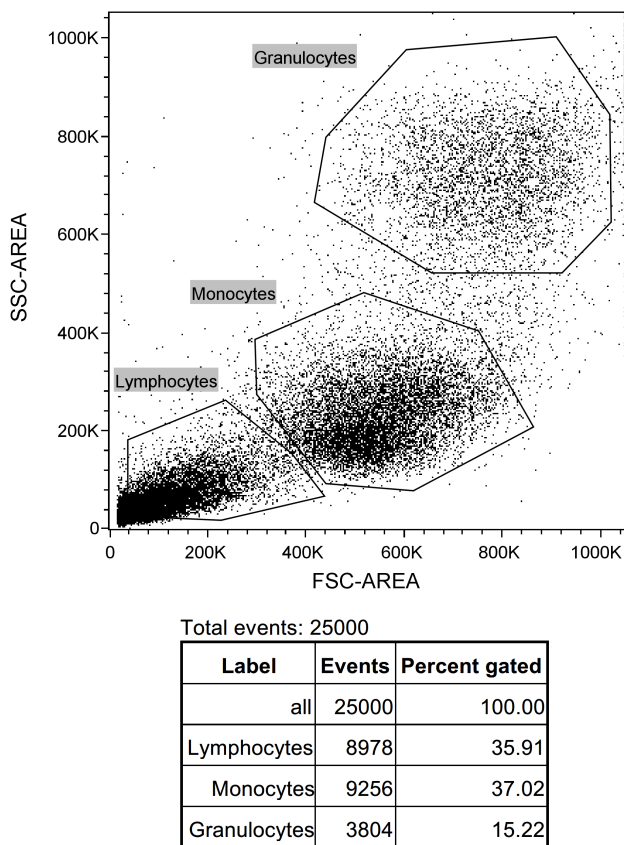


Fig. 24 Subpopulations (%) of PBMC. The percentages of lymphocytes, monocytes and granulocytes in isolated PBMC were indicated via flow cytometric analysis.

In addition to the multi-nuclear morphology of monocyte fusion, the cell phenotype of type 2 macrophages (M2) during monocyte/macrophage differentiation was confirmed with flow cytometric analysis (Fig. 25). Here, the macrophage pan marker-CD 68<sup>+</sup> was used to distinguish the macrophages from the PBMC cluster. Then, the surface antigen-CD 163<sup>+</sup> was stained to classify the M2 subpopulation from all CD 68<sup>+</sup> cells (all subtypes of macrophages). In Fig. 25, the percentage of M2 (CD 68<sup>+</sup> CD 163<sup>+</sup>) at day 7 in the H+P+Mg conditions of the

transwell coculture system is shown. First, debris and dead cells were removed (positive propidium iodide (PI) staining). Then, CD 68<sup>+</sup> cells (Fig. 25a, blue dots) were gated from the total cells. Finally, the profile shown in Fig. 25b was obtained, and the M2 macrophages in this CD 68<sup>+</sup> subgroup were automatically calculated (approximately 60%).

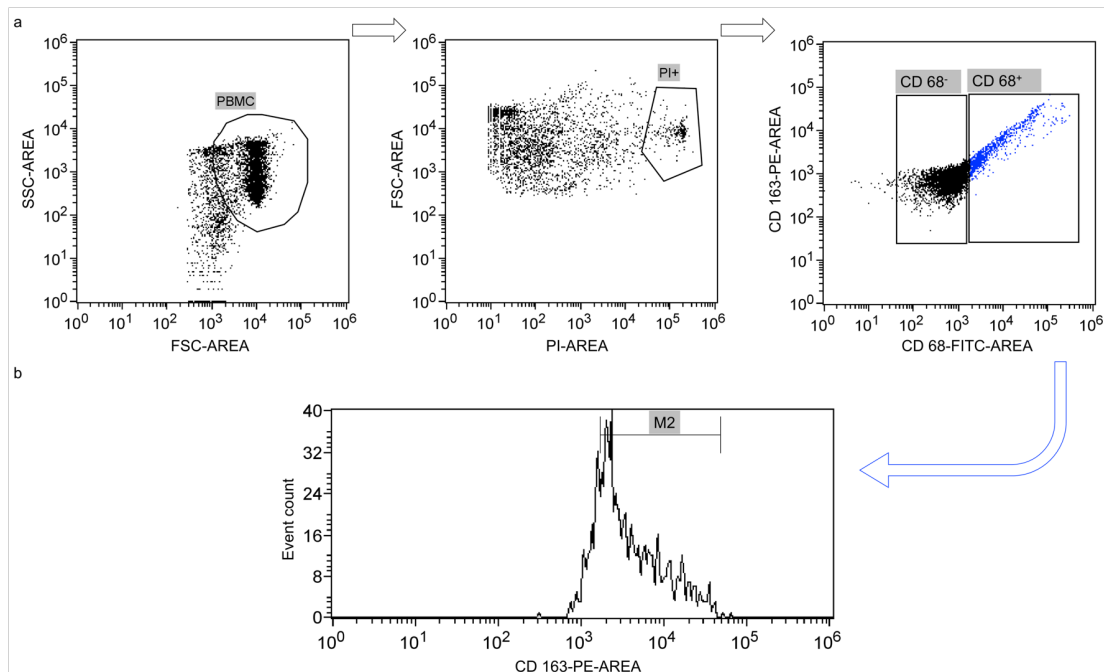


Fig. 25 Flow cytometric analysis of the M2 subpopulation. (a) The selection of macrophages (CD 68<sup>+</sup>). In brief, the live cells were first gated out, followed by the CD 68<sup>+</sup> cells. (b) The selection of M2 macrophages in this CD 68<sup>+</sup> subgroup. CD 163 was used as a specific marker to identify M2 macrophages from the total macrophage population.

In PBMC, the monocytes differentiating into M2 macrophages were indicated by phenotypic changes after 1, 4 and 7 days detected *via* flow cytometry (Fig. 26). PBMC were labelled with anti-human CD 68<sup>+</sup> (a pan marker for macrophages) and anti-human CD 163<sup>+</sup> (surface marker for the M2 phenotype).

Flow cytometry (Fig. 26a) revealed an elevated percentage of M2 macrophages in the total macrophage population at day 1 when PBMC were exposed to HUCPV (P vs. H+P). In addition, compared to the H+P condition, the M2/CD 68<sup>+</sup> cell population increased under the H+P+Mg condition from day 4 onward. At day 7, Mg in synergy with HUCPV promoted the M2 macrophage phenotype. Similarly, the M2/CD 68<sup>+</sup> population increased in the conditioned media system (Fig. 26b) between P+(H CM) and P+(H+Mg CM) conditions after 1 day of culture. Additionally, a clear increase was observed under the conditions of P alone and P+(Mg CM) on day 4. These data suggest that this polarisation may derive from the effect of Mg on the immunomodulatory properties of HUCPV.

The results also indicate the regulation of stem cells on M2 macrophage polarisation. For instance, an elevated percentage of M2 macrophages was exhibited at day 1 in both the transwell coculture (P and H+P) and conditioned media systems (P+(Mg CM) and P+(H+Mg CM)).

Compared to the role of HUCPV on the M2 phenotype, the effect of Mg on the M2 phenotype in different indirect coculture systems notably could be seen. Mg significantly elevated the M2 phenotype in PBMC compared to HUCPV in either P+Mg vs. H+P (transwell coculture) or P+(Mg CM) vs. P+(H CM) in conditioned media system at day 4 or 7.

Taken together, these data imply that Mg could promote macrophage differentiation into M2 cells with and without HUCPV cell exposure.

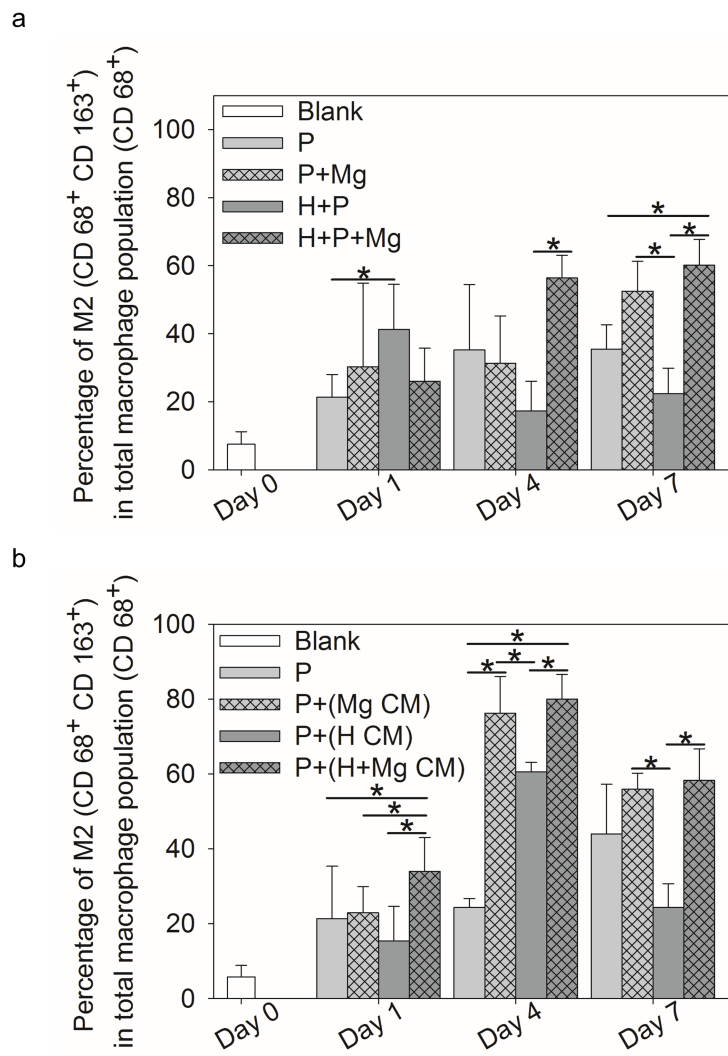


Fig. 26 The percentage of M2 cells in the total macrophage population in the transwell coculture and conditioned media systems. (a) M2 in transwell coculture. (b) M2 in conditioned media system. The bars represent the mean  $\pm$  SD ( $n \geq 12$ ). Significant differences are represented by asterisks and were obtained from post hoc multiple comparisons between each group or compared to controls in ANOVA ( $\alpha=0.05$ ,  $*P \leq 0.05$ ). H: HUCPV; P: PBMC; CM: conditioned media.

### 5.1.5. Migratory ability of HUCPV

Referring to the former section, migration-specific cytokines were significantly upregulated by Mg exposure. Thus, a scratch assay was performed to investigate the migration potential of HUCPV upon stimulation with PBMC and/or Mg discs under physiological conditions.

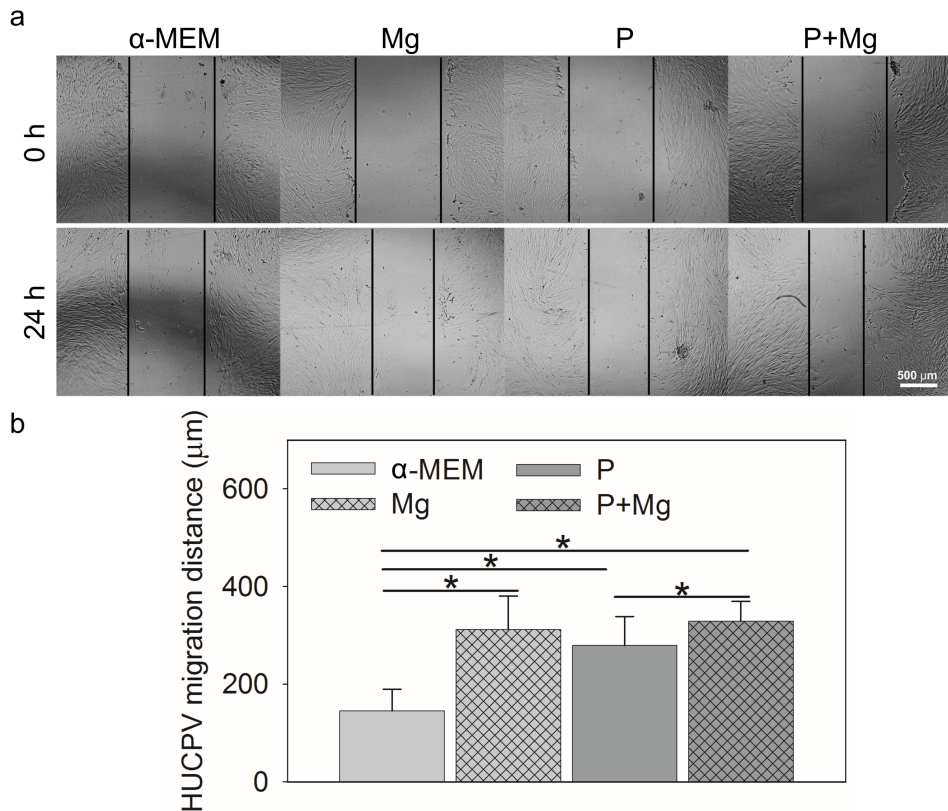


Fig. 27 The migration distance of HUCPV when cultured in the supernatant from the transwell coculture system. (a) The scratches at 0 h and 24 h were quantified by the gap width. (b) HUCPV cell migration distance in the transwell coculture system. The scale bar represents 500  $\mu\text{m}$ . The migration distance was calculated by the scratch width difference between 0 h and 24 h. The bars represent the mean  $\pm$  SD ( $n \geq 12$ ). Significance differences are represented by asterisks and were obtained from post hoc multiple comparisons between each group or compared to controls with ANOVA ( $\alpha=0.05$ , \* $P \leq 0.05$ ). H: HUCPV; P: PBMC.

The migration distance of HUCPV was qualified by the scratch area difference between 0 and 24 h (Fig. 27 and 28). As shown in Fig. 27b, compared to the α-MEM control group, treatment with Mg or PBMC (P) or both (P+Mg) significantly increased the migratory ability of HUCPV. Similarly, a stimulated migration capacity of HUCPV was observed in P+Mg compared with HUCPV in P. In the captured bright light micrographs, a large number of HUCPV crossed the edge of the scratch in the transwell coculture after 24 h (Fig. 27a). These results reveal that HUCPV have a greater capacity to migrate when cultured with Mg and/or PBMC for 24 h in the transwell coculture system.

No difference was observed when HUCPV were cultured in the conditioned media system of all experimental conditions (Fig. 28). Interestingly, Mg stimulated HUCPV cell migration capacity in the transwell coculture system but not in the conditioned media system. This difference may be due to the various Mg concentrations of the Mg group in the transwell coculture and conditioned media systems. The Mg group contained 8 mM or 3.8 mM Mg ion in the transwell coculture or conditioned media system, respectively.

Therefore, the significantly increased migration of HUCPV may be influenced by the Mg concentration itself.

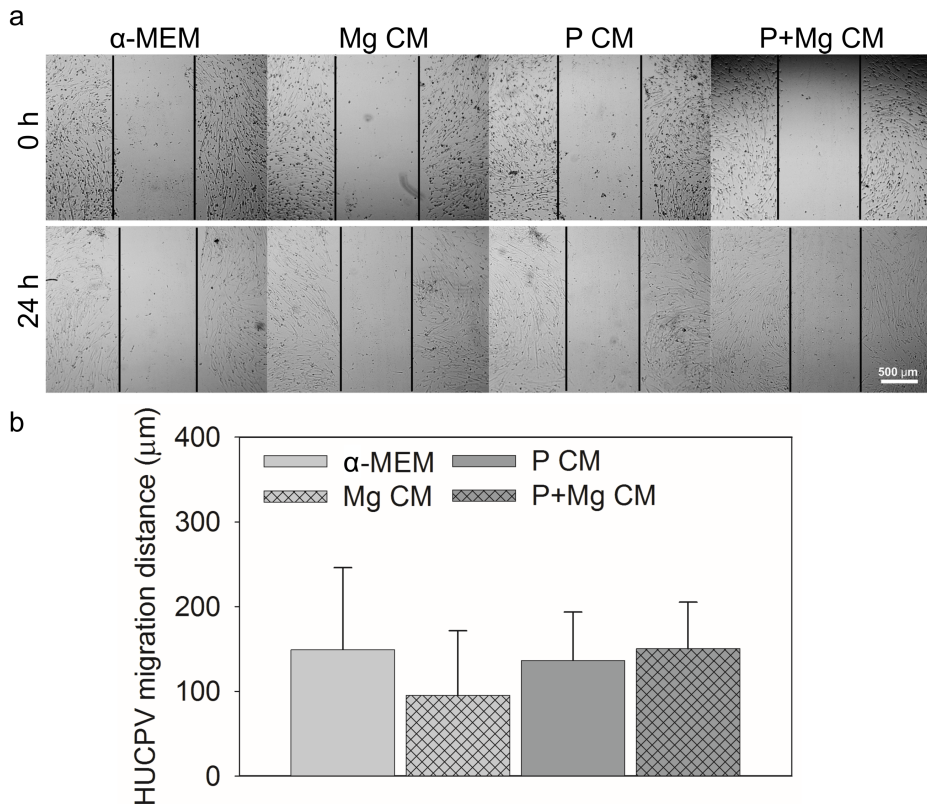


Fig. 28 The migration distance of HUCPV when cultured in the supernatant from the conditioned media system. (a) The scratches at 0 h and 24 h were quantified by the gap width. (b) HUCPV cell migration distance in the conditioned media system. The scale bar represents 500  $\mu\text{m}$ . The migration distance was calculated by the scratch difference between 0 h and 24 h. The bars represent the mean  $\pm$  SD ( $n \geq 12$ ). Significant differences were obtained from post hoc multiple comparisons in ANOVA ( $\alpha=0.05$ ). H: HUCPV; P: PBMC; CM: conditioned media.

### 5.1.6. Osteogenic potential of HUCPV

ALP activity acts as an indicator of HUCPV cell osteogenic differentiation. ALP activity at day 7 can be attributed to HUCPV as the PBMC/macrophages do not significantly produce ALP activity [211]. Hence, only treatment conditions involving HUCPV are presented to indicate HUCPV differentiation: H, H+Mg, H+P, H+P+Mg in the transwell coculture system (Fig. 29a and 30a) and H, H+(Mg CM), H+(P CM), H+(P+Mg CM) in the conditioned media system (Fig. 29b and 30b).

The ALP activities were normalised to the respective DNA contents of the HUCPV to reduce variation induced by proliferation. The ALP activities at day 7 can be attributed to HUCPV as the PBMC/macrophages do not significantly produce ALP [211].

In the transwell coculture system, when HUCPV were exposed to Mg or PBMC+Mg (Fig. 29a), significantly increased ALP activity was observed compared to HUCPV cell monoculture in the control cell culture medium. The ALP level of PBMC on inserts (H+P) was not affected; however, in the presence of Mg discs (H+P+Mg), ALP activity was significantly upregulated. In the conditioned media system (Fig. 29b), no difference in ALP activity between the controls (HUCPV monoculture) and other treatments was measured.

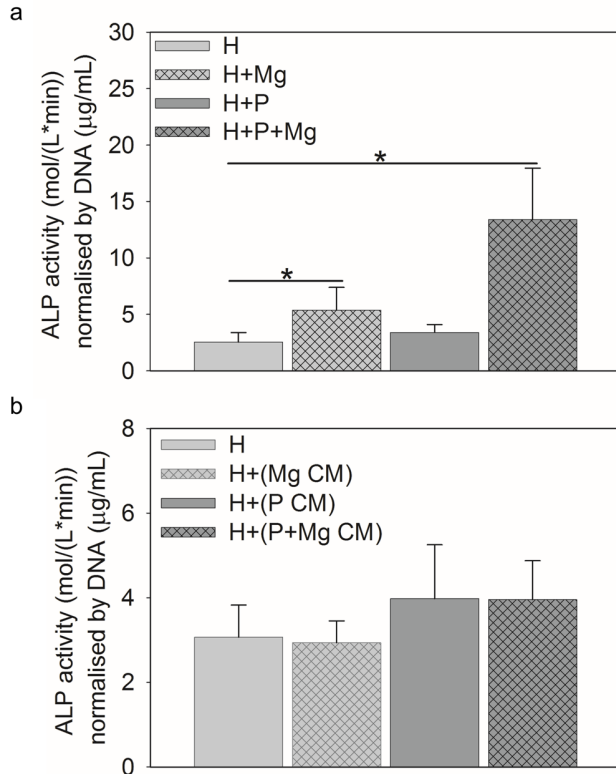


Fig. 29 The osteogenic potential of HUCPV indicated by ALP activity in the transwell coculture and conditioned media systems at day 7. ALP activity in the transwell coculture (a) and conditioned media systems (b) was normalised by the respective HUCPV DNA content. The bars represent the mean  $\pm$  SD ( $n \geq 12$ ). Significant differences are represented by asterisks and were obtained from post hoc multiple comparisons between each group or compared to controls with ANOVA ( $\alpha=0.05$ ,  $*P \leq 0.05$ ). H: HUCPV; P: PBMC; CM: conditioned media.

In addition, the fold change of osteogenesis-related gene expression of *COL1A1*, *OC* and *OPN* in HUCPV is indicated by the colour scale in Fig. 30a and 30b.

In the transwell coculture system, the coculture with PBMC enhanced the expression of *OC* in HUCPV. Similarly, increases in *COL1A1*, *OC* and *OPN* were found when Mg was applied. Even a synergistic effect of P and Mg could be seen for *OC* (regulation fold reached 20).

In the conditioned media system, *COL1A1* and *OPN* were upregulated in all coculture groups, accompanied by a slight decrease in *OC* expression in (H+P+Mg CM). A higher fold change was observed for the *COL1A1* gene (regulation fold from 8.5 to 11.0).

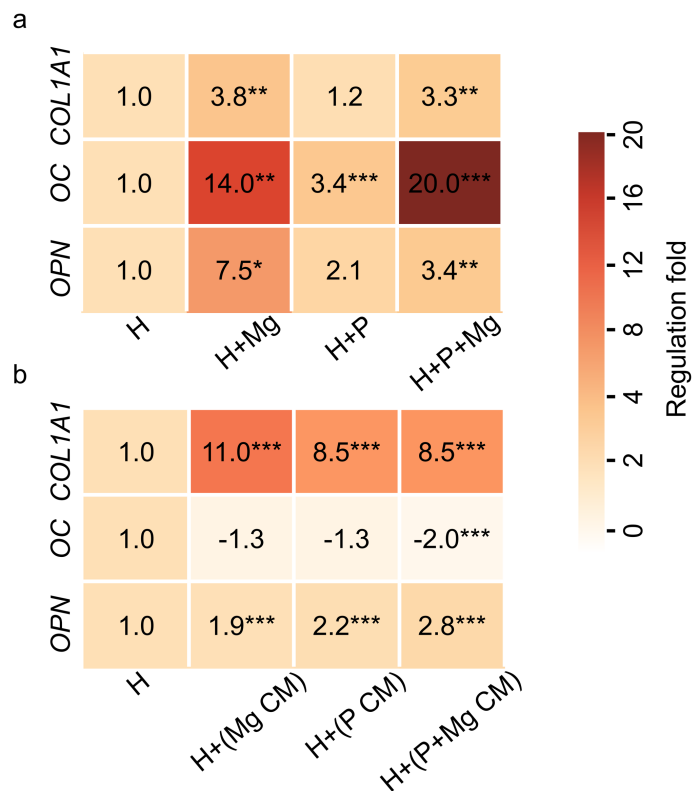


Fig. 30 Osteogenesis-related gene expression in transwell coculture and conditioned media system at day 7 in HUCPV was measured by RT-qPCR. The gene expression fold change was compared to controls (H) in transwell coculture (a) and conditioned media system (b). The bars represent the mean  $\pm$  SD ( $n \geq 12$ ). Significant differences are represented by asterisks and were obtained from post hoc multiple comparisons between each group or compared to controls with ANOVA ( $\alpha=0.05$ , \* $P \leq 0.05$ , \*\* $P \leq 0.01$  and \*\*\* $P \leq 0.001$ ). H: HUCPV; P: PBMC; CM: conditioned media.

## 5.2. Interactions between macrophages and HUCPV in a direct coculture system

### 5.2.1. Mg concentration, pH, osmolality, and corrosion rate characterisation

To characterise the experimental conditions, the Mg concentration, pH, osmolality and corrosion rate of the supernatants at each time point were analysed. Because of the degradation of Mg and Mg-10Gd over time, the specimen characterisation under different conditions of a direct coculture system was determined at days 7 and 14 (Table 16).

Table 16 The Mg concentration, pH, osmolality and corrosion rate characterisation of the solutions for all experimental conditions in the direct coculture system. The blank group at day 0 was also characterised (Mg concentration: 0.71 mM; pH: 7.60; osmolality: 0.31 Osmol/kg). The data were obtained from biological duplicates of three independent experiments, resulting in a sample size of n=6. H: HUCPV; M: macrophages.

Timepoints	Conditions	Mg (mM)	pH	Osmolality (Osmol/kg)	Corrosion rate (mm/y)
Day 7	H	0.57±0.12	8.15±0.03	0.33±0.01	/
	H+M	0.41±0.01	8.18±0.03	0.34±0.01	/
	H+Mg	30.36±5.41	8.46±0.14	0.40±0.01	1.16±0.24
	H+M+Mg	23.59±1.62	8.44±0.02	0.40±0.02	1.31±0.28
	H+Mg-10Gd	16.31±3.38	8.55±0.02	0.38±0.01	1.29±0.03
	H+M+Mg-10Gd	15.87±1.05	8.53±0.04	0.38±0.01	1.31±0.01
Day 14	H	0.45±0.01	8.20±0.02	0.35±0.04	/
	H+M	0.40±0.01	8.19±0.03	0.34±0.01	/
	H+Mg	35.26±9.11	8.46±0.01	0.41±0.02	0.73±0.06
	H+M+Mg	29.76±0.65	8.46±0.06	0.40±0.02	0.63±0.07
	H+Mg-10Gd	16.33±0.75	8.50±0.04	0.36±0.01	0.69±0.03
	H+M+Mg-10Gd	18.30±1.95	8.50±0.02	0.36±0.01	0.59±0.04

In the direct coculture system, the Mg concentration in the blank group at day 0 was 0.71 mM. The Mg concentration under conditions without an Mg disc ranged from 0.40 to 0.57 mM. Different Mg concentrations were measured upon treatment with Mg or Mg-10Gd in cell-seeded conditions. The Mg concentration in cell-seeded conditions (*i.e.*, H+Mg, P+Mg and H+P+Mg) ranged from 23.59 to 35.26 mM at various time points. The Mg concentration in those cell-seeded conditions with Mg-10Gd dropped from 15.87 to 18.30 mM.

As shown in Table 16, the pH value varied from 8.44 to 8.55 in the presence of Mg or Mg-10Gd at day 7. The pH value under each condition was clearly higher compared to the blank group (pH: 7.60).

Under different conditions of the direct coculture system, the osmolality in the supernatants ranged from 0.33 to 0.41 Osmol/kg (osmolality in blank group: 0.31 Osmol/kg).

Consistently, both the Mg- and Mg-10Gd-treated groups showed a higher corrosion rate of approximately 1.30 mm/y before 7 days. Up to 14 days, the corrosion rate slowed to

approximately 0.70 mm/y. At the same timepoint, no significant differences in the corrosion rate between Mg and Mg-10Gd were found.

### 5.2.2. Cell viability and proliferation

To determine the roles of the Mg disc on cell viability and proliferation, live/dead staining (Fig. 31) and DNA content (Fig. 32) of HUCPV/macrophages were investigated in direct coculture systems. After staining, the live cells were labelled green, while the dead cells were red. Cell proliferation, indicated by the DNA content, shows the cell number in mono- and co-culture with Mg or Mg-10Gd at various timepoints (days 7 and 14).

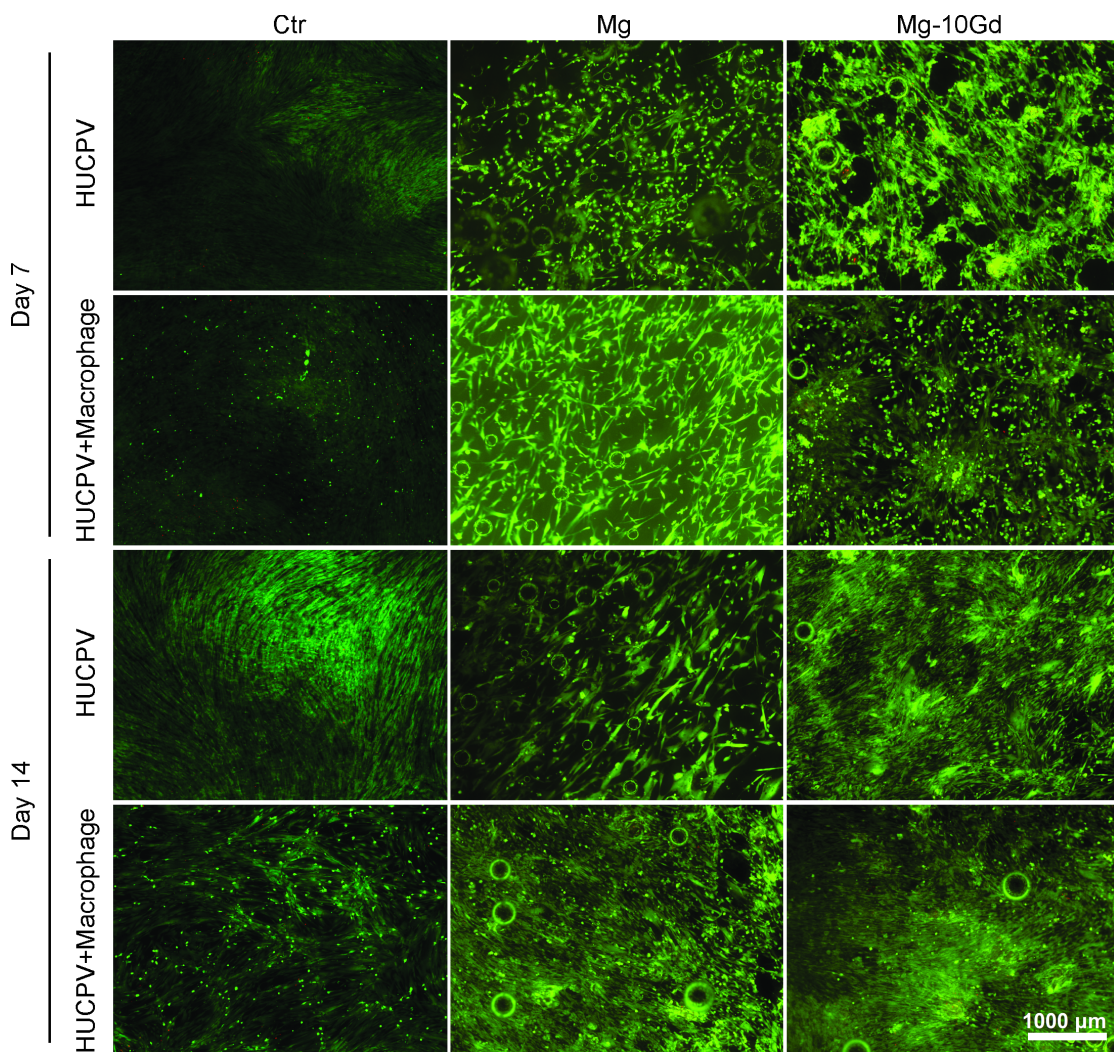


Fig. 31 Live/dead staining of HUCPV alone or cocultured with macrophages at days 7 and 14. The scale bar represents 1000  $\mu$ m.

As shown in Fig. 31, in a direct coculture system, adherent HUCPV and cocultured HUCPV-macrophages could be observed in blank (Ctr), Mg and Mg-10Gd wells during the entire culture period. The numbers of dead (red) and live cells (green) in the HUCPV monocultures in control wells and HUCPV cell-macrophage cocultures were not affected by the presence of Mg or Mg-10Gd.

Comparing Mg and Mg-10Gd (Fig. 32), no difference was found for cell growth. At days 7 and 14, the cell monoculture and cocultures in the controls exhibited a consistent DNA content (approximately 5 µg/mL). Even though the materials reduced the DNA content at day 7, a recovery of HUCPV proliferation was observed at day 14, especially with Mg-10Gd.

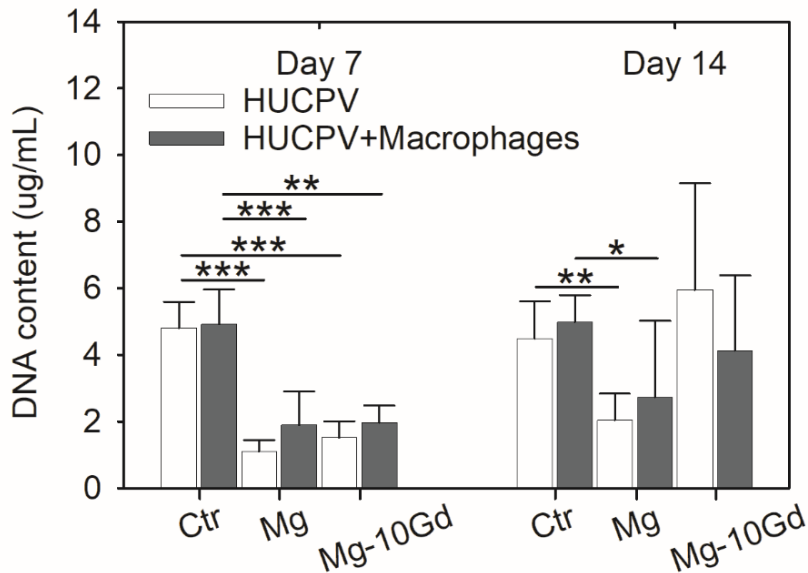


Fig. 32 The DNA content of HUCPV alone and in coculture with macrophages at days 7 and 14. The bars represent the mean  $\pm$  SD ( $n\geq 12$ ). Significant differences are represented by asterisks and were obtained from post hoc multiple comparisons between each group or compared to controls with ANOVA ( $\alpha=0.05$ ,  $*P\leq 0.05$ ,  $**P\leq 0.01$  and  $***P\leq 0.001$ ).

### 5.2.3. Subpopulations of HUCPV cell and macrophage cocultures

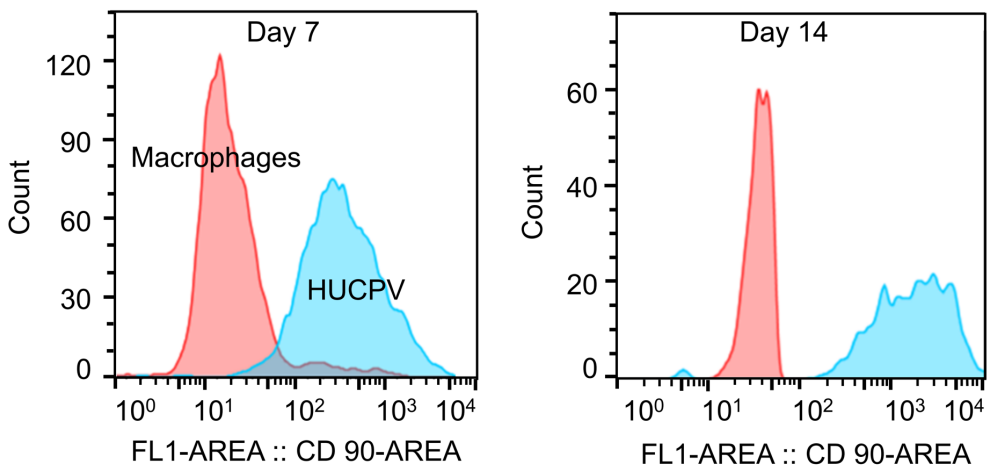


Fig. 33 The cell distribution in the direct coculture groups at days 7 and 14. The histograms represent HUCPV (blue) and macrophages (red).

As shown in Fig. 33, HUCPV were confirmed as CD 90 positive while macrophages did not express the CD 90 antigen during the culture period. Immunophenotyping analysis utilising the CD 90 marker was applied to reveal the cellular proportion of HUCPV and macrophages in direct coculture upon stimulation by materials.

Comparing the groups exposed or not to Mg or Mg-10Gd, no significant effects were found on the cell ratios after 14 days (Fig. 34). This result implies that the cell ratios should not be considered as a parameter that could either influence cell-cell direct interactions or explain results.

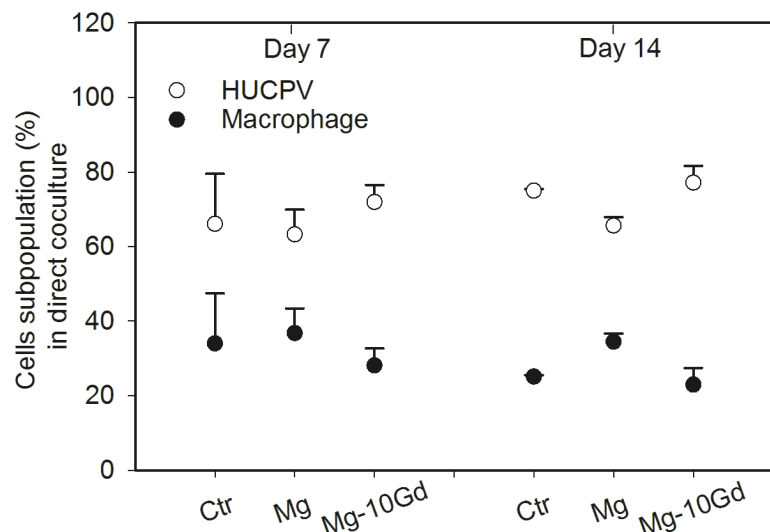


Fig. 34 Cell subpopulations (%) in the direct coculture groups at days 7 and 14. The bars represent the mean  $\pm$  SD ( $n\geq 12$ ). Significant differences were investigated by post hoc multiple comparisons between each group or compared to controls with ANOVA ( $\alpha=0.05$ ).

#### 5.2.4. Mg and Mg-10Gd stimulated the pro-osteogenic activity of HUCPV

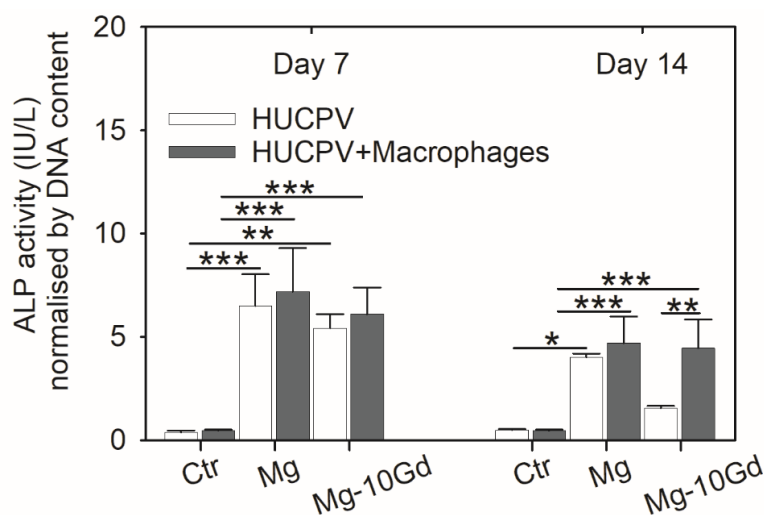


Fig. 35 The ALP activity in HUCPV and cocultures. The ALP activity was normalised by the corresponding DNA content. The bars represent the mean  $\pm$  SD ( $n\geq 12$ ). Significant differences are represented by asterisks and were obtained from post hoc multiple comparisons between each group or compared to controls with ANOVA ( $\alpha=0.05$ , \* $P\leq 0.05$ , \*\* $P\leq 0.01$  and \*\*\* $P\leq 0.001$ ).

As shown in Fig. 35, the ALP activities were markedly enhanced at day 7 by Mg and Mg-10Gd in both the HUCPV cell monoculture and cocultures. The stimulation by Mg-10Gd was more efficient than pure Mg.

Shown in Fig. 36, HUCPV cocultured with macrophages and/or Mg or Mg-10Gd expressed markedly higher levels of osteogenic-related genes. Specifically, the expression levels of *ALP*, *OC* and *OPN* were significantly higher under stimulation by Mg and Mg-10Gd in both the HUCPV cell monoculture or coculture systems. The RT-qPCR results showed that *OC* (fold change: 70) and *ALP* (fold change: 200) genes exhibited the highest expression upon stimulation by Mg in the cocultures. The expression of *OPN* was also significantly higher under stimulation by Mg-10Gd in both the HUCPV cell monoculture and cocultures.

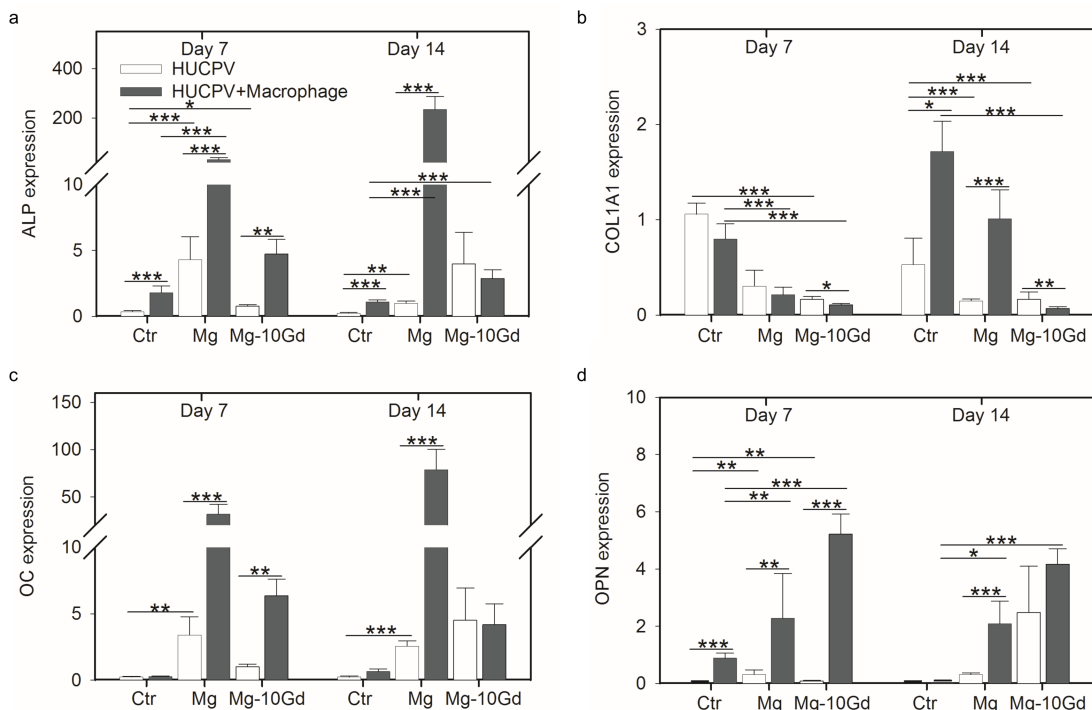


Fig. 36 Selected gene expression in HUCPV alone or in cocultures at days 7 and 14. The expression levels of *ALP* (a), *COL1A1* (b), *OC* (c), and *OPN* (d) were investigated with RT-qPCR. The “gene expression” on the y-axis defines the changes in the selected genes normalised to the levels of the reference genes. The bars represent the mean  $\pm$  SD ( $n \geq 12$ ). Significant differences are represented by asterisks and were obtained from post hoc multiple comparisons between each condition ( $\alpha=0.05$ , \* $P \leq 0.05$ , \*\* $P \leq 0.01$ , and \*\*\* $P \leq 0.001$ ).

### 5.2.5. Possible signalling factors (OSM/IL6/BMP6/TNF $\alpha$ /IL1 $\beta$ ) involved in the pre-osteogenic activity of HUCPV

Among the signalling factors secreted by macrophages, immune-regulatory cytokines have been extensively investigated. Members of the IL6 family (OSM) can stimulate bone formation. Acting as pro-inflammatory cytokines, TNF $\alpha$  and IL1 $\beta$  can modulate bone formation by inhibiting osteoblast differentiation. In addition, macrophages can also release growth factors, such as BMP. The involvement of BMP has also been reported to have a stimulatory effect on bone formation.

To confirm the involvement of these signalling factors on the pro-osteogenic activity of HUCPV, the levels of OSM, IL6, TNF $\alpha$ , and IL1 $\beta$  were measured by ELISA. The related gene expression of the BMP/Smad signalling pathway members was also studied.

### 5.2.5.1. The effects of OSM/IL6 on osteogenic behaviour are OSM- and gp130-dependent

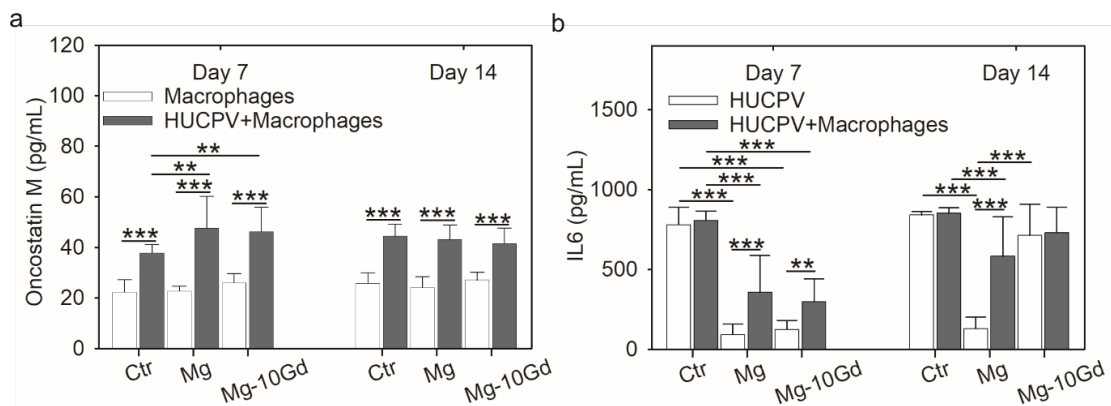


Fig. 37 The OSM and IL6 levels in the supernatant of cocultured HUCPV and macrophages in a direct culture on metallic biomaterial. The bars represent the mean  $\pm$  SD ( $n\geq 12$ ). Significant differences are represented by asterisks and were obtained from post hoc multiple comparisons between each group or compared to controls with ANOVA ( $\alpha=0.05$ , \* $P\leq 0.05$ , \*\* $P\leq 0.01$  and \*\*\* $P\leq 0.001$ ).

The ELISA assays highlighted that extracellular OSM was significantly stimulated up to 14 days (Fig. 37a). At day 7, OSM was significantly higher in the presence of Mg and Mg-10Gd. The OSM level was also increased by coculture of HUCPV and macrophages. At day 14, OSM was significantly upregulated only in the cocultures, regardless of the presence or absence of Mg-based materials. These results indicated that cocultures in synergy with materials (Mg and Mg-10Gd) contributed to the higher secretion of OSM.

As shown in Fig. 37b, no difference in the IL6 levels between HUCPV cell monoculture and cocultures in the controls was detected during the 14-day experiment. Even though a clear decrease was shown by both additives in the HUCPV cell monoculture or cocultures, nevertheless, in the cocultures, the reduced IL6 secretion was attenuated by both Mg-based materials. Taken together, these data show that the OSM and IL6 secretions are influenced by Mg-based (Mg and Mg-10Gd) materials, especially in the cocultures.

To further investigate the OSM- [166] and IL6-mediated [160] osteoblastogenesis, OSM and gp130 were neutralised in the cell cocultures. After neutralisation, ALP activities in the cocultures were investigated.

As shown in Fig. 38, the ALP activities in the cocultures were normalised by the corresponding DNA content. The neutralisation of OSM and OSM+gp130 significantly decreased the ALP activity in the cocultures exposed to the Mg disc at both days 7 and 14. When the cocultures were exposed to Mg-10Gd, the ALP activity was also reduced after anti-gp130 treatment, but this result was only statistically significant at day 7. In the isotype control groups, IgG1 and IgG2a, the ALP level was unchanged compared to the blank control group (only the cell cocultures). These results collectively indicate that the roles of OSM and IL6 on the osteogenic differentiation of HUCPV are OSM- and gp130-dependent.

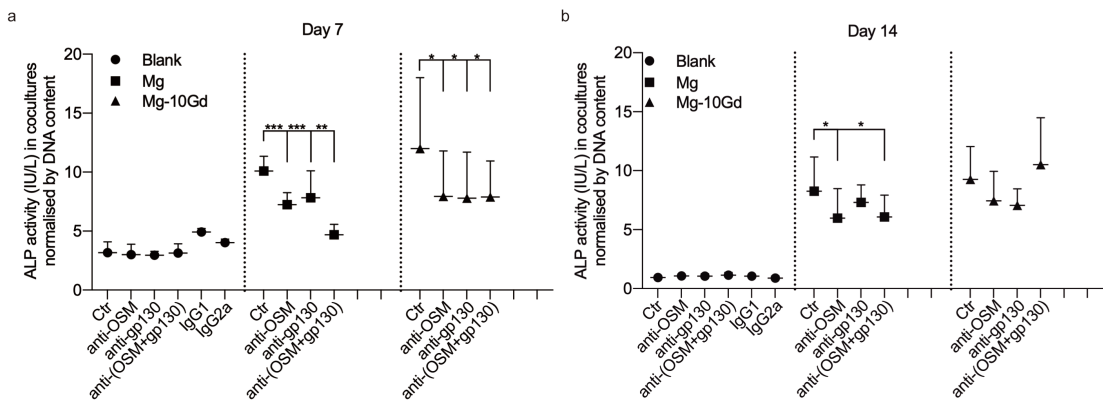


Fig. 38 ALP activity after OSM and gp130 neutralisation in the cocultures at days 7 and 14. HUCPV and macrophages were cocultured (blank) and seeded on Mg or Mg-10Gd for 14 days and were treated with anti-OSM (0.2 µg/mL), anti-gp130 (0.2 µg/mL) or both antibodies. The condition without anti-OSM and anti-gp130 served as the control (Ctr). IgG1 and IgG2a were applied as isotype controls. ALP activity in the supernatant was assessed and normalised by the corresponding DNA content. The bars represent the mean ± SD ( $n \geq 12$ ). Significant differences were investigated by ANOVA and indicated by an asterisk ( $\alpha=0.05$ , \* $P \leq 0.05$ , \*\* $P \leq 0.01$ , and \*\*\* $P \leq 0.001$ ).

#### 5.2.5.2. BMP6/Smad signalling is involved in the osteogenic differentiation of HUCPV

The osteogenic mediation between HUCPV and macrophages requires signalling cascades such as BMP/Smad, which involves the receptors BMPR1A and BMPR2 as well as Smad 1/4/5. To follow this cascade, the expression of several factors including *BMP6*, *BMPR1A/2* and *Smad 1/4/5* was measured via RT-PCR. As shown in Fig. 39, the gene expression of *BMP6* in the macrophages was significantly upregulated by Mg (days 3, 7 and 14) and Mg-10Gd (days 7 and 14).

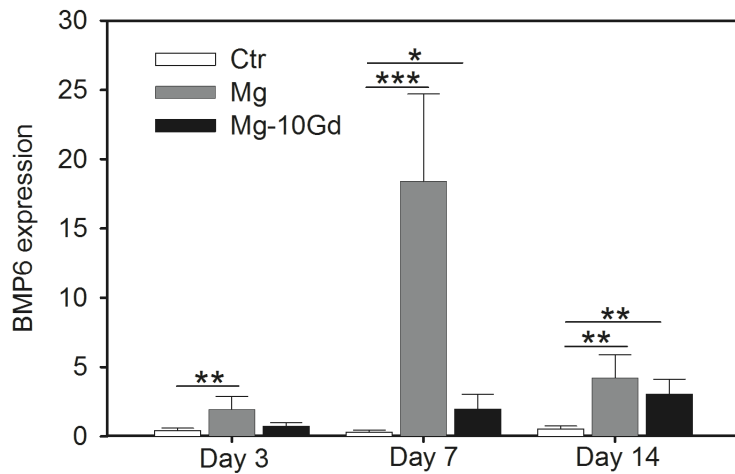


Fig. 39 *BMP6* expression in macrophages under stimulation by Mg and Mg-10Gd. Control (Ctr): cell culture medium. The y-axis shows the change in the selected gene normalised to the level of the reference gene. The bars represent the mean ± SD ( $n \geq 12$ ). Significant differences were investigated by t-test and are indicated by an asterisk ( $\alpha=0.05$ , \* $P \leq 0.05$ , \*\* $P \leq 0.01$  and \*\*\* $P \leq 0.001$ ).

To confirm *BMP6*-related cascade involvement, the macrophages were cocultured with HUCPV for 14 days in a direct coculture system upon stimulation with Mg and Mg-10Gd.

First, the expression of the receptors for BMP6, *BMPR1A* and *BMPR2* in the HUCPV and cocultures was quantified using RT-qPCR (Fig. 40). A great increase in *BMPR1A* and *BMPR2* expression was measured upon the stimulation by materials during the culture period, even though there was a slight decrease at day 14 when the cocultures were exposed to Mg-10Gd. Moreover, a much greater expression of *BMPR1A/2* in the cocultured cells was detected upon Mg stimulation but not in those seeded on Mg-10Gd.

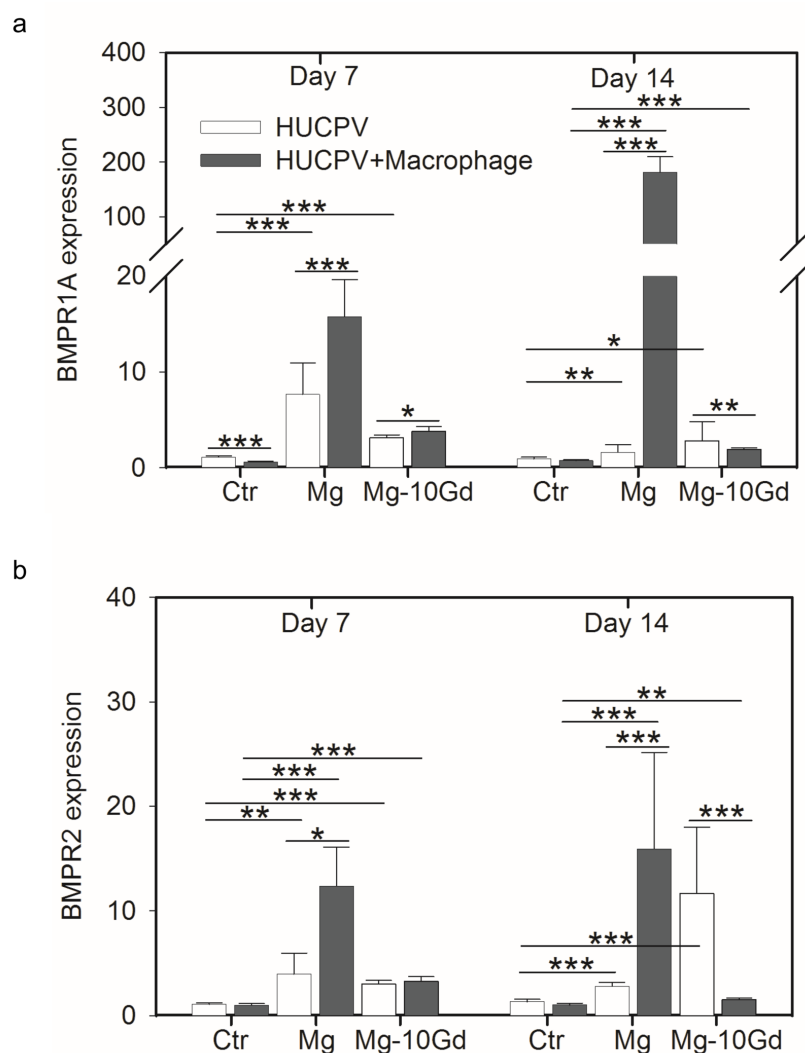


Fig. 40 *BMPR1A* and *BMPR2* expression in HUCPV and cocultures under stimulation of Mg and Mg-10Gd. The y-axis represents the change in the selected gene normalised to the level of the reference gene. The bars represent the mean  $\pm$  SD ( $n \geq 12$ ). Significant differences were investigated by ANOVA and are indicated by an asterisk ( $\alpha=0.05$ ,  $^*P \leq 0.05$ ,  $^{**}P \leq 0.01$  and  $^{***}P \leq 0.001$ ).

To further explore the signalling mechanisms behind the osteogenic stimulation, the BMP-related Smad genes, *Smad1*, 4 and 5, were also analysed (Fig. 41).

A similar increase was detected in HUCPV and cocultures in the presence of Mg and Mg-10Gd. The cell cocultures exposed to the Mg discs showed the highest gene expression of *Smad1/4/5* at day 14.

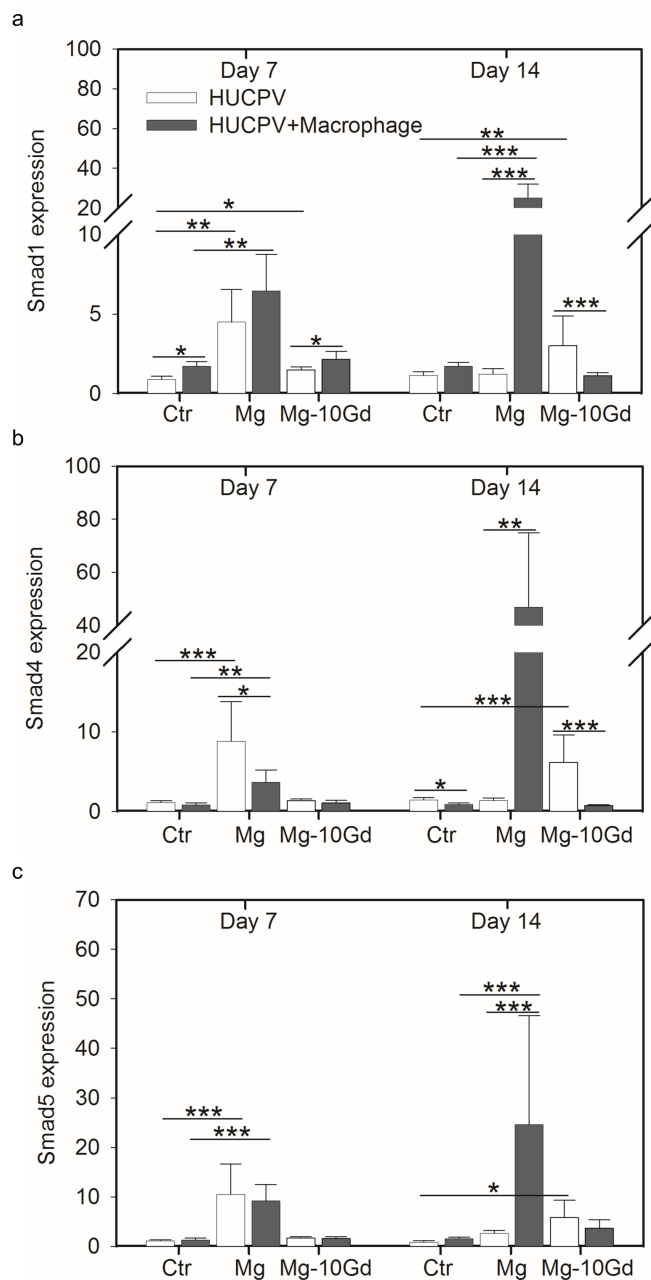


Fig. 41 *Smad 1/4/5* expression in HUCPV and cocultures under stimulation by Mg and Mg-10Gd. The y-axis represents the change in the selected gene normalised to the level of the reference gene. The bars represent the mean  $\pm$  SD ( $n \geq 12$ ). Significant differences were investigated by ANOVA and are indicated by an asterisk ( $\alpha = 0.05$ ,  $*P \leq 0.05$ ,  $**P \leq 0.01$  and  $***P \leq 0.001$ ).

5.2.5.3. Inflammatory cytokines ( $\text{TNF}\alpha$  and  $\text{IL1}\beta$ ) contributed to the osteogenic activity of HUCPV

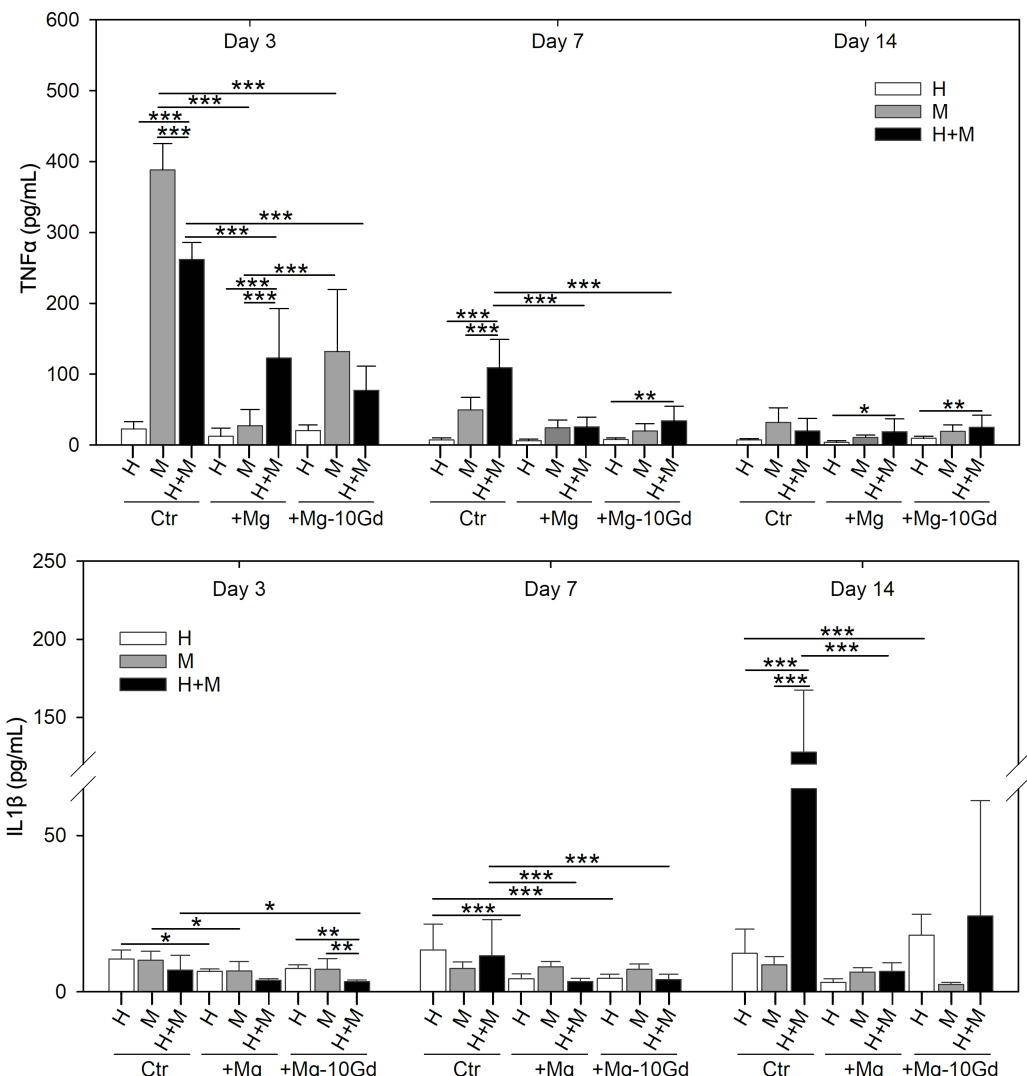


Fig. 42 TNF $\alpha$  and IL1 $\beta$  levels in the monoculture and cocultures. The bars represent the mean  $\pm$  SD ( $n\geq 12$ ). Significant differences were investigated by ANOVA and are indicated by an asterisk ( $\alpha=0.05$ ,  $*P\leq 0.05$ ,  $**P\leq 0.01$  and  $***P\leq 0.001$ ). H: HUCPV; M: macrophages.

The ELISA results indicated a greater inflammatory TNF $\alpha$  release by macrophages compared to HUCPV especially at day 3 (Fig. 42); however, compared to macrophages alone in the Ctr groups, the cocultures presented different effects on the TNF $\alpha$  level including a significant decrease in TNF $\alpha$  at day 3 but an increase at day 7. In both the macrophage monoculture and the cocultures, the materials (Mg and Mg-10Gd) reduced TNF $\alpha$  during the early culture period, especially the pure Mg at day 3.

The secretion of IL1 $\beta$  from both the HUCPV cell and macrophage monoculture remained constant. A remarkable increase in the IL1 $\beta$  level was measured in the HUCPV cell and macrophage coculture at day 14. Nevertheless, consistent with the effects measured for TNF $\alpha$ , the IL1 $\beta$  level in the cocultures was reduced by Mg and Mg-10Gd at day 7, and this decrease by Mg was still observed at day 14.

## 6. Discussion

Mg-based biomaterials have been extensively studied in regenerative medicine, and tissue engineering and repair in this context depend on their excellent manufacturing and biocompatibility. To develop these promising implants for clinical trials, their biological activity must be clearly understood.

In view of the complexity of local *in vivo* protagonists, a biomaterial triggers host immune reactions after implant prior to MSC recruitment [19, 212]. MSC can interact with immune cells by modulating immune responses and promoting bone regeneration (osteoimmunomodulation); indeed, MSC and immune cells can share secreted cytokines [187, 213]. In addition, immune responses can affect the mechanical properties and performance of biomaterial [214]. However, comprehensive knowledge of the effects of degradable Mg on paracrine signalling between immune cells (PBMC/macrophages) and MSC remains lacking. Thus, the roles of degradable Mg in the immunomodulatory properties of MSC and immune-mediated MSC behaviour, such as MSC migration and osteogenic differentiation, were studied. Furthermore, the underlying mechanisms of MSC differentiation into osteoblasts-like cells were studied.

Tissue repair cells, immune cells, and Mg ions are three protagonists involved in the cascades of degradable Mg-modulated fracture healing. HUCPV are defined as mesenchymal progenitor, multipotent and allogeneic stem cells [203]. Compared to bone marrow mesenchymal stem cells (BMMSC), HUCPV, as an alternative foetal MSC, possess differentiation capacity and immunomodulatory properties as well [203, 215-217]. Macrophages are one of the key types of immune cells (PBMC) that participate in fracture healing given their polarisation plasticity [84]. Mg and Mg-based alloys are potential degradable materials for regenerative applications [218-220]. In the current study, initially pure Mg was selected to avoid an increase in biological complexity due to alloying elements. To widely evaluate the roles of Mg-based biomaterials in osteoblastogenesis, Mg-10Gd, which exhibits good physically properties, was also applied.

To elucidate the interaction between MSC and immune cells, cocultures are widely applied. In the present study, we successfully established indirect *in vitro* coculture in a transwell coculture and conditioned media system. In the transwell coculture system, PBMC were typically seeded on the top of chamber, and HUCPV were seeded in the lower compartment. Cell-cell contact was avoided, allowing monocytes to differentiate into macrophages and HUCPV to differentiate into osteoblast-like cells. Thus, the individual cell type can be evaluated (individual cell proliferation, microscopic examination and gene expression). Moreover, in transwell coculture, interactions between various cell subtypes exist. In addition, MSC can influence various pathways of the immune responses in a paracrine manner [187, 188], so a conditioned media system should be applied. Regarding our conditioned media system, HUCPV-conditioned media were utilised to examine direct M2 differentiation, whereas PBMC-conditioned media induced HUCPV towards a pro-calcific phenotype. Together, these two systems were feasible to mimic the initial inflammation stage (up to 7 days) of Mg-modulated fracture healing. To evaluate the roles of Mg and Mg-10Gd in the following inflammation stage (7-14 days) of fracture healing, a direct coculture system was applied. HUCPV mono- and cocultured with macrophages were separately seeded on Mg/Mg-10Gd. Both cell types could communicate

with each other *via* autocrine or paracrine signalling. Here, a direct coculture system was used to mimic the subsequent *in vivo* phenomenon. In addition, as reported, the osteoblastogenesis process of MSC relied on physical interactions with monocytes or macrophages *via* direct cell-cell contact [165]. In addition, auto/paracrine signals can also be analysed.

As indirect *in vitro* models, results from conditioned media system and transwell coculture were not comparable given their distinct procedures, various conditions (Mg contents and cytokine levels) and particular purposes. As summarized in Fig. 43, more significant differences in cell behaviour were exclusively noted in the transwell coculture system. To be specific, conditioned media system was a static process, whereas transwell coculture was relatively dynamic. For instance, Mg concentrations were normally 3-4 mM in conditioned media system but varied from 0.5 mM to 18 mM in transwell coculture as a consequence of Mg degradation. Moreover, in transwell coculture, the participants were consistently communicating with each other. Hence, as a more suitable indirect system for the evaluation of osteo-immunomodulation [197], transwell coculture is highly relevant for microenvironment studies and allows in-depth tracking of the effects of biodegradable Mg on cell-cell interactions in the initial inflammation stage of biomaterial-mediated fracture healing. In addition, compared to indirect cocultures, higher Mg contents and pH but inconstant osmolarities were observed when cells and materials were cocultured together (direct coculture) in the late inflammation stage.

After fracture, osteogenesis is one of the key processes of fracture healing. This process could be affected by its local environment (e.g., paracrine signalling) and the inflammatory response. The immune response is accompanied by tissue repair reactions in the following 2-10 days [19]. Osteogenesis relies on the good performance of MSC through proliferation and differentiation of osteoblasts. Additionally, clinical tests revealed that the success of MSC-based immunomodulation relies on the assessment of molecule secretion and their interaction with immune cells [213]. Multiple auto/paracrine signalling pathways work closely to modulate osteogenesis.

Bone regeneration is a complex and well-organized physiological process of osteogenesis that remains a medical challenge in the field of orthopaedic surgery. *In vitro* evaluations of Mg-based biomaterials generally focus on several areas: cell growth and cell maturation (activation or differentiation). The current study also provides insight into the development of Mg-based biomaterials in osteogenesis and bone regeneration. This study consists of cellular mechanisms (paracrine signalling), biological therapies (osteo-immunomodulatory properties of MSC and paracrine secretions of inflammatory factors and growth factors), and tissue engineering approaches stimulating bone regeneration by targeting osteoblastogenesis through the interactions between MSC and immune cells.

## **6.1. HUCPV and immune cell growth correlates with Mg contents as well as physiological osmolality and pH**

The environment significantly influences the degradation behaviour of various materials. Furthermore, the physiological environment is rather corrosive. Components (e.g., serum) in body fluids are able to adsorb onto the material's surface and subsequently affect the corrosion behaviour and cell attachment on Mg implants, thus further conditioning the fate of the implant [221]. Considering the ideal medium for growth of both cells (PBMC/macrophages and HUCPV),

$\alpha$ -MEM medium with human blood serum (plasma) or FBS was applied to prevent variance in medium components. In the current studies, pure Mg and Mg-10Gd discs were preincubated in medium with FBS, and improved cell adhesion and viability were observed as other reported [222]. The present results suggest various roles of degradable Mg in stromal and immune cells, such as HUCPV (MSC) and PBMC, and further differentiated macrophages in different *in vitro* systems.

Viability measurements are used to determine the cytotoxicity of immune cells that respond to the material. If the cell response is poor and the viability is reduced, the biomaterial may not be able to support optimal wound healing in the body. Conversely, a significant increase in the viability of immune cells may not be the best result, likely indicating a certain degree of activation of the material [223]. Therefore, the use of immune cell viability as a single method for determining immune response may not be the best method for determining *in vivo* acceptance. In addition, cell proliferation was also used to evaluate cell growth.

Such unstable physical factors could increase cell viability in transwell coculture but suppress them in cell-materials direct coculture. Similarly, DNA contents exhibited the same trend, e.g., higher anti-proliferous effects were measured in the direct coculture system. Taken together, different *in vitro* systems contributed to various physical microenvironments, resulting in the growth of various cells.

In most mammalian cells, the total concentration of cellular Mg ranges from 17 to 20 mM [224], and concentrations in serum range between 0.65 and 1.05 mM [225]. In our system, the Mg concentration in cell culture medium ( $\alpha$ -MEM) was 0.71 mM, which is consistent with the supplier's information. Moreover, many cells maintain Mg at a physiological level, which is irrelevant to extracellular Mg concentrations [74]. In addition,  $Mg^{2+}$  is an important regulator of biological reactions because it is similar to other biologically important metal ions, such as  $Ca^{2+}$  and zinc ( $Zn^{+}$ ) in terms of radius, coordination sphere [226], and soft and hard properties of boundaries [227-229]. In addition,  $Mg^{2+}$  is most likely to replace other metal ions in functional biomolecules, such as enzyme cofactors or enzymes that affect DNA activity [230, 231].

As summarised in the published literature, Mg plays various roles in cell growth, including stimulation of cell proliferation [75] or inhibition of cell number [76]. For instance, in U2OS cells, an osteosarcoma cell line, a slight inhibition of cell proliferation was observed with Mg concentrations greater than 5 mM [77]. Other studies suggested Mg significantly inhibits cell growth in the range of 12.5 to 50 mM [78-82]. As shown in Fig. 19 in transwell coculture, HUCPV exhibit reduced DNA content in presence of Mg (13.81 mM), whereas increased DNA content in HUCPV was observed upon exposure to Mg and P+Mg (5.74 mM and 17.91 mM). In addition, various Mg contents ranging from 0.54 to 17.91 mM promoted PBMC proliferation. Nevertheless, there was no clear difference in presence of Mg in the conditioned media system (Mg: 0.63 to 3.82 mM) regardless of the cell subtype (Fig. 20). Again, as shown in Fig. 32, a significant decrease of DNA contents caused by Mg was noted up to 14 days in a direct coculture system (Mg: approximately 30.00 mM). Viability staining demonstrated that cells were able to grow and proliferate on the materials present in these three *in vitro* systems. The influence of Mg on proliferation was attributed to the chemical properties of metal ions, which are related to molecular or biological activities. The differences in various models, conditions and time points are potentially caused by other metal ions present in metabolic enzymes or

DNA enzymes, such as Ca and Zn [226-229]. Magnesium ions can affect cell proliferation by displacing other ions from their biological functional molecules, thereby interfering with, for example, enzyme cofactors [230, 231]. Thus, the effects of Mg on cellular proliferation could be biphasic [83] or dependent on the microenvironment between materials and cells.

To meet cell culture standards, the physiological osmolality should be around 0.29 Osmol/kg [232]. Cecchinato *et al.* (2015) noted a reduction in viability after cells were seeded on specimens probably due to changed surface properties and microenvironments (pH and osmolality) [233]. Here, the direct system exhibited a higher osmolality (0.36-0.41 Osmol/kg) in cell monoculture or coculture on the material's surface. Thus, the increased osmolality due to Mg-induced cell-material contact may explain the decrease in HUCPV and/or PBMC growth in the presence of degradable Mg or Mg-10Gd.

Changes in pH values exert remarkable influences on cell metabolic activity. In transwell coculture, conditioned media system, and direct coculture, pH values were slightly alkaline (8.0 and 8.6). Some results support the advantageous effects of pH greater than 9.0 on cell viability [234, 235]. Furthermore, alkalosis was reported to increase osteoblastic formation *in vivo* [236]. In addition, an opposite stimulatory effect on cell viability was observed for pH values greater than 8.5 [237]. Hence, pH guides the microenvironment and subsequently influences the growth of bone-forming MSC and regulatory immune cells. In addition, a higher pH was noted in HUCPV and PBMC cocultured in the presence of an Mg disc at days 1 and 4. Under the present circumstances, the high pH could also enhance osteogenic differentiation. Previously, D.A. Bushinsky *et al.* (1983) suggested that a higher pH can induce  $\text{Ca}^{2+}$  influx to stimulate bone formation [238]. In addition to the new bone formation, an increased initial microenvironment pH *in vivo* is associated with a later response in TRAP (tartrate-resistant acid phosphatase)-positive osteoclast-like cells [239]. These results suggest that Mg material-mediated pH variation may play a role in osteogenic activity in the current study.

## **6.2. Interactions between PBMC/macrophages and HUCPV in indirect coculture (transwell coculture and conditioned media) system**

Based on the current results of interactions between PBMC/macrophages and HUCPV in the indirect coculture system (transwell coculture and conditioned media system), the possible roles of degradable Mg on the interactions between immune cells and HUCPV in transwell coculture and conditioned media system are presented in Fig. 43.

The obvious difference caused by Mg and/or immune cells is described in detail as followings:

- Roles of degradable Mg in immunomodulatory properties of HUCPV (in section 6.2.1.);
- 1) Synergetic effects of Mg and HUCPV on attenuating inflammation *via* a moderate inflammatory cytokine production in a transwell coculture system;
- 2) Synergetic effects of Mg and HUCPV on enhancing M2 macrophages phenotype in PBMC in the transwell coculture and conditioned media system.
- Roles of degradable Mg in inflammatory secretion-mediated fracture healing (in sections 6.2.2. and 6.2.3.).

- 1) Synergetic effects of Mg and PBMC on stimulating the migratory ability of HUCPV in a transwell coculture system;
- 2) Enhanced pro-osteogenic potential of HUCPV by Mg but not PBMC in a transwell coculture system.

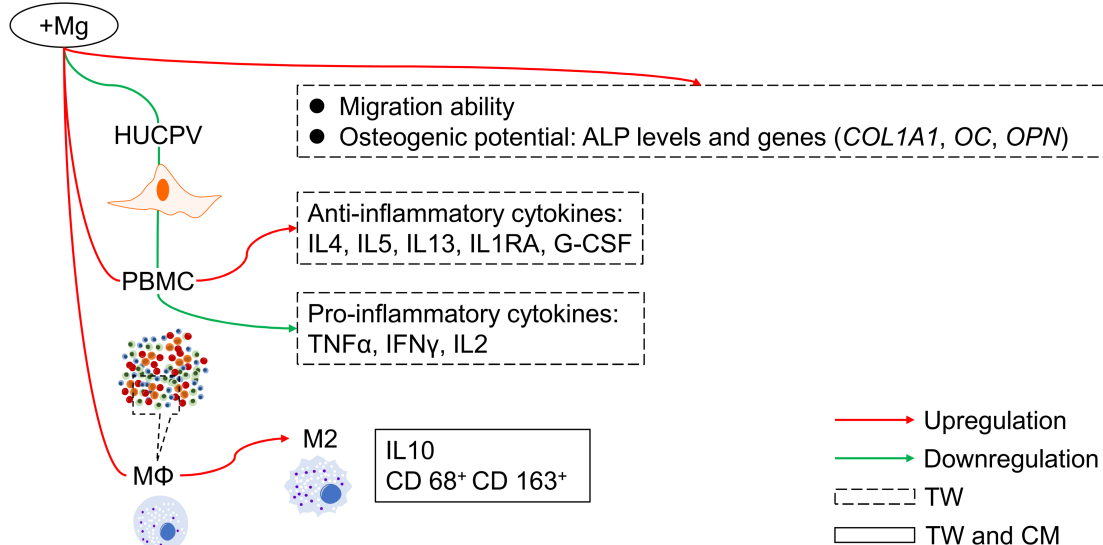


Fig. 43 Possible roles of degradable Mg on the interactions between immune cells and HUCPV in a transwell coculture and conditioned media system. TW: transwell system; CM: conditioned media.

#### 6.2.1. Inflammation

Immune rejection has become a common and end result of the clinical use of popular biological materials. The immune response is caused by the biomaterial's interaction with the immune system, which includes innate and adaptive responses. The innate response includes a wide variety of cells, such as polymorphonuclear cells (granulocytes, eosinophils, and basophils), mononuclear phagocytes (dendritic cells, monocytes and macrophages) and lymphocytes (NK cells, gamma delta T cells and innate lymphoid cells), whereas the adaptive response includes T and B lymphocytes [240]. The immune response to a biomaterial typically comprises non-specific inflammation [241]. PBMC have been widely used as immune cells to evaluate the *in vitro* inflammatory reaction to biomaterials [242, 243]. PBMC consist of lymphocytes (T cells, B cells, NK cells) and monocytes (10-20 %).

Recent studies based on protein secretions tend to use multiple kits to measure several markers of immune cell activation. The advantage of this technique is that it can provide information on the levels of protein secretion associated with pro-inflammatory and anti-inflammatory properties. Therefore, the information obtained from multiple markers, such as multiplex immunoassays, provide more clear information to predict the *in vivo* immune acceptance of a biomaterial.

As an *in vitro* model of the initial immune reaction after biomaterial implantation, secretion of cytokines by PBMC could be instructive. *In vitro* secretion of cytokines by PBMC could serve as a measurement of their activation after *in vivo* implantation. PBMC are able to secrete a broad

series of cytokines in non-specific inflammatory responses, including pro-inflammatory IL1 $\beta$ , IL2, TNF $\alpha$ , and IFNy [244], as well as anti-inflammatory cytokines, such as IL10 [245]. Additionally, immune cell activation mainly focuses on the assessment of secretion of specific cytokines. This is a common method used to characterise the *in vitro* immune response to a biomaterial. Therefore, PBMC were isolated from blood, and released cytokines were measured after 1, 4, and 7 days to follow the initial immune reaction to Mg degradable material. For instance, a high pro-/anti- ratio indicates that the material may cause a serious foreign body reaction, and a high anti-/pro- ratio is associated with pro-healing processes in the body [246, 247]. Common cytokines have been used to evaluate the immune acceptance or rejection for a biomaterial.

Cytokines were investigated using an *in vitro* indirect system-transwell coculture system. In this cell-cell noncontact model, HUCPV and PBMC were seeded on the material's surface or inserts, respectively, in the upper chamber. Monocytes (PBMC) can activate and differentiate into macrophage phenotypes. Meanwhile, without competition for a well's surface, HUCPV can proliferate and/or differentiate into osteoblast-like cells. In addition to preventing cell-cell physical contact, the membrane of transwell coculture allows secretory factors transfer and communication between these two cell types. A previous transwell coculture study reported that the influence of cytokine secretion can be observed between macrophages and MSC [84].

After infiltrating onto injurious tissue or the material's surface, monocytes can be stimulated to secrete cytokines, chemokines and other soluble factors to contribute to injurious tissue repair [248]. Once recruited to targets, monocytes can differentiate into macrophages. The main subtypes of macrophages are M1 and M2 phenotype macrophages, which are vital factors in the resolution of inflammation and tissue remodelling [249-251]. Macrophages are essentially phagocytic and have specific phenotypic characteristics. Macrophages are a group of differentiated immune cells and are polarized by various microenvironments to generate heterogeneous populations with different characteristics and functions. Macrophages are involved in tissue homeostasis, immune reactions and wound healing.

M1 phenotype macrophages are often induced by TLR ligands or T helper type 1 (Th1) cytokines (TNF $\alpha$  and IFNy) [252]. These macrophages release cytokines, such as IL6, IL12, and TNF $\alpha$ , which are associated with pro-inflammatory activities [253]. In addition, M2 phenotype macrophages are polarized by Th2-derived cytokines, including IL4, IL10, IL13, TGF $\beta$  or prostaglandin E2 (PGE2) [252]. They are called "tissue repair macrophages" because they promote tissue repair through immune tolerance and tissue remodelling, removal of debris, and immune regulation [254]. Regarding implant-mediated fracture healing, M2 macrophages also secrete VEGF to support angiogenesis and express immunosuppressive molecules, such as IL10 and IL1RA, which are conducive to the resolution of inflammation [223]. The M2 phenotype has three subtypes: allergic M2a, immune-regulatory M2b, and wound-healing M2c [255, 256]. Despite their importance, M2a and M2b types have a smaller role in biocompatibility assessment. M2c has anti-inflammatory effects and promotes wound healing, extracellular matrix deposition, and tissue remodelling [257, 258]. Additionally, pro-inflammatory secretions of IL1 $\beta$ , IL6, IL8 and TNF $\alpha$  defined the pro-inflammatory response, whereas anti-inflammatory TGF $\beta$ , IL4, IL10, IL13 and IL1RA exhibit anti-inflammation and wound healing activities [257, 258].

In the host immune response after Mg implantation, secretory cytokines are vital players in the regulation of inflammation. Given the pro- and anti-inflammatory properties of MSC and PBMC/macrophages [259, 260], this correlation was evaluated *via* the production of cytokines in the inflammatory panel (TNF $\alpha$ , IFN $\gamma$ , IL1 $\beta$ , IL2, IL4, IL5, IL10, IL13, IL1RA, and G-CSF) in the current transwell coculture system. In the presence of Mg, HUCPV secreted reduced amounts of pro-inflammatory TNF $\alpha$ , IFN $\gamma$ , IL1 $\beta$ , and IL2 on day 4 when the Mg concentrations in supernatants reached 18 mM. Moreover, at days 1 and 7 (Mg concentrations range from 5 and 8 mM), Mg-stimulated PBMC exhibited an intensive inflammation state, releasing higher levels of pro- and anti- inflammatory cytokines; this stimulation is potentially recognised by an inflammatory response and cell activation [31]. In addition, 16 mM Mg did not affect inflammatory cytokine production in PBMC (day 4). Therefore, the effects of degradable Mg on the production of inflammatory cytokines in mono HUCPV or PBMC cultures were biphasic. However, coculture with HUCPV downregulated Mg-induced increased levels of pro-inflammatory cytokines on day 1 (7 mM Mg) and day 4 (18 mM Mg) individually. Similarly, on day 7, HUCPV attenuated the increased secretion of anti-inflammatory cytokines from PBMC exposed to 15 mM Mg (colour scale: dark red to light red). These comparisons in cocultures revealed the immuno-suppressive role of HUCPV interacting with PBMC under Mg stimulation regardless of Mg concentrations. Thus, the interface of the Mg biomaterial-tissue retains a more moderate status of inflammation. This finding is consistent with the study on the immuno-suppressive capacity of MSC wherein MSC regulate the transition from a Th1-driven response to an anti-inflammatory Th2 response. This response is characterised by lower concentrations of TNF $\alpha$ , IFN $\gamma$  and IL2 and increased production of IL4, IL5, IL10 and IL13 [259].

Despite the complexity of cytokine signalling, immunomodulation by MSC is crucial for macrophages maturation [223, 252-254]. The maturation of immune cells mainly also focuses on the assessment of cell surface markers, especially for macrophages. Cell surface markers are variably expressed at different stages of macrophage maturation, so measurement of surface markers in cells in response to a material can enable researchers to determine whether a material induces cell differentiation/maturation [223]. Activated macrophages differentiate into M1 and M2. The CD 86 surface marker is normally used to identify M1 macrophages. Cellular surface markers for all M2 phenotypes include CD 163 or CD 206 [256]. Flow cytometry is one method used by researchers to evaluate cell surface markers, which allows qualification of specific cell types [261].

Multiple studies confirmed that MSC induce M2 polarization [84, 102, 106]. Mg influences M2 macrophage polarization in various microenvironments, as indicated by flow cytometry [262, 263]. Current results of both transwell coculture and conditioned media system suggested that M2 subpopulations increased on day 1 upon coculture with HUCPV. Furthermore, in the presence of Mg, M2 subpopulations were dramatically increased in both transwell coculture and conditioned media system with or without HUCPV. PGE2 also influenced M2 macrophages polarization [264, 265] based on evaluation of prostaglandin E synthase 2 (*PTGES2*) gene expression in HUCPV. *PTGES* is a key enzyme in the production of PGE2 [266]. As shown in Fig. S1 (supplementary data), Mg and/or PBMC upregulated *PTGES2* gene expression at day 7. These results in transwell coculture and conditioned media system conjointly suggest that the M2 percentage of macrophages is probably influenced by Mg and that other factors, such as cell interactions, are also involved (e.g., *PTGES2* expression).

Moreover, mediators, such as TNF $\alpha$ , IL1 $\beta$ , IL4, IL10, HGF (hepatocyte growth factor), PGE2 and IDO (indoleamine 2,3-dioxygenase 1), which are expressed by MSC and released by immune cells [267], lead to the activation of immunosuppressive Treg cells [268] to regulate the last phase and intensity of inflammation in fracture healing. Thus, higher levels of TNF $\alpha$  and IL10 are secreted by PBMC under Mg stimulation for 7 days, and upregulated prostaglandin E synthase 2 (*PTGES2*) gene expression is noted on day 7 (Fig. S1). These findings indicate that Mg positively influences the immuno-regulatory role of MSC on PBMC via multiple factors.

### 6.2.2. Migration/wound healing

During fracture healing, MSC initially migrate to the bone injury site to participate in healing before differentiating into osteoblasts-like cells [267, 269-271]. MSC migrate into fracture sites to participate in repair of damaged tissue and fracture healing [267, 269-271].

MSC recruitment is influenced by a series of secretory cytokines, such as MCP-1, MIP-1 $\alpha/\beta$ , and IL8 [125, 272]. For instance, MCP-1 acts as a homing factor to recruit macrophages and MSC into the sites of bone repair [273, 274]. Other reports also implicate the stimulation of MCP-1 on ultimate bone formation by promoting callus formation and accelerating bone resorption [275, 276]. In addition, MIP-1 $\alpha/\beta$  contributes to migration of immune cells and regulates bone regeneration by controlling the dynamic balance of osteoblasts and osteoclasts [277, 278]. IL8 not only enhances therapeutic effects of MSC on bone regeneration but also stimulates osteoclasts activity and bone resorption [279, 280]. GM-CSF is also well-known for stimulating human MSC mobilization [281].

As shown in Fig. S2, cytokines inducing MSC migration, such as IL8, GM-CSF, MCP-1, and MIP-1 $\alpha/\beta$  in PBMC, were dramatically upregulated by Mg, especially on days 1 and 7. Thus, attempting to further examine the migration potency of HUCPV affected by Mg, an *in vitro* wound healing assay was performed with supernatants collected at day 1 from various transwell coculture conditions, including Mg, P, and P+Mg.

As previously shown in section 5.1.5, compared with  $\alpha$ -MEM (Ctr), Mg or PBMC (P) or both (P+Mg) significantly stimulated HUCPV migration into the closure area in transwell coculture. Similarly, a stimulated migratory distance of HUCPV was observed in P+Mg compared with HUCPV in P. The results revealed that HUCPV exhibits an increased capacity to migrate when cultured with Mg and/or PBMC for 24 hours.

In the transwell coculture system, the addition of Mg discs resulted in a concentration-dependent stimulation of IL8, MCP-1, and MIP-1 $\alpha/\beta$ . Indeed, higher concentrations of Mg (4-19 mM) upregulated extracellular IL8, MCP-1, and MIP-1 $\alpha/\beta$  levels. Although enhanced HUCPV migration was measured in transwell coculture supernatant (4-8 mM Mg), no significant migration was observed in conditioned media system groups with Mg concentrations of 0.5-4 mM. It is therefore reasonable to assume that the effects of Mg on HUCPV migration are concentration dependent. To some extent, local Mg $^{2+}$  concentrations may mediate HUCPV migration since the shift of local extracellular Mg $^{2+}$  and Ca $^{2+}$  impacts cell-cell and cell-extracellular matrix interactions during would healing [282].

Therefore, the enhanced migratory ability of HUCPV was not only due to Mg itself (Mg contents) but also due to the involvement of Mg-induced paracrine signalling of IL8, GM-CSF, MCP-1, and MIP-1 $\alpha/\beta$ .

#### **6.2.3. Osteogenic potential of HUCPV**

High ALP activity and specific upregulated pro-osteogenic genes are indicators osteogenic differentiation of MSC populations. It is well documented that Mg-based biomaterials enhance pro-osteogenic activities of MSC [283, 284]. In addition, evidence supports roles of monocytes in upregulating the osteogenic potential of MSC [285].

Compared with the conditioned media system, the transwell coculture system induces HUCPV differentiation towards a pro-calcific phenotype (ALP activity). In the evaluation of osteogenesis in the conditioned media system, PBMC-, Mg- or (PBMC+Mg)-conditioned media induced increased *COL1A1* and *OPN* gene expression. In the transwell coculture system, Mg alone and PBMC+Mg induced various osteogenic parameters in HUCPV, such as increased ALP activity, upregulated collagen synthesis, and OC and *OPN* expression. Due to the more interactive communication between HUCPV and PBMC in transwell coculture model, these results particularly imply the pro-osteogenic roles of Mg but not PBMC.

In addition, increased levels of IL12, bFGF, and VEGF are recognized as markers of foetal-derived osteoblastogenesis [217]. As shown in Fig. S3, Mg elevated the production of bFGF (H vs. H+Mg at day 1), VEGF (H vs. H+Mg, or H+P vs. H+P+Mg at day 7), and IL12 (H vs. H+Mg at day 7). Interestingly, at days 1 and 4, PBMC significantly reduce production of these three cytokines (H vs. H+P or H+Mg vs. H+P+Mg).

Mg stimulated increased secretions of IL12, bFGF, and VEGF and induced various osteogenic parameters, such as ALP activity, collagen synthesis and OC and *OPN* expression, indicating that Mg enhance the osteogenic differentiation of MSC [283, 284]. As reported, monocytes enhance osteogenic gene expression in MSC [285] and further promote osteoblast formation [165, 166]. Furthermore, it has also been well-documented that macrophages engage in the degradation of biomaterials and contribute to the osteogenic behaviour of MSC, which aid in bone regeneration [286]. The immune microenvironment can effectively stimulate osteogenesis; therefore, the roles of degradable Mg via paracrine secretions in immune-mediated osteogenesis will be further studied for longer periods (7 days reflect early osteogenesis).

### **6.3. Mechanisms of macrophage-mediated osteogenic activity of HUCPV in direct coculture systems**

Communication between MSC and immune cells induces MSC differentiation into pre-osteoblasts and subsequently mature osteoblasts. These processes normally occur after MSC recruitment until they direct contact with local immune cells or implants.

The applied direct coculture model clearly showed the improved osteogenic ability of HUCPV in the context of Mg, and a more pronounced effect was noted with Mg-10Gd. In detail, both materials induced ALP secretion and upregulated expression of specific osteogenic gene (*ALP*, *OC*, and *OPN*) on days 7 and 14 compared with control groups. Furthermore, Mg-10Gd was a more efficient stimulator than pure Mg. Importantly, such positive regulation of bone-forming

differentiation is not only dependent on formerly discussed  $Mg^{2+}$  released by materials but also relies on macrophage production of regulatory factors, including inflammatory factors (OSM/IL6,  $TNF\alpha$  and  $IL1\beta$ ) and growth factors (BMP6).

Summarized results from the direct coculture system are presented in Fig. 44. The possible mechanisms of Mg-based material-induced osteogenic differentiation include the following:

- Stimulatory roles of OSM and gp130;
- Stimulatory roles of BMP6;
- Inhibitory roles of  $TNF\alpha$  and  $IL1\beta$ .

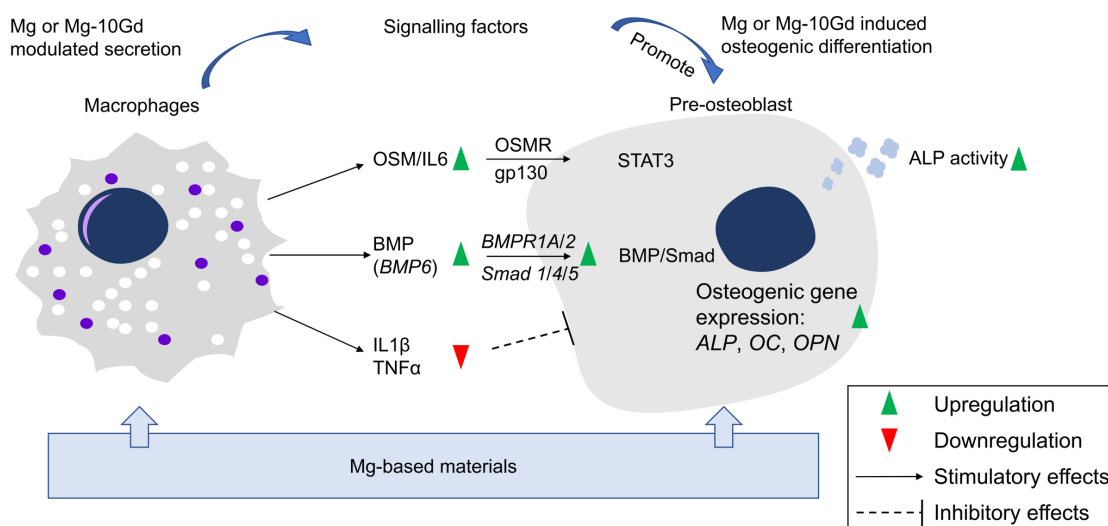


Fig. 44 Mechanisms of Mg-based material-induced secretion of signalling factors by macrophages promoting the osteogenic differentiation of HUCPV in a direct coculture system.

One method to measure inflammatory cytokines secreted from immune cells, especially macrophages, is ELISA. ELISA is a plate-based measurement technique that can quantify specific proteins in liquid samples using highly specific antibodies linked to enzymes. Detection is achieved by evaluating the activity of the coupled enzyme through colour changes. In the current test, ELISA was used to quantify the concentration of inflammatory cytokines from macrophages exposed to Mg and Mg-10Gd. Single marker assays include  $TNF\alpha$ ,  $IL1\beta$ ,  $IL6$  and OSM.

The present study also focuses on gene expression of growth factor markers based on immune cells' interactions with biomaterials. A more modern method of gene expression analysis, namely RT-qPCR [287] uses oligonucleotide probes specifically designed to anneal to the target gene sequence to quantify the target DNA amplified from the sample in real time. During the amplification process, the probe is cleaved to release specific fluorescent labels. In many cycles, gene-specific fluorescence is measured in real time and is proportional to the starting amount of each target gene in the template sample. Target gene expression is calculated relative to the baseline sample (reference genes). This analysis reduces the experiment time, thereby improving the efficiency of biomaterial evaluation. In the current study, *BMP6* gene expression in response to Mg/Mg-10Gd was analysed. The following cascades

related to the BMP/Smad signalling pathway, such as *BMPR1A*, *BMPR2*, and *Smad 1/4/5/8*, were also analysed.

### 6.3.1. OSM and gp130 dependency

OSM, a multifunctional cytokine of the IL6 family, has been implicated in the inflammation and bone tissue regeneration. OSM is produced by activated CD 14<sup>+</sup> monocytes/macrophages and enhances MSC osteogenesis. This stimulation could be inhibited using neutralizing antibodies to OSM, OSM receptor (OSMR and gp130), or downstream STAT3 pathway signal transducers [166]. Another recent study also demonstrated that the pro-osteogenic differentiation of human adipose-derived stem cells was stimulated after OSM pre-treatment [164]. IL6 is secreted by immune cells and acts as a pro-inflammatory cytokine, but it is also produced by stromal cells to promote osteogenesis [159]. Research indicates that expression of osteogenic genes, such as *COL1A1* and *OPN*, is not altered in MC3T3-E1 cells by IL6, but ALP activity is increased by IL6 and reduced upon IL6 neutralization [288].

These lines of evidence collectively consolidate the pro-osteogenic induction of OSM and IL6. However, the roles of Mg/Mg-10Gd in OSM/IL6-mediated pro-osteogenic activity are not well characterized. Hence, in the present study, OSM production was stimulated in direct cocultures, particularly upon exposure to Mg and Mg-10Gd. Secretion of pro-inflammatory IL6 in HUCPV monoculture and cocultures was significantly decreased by materials at day 7 but restored after an additional 7 days. Meanwhile, a clear difference between HUCPV alone and cocultures under Mg stimulation was noted on day 14. The IL6 difference was consistent with the highest ALP levels and osteogenic-specific gene expression in HUCPV-macrophage cocultures exposed to materials. In addition, anti-human OSM and anti-human gp130 inhibit the functions of osteogenic factors (OSM and IL6) and clearly antagonized extracellular ALP activity in osteogenic differentiation of HUCPV cocultured with Mg and Mg-10Gd.

Taken together, the current study highlights that Mg and Mg-10Gd mediate pro-osteogenic activity through regulating OSM/IL6, and the process is OSM and gp130 dependent.

### 6.3.2. Stimulatory roles of BMP/Smad signals

Macrophages have a role in BMP-dependent differentiation of MSC *via* production of BMPs. BMP2 or BMP6 bind to BMP receptors, such as BMPR1 and BMPR2, which subsequently activate Smad signalling receptors and increase osteogenic differentiation of MSC.

In direct contact cocultures, *BMP6* upregulation was first demonstrated in macrophages exposed to Mg-based materials. BMP proteins induce Smad 1/5/8 phosphorylation. Smad 4 is recognized as vital player in the BMP/Smad signalling pathway involved in osteogenic differentiation [289, 290]. Increased expression of Smad signalling receptors, such as *BMPR1A*, *BMPR2*, and *Smad 1/4/5/8*, was observed in cocultures with Mg and Mg-10Gd compared with cocultures without biomaterials (controls).

BMP2 enhances bioactivity [291, 292] and repair [293] incorporating with Mg-based biomaterials. Accordingly, present findings support the hypothesis that macrophages express the *BMP6* gene, which synergizes with Mg and Mg-10Gd, further regulating the osteogenic differentiation of HUCPV *via* the BMP/Smad signalling pathway. Hence, BMP protein

represents a promising mediator of Mg-based biomaterials by enhancing bioactivity and tissue repair.

### 6.3.3. Inhibitory roles of TNF $\alpha$ and IL1 $\beta$

Increasing evidence suggests that the secretion of macrophages in response to Mg-based biomaterials induced profound changes in MSC differentiation.

In particular, upon exposure to Mg ions or Mg-based materials, macrophages are polarized into an anti-inflammatory phenotype termed M2 [263, 294-296]. M2 phenotype macrophages secrete less TNF $\alpha$ , IL1 $\beta$  and release higher level of IL10. Furthermore, a dose-dependent, negative correlation between TNF $\alpha$  and IL1 $\beta$  production and osteogenic differentiation was confirmed [297-299]. In current experiments, a significant decrease in TNF $\alpha$  and IL1 $\beta$  were observed in macrophages (-/+HUCPV) when seeded on Mg and Mg-10Gd, supporting the hypothesis of anti-inflammatory effects of osteoblastogenesis. Similar results were also shown in other studies using a Mg–Ca phosphate cement extract, in which the pro-inflammatory cytokines, including TNF $\alpha$  and IL-6, were less expressed in macrophages [80].

In summary, excessive production of pro-inflammatory cytokines (TNF $\alpha$  and IL1 $\beta$ ) could cause the loss of implants, whereas suitable concentrations of pro-inflammatory factors (OSM and IL6) could synergize to stimulate bone formation. Thus, the balance of pro- and anti-inflammation is necessary to consider as a feature to evaluate the property of biomaterials. As degradable biomaterials, Mg and Mg-10Gd result in enhanced osteogenic differentiation of HUCPV based upon the release of osteogenic factors, such as proteins (OSM/IL6) and growth factors (*BMP6*).

## 7. Outlook

Biomaterial-mediated bone healing involves early inflammation, bone formation and remodelling phases. The specific stages include coagulation, immune response, and bone formation. The early stage of tissue repair is mainly modulated by an immune response, where the majority of monocytes are activated into pro-inflammatory macrophages (phenotype M1). The switch pattern of the macrophage phenotype to an anti-inflammatory phenotype (M2) occurs in the bone formation phase, resulting in osteogenic-related cytokine secretion to manage the formation of new tissue and bone. A continuous M1 phenotype contributes to chronic inflammation, whereas excessive M2 induces fibrous encapsulation, which could be enhanced by the secreted cytokines and ultimately lead to biomaterial implantation failure. In light of unavoidable immune response, a bone substitute material could be designed to utilise the crosstalk between immune cells and MSC and consequently improve bone regeneration.

Based on results from the current study, the outlook for the orthopaedic applications are presented from two aspects:

- Possible strategies for bone substitute materials;

e.g., modification by incorporating relevant metallic ions or specific cellular mechanisms (auto/paracrine signalling; secretions of inflammatory factors and growth factors).

- Therapeutic potential of utilizing MSC (HUCPV)-macrophages for bone formation.

e.g., biological therapies (osteo-immunomodulatory properties of MSC) as well as tissue engineering approaches stimulating bone regeneration by targeting osteoblastogenesis through interactions between MSC and immune cells.

### 7.1. Possible strategies for bone substitute materials

Bone substitute materials could be improved to modulate the immune response of PBMC, macrophages, and lymphocytes; specifically, the surface properties (surface roughness, surface wettability and surface charge), particle size, pore size, and ion release properties could be improved [300-302]. Hence, based on the results of this study, Mg-based biomaterials could be manufactured to form more desired immunomodulation properties based on the following methodologies.

#### 7.1.1. Modification by incorporation of Ca, Strontium (Sr), and Zn

The consistent corrosion of materials after implantation is mainly dominated by physiological microenvironment and cell-mediated material dissolution. Many metals or inorganic elements could be applied to optimize the degradation while controlling the release profile from materials that are important in interacting with the microenvironment (Fig. 45).

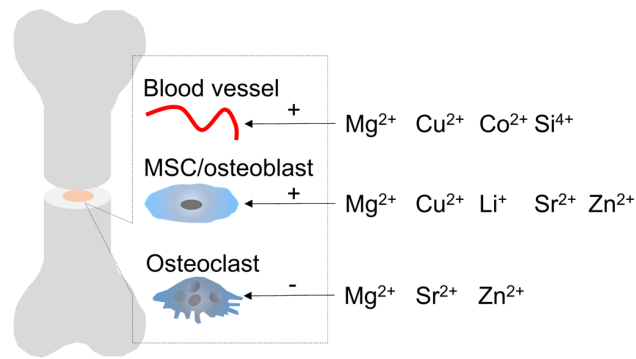


Fig. 45 Common specific targets of relevant metallic ions and their therapeutic roles in the human body. The figure is adapted from previous work [303] with permission under the license of "CC BY 4.0": <https://creativecommons.org/licenses/by/4.0/>.

For instance, Ti coated with Sr-, Mg-, and Si-containing  $\text{Sr}_2\text{MgSi}_2\text{O}_7$  (SMS) ceramics promote the anti-inflammatory M2 phenotype and suppress inflammation *via* inhibiting Wnt family member 5A (Wnt5A)/Ca<sup>2+</sup> and TLR pathways in macrophages [40]. Additionally, this SMS coating maintains comparable osteogenesis and reduces osteoclast activities. Another study based on Ti conducted with nutrient element-based bioceramic coatings ( $\text{Sr}_2\text{ZnSi}_2\text{O}_7$  (Szs)) reported that coating enhance osteogenic differentiation of bone marrow-MSC but downregulate osteoclastogenesis *via* inhibition of the RANKL (receptor activator of nuclear factor kappa-B ligand)/RANK (receptor activator of nuclear factor kappa-B) pathway [304]. The Ca element was also a potential candidate to decrease M1 polarization and the M2 phenotype through the TLR signalling pathway, in which Ca-incorporated implants ( $\text{Ca}_{11}\text{Si}_4\text{B}_2\text{O}_{22}$ ) improve osteogenesis [305].

Current findings suggest that Mg possesses osteo-immunomodulatory properties. Thus, specific metallic elements could be incorporated with Mg to design a bone substitute material to achieve improved inflammation and osteogenesis.

### 7.1.2. Functionalization with inflammatory mediators (IL4, IL10 and OSM) and growth factors (TGF $\beta$ 1, BMP and VEGF)

Many cytokines and large molecules, such as IL4, IL10, and LPS, mediate inflammation *via* influencing immune cell activities. Importantly, these factors cooperate with biomaterials to improve clinical outcomes.

For instance, IL4 delivery by osmotic pumps was reported to induce M2-like phenotype polarization from macrophages *in vitro* [306]. Additionally, the release of such components could be controlled by materials to modify inflammation status. The release of components (IL4/IL10/TGF $\beta$ 1) loaded on gelatine/tyraminated films could be controlled to increase tissue repair by retaining an anti-inflammatory environment with decreased levels of pro-inflammatory cytokines [307]. As documented in the current results, secretory mediators not only regulate inflammation but also modulate osteoblastogenesis. OSM carried by an inactive demineralized bone matrix (DBM) stimulated osteogenesis in a rabbit model [181]. Importantly, BMP2 and BMP7 have been approved for clinical trials in open fractures of long bones, non-unions and

spinal fusion [308]. Moreover, BMP2 and VEGF are upregulated in macrophages and MSC seeded on Ca-incorporated materials, leading to activation of BMP2 signalling and subsequent osteogenic cascades [305]. Other reports also revealed that factors used for coating are associated with osteogenic outcomes. For example, scaffolds could be doped with osteogenic-specific BMP to regulate bone formation [309]. BMP coating on metal implants represents a strategy to increase osteogenic differentiation in a dose-dependent manner [182]. Moreover, BMP2 incorporation into the coating increases osteoinductive efficacy and attenuates inflammation compared with direct absorption on implants [310]. The results of the current study suggest that Mg ions potentially could be designed as carriers or scaffolds to achieve good performance of fracture healing. Additionally, the coating of cytokines and growth factors (IL4, IL10, OSM, TGF $\beta$ 1, BMP and VEGF etc.) on Mg-based biomaterials could represent a method to improve clinical trials of fracture healing.

#### **7.1.3. Combinations with anti-inflammatory drugs**

To prevent and even control local inflammation after biomaterial implantation, many applications of implantable medical devices have been developed to modulate the release or administration of anti-inflammatory drugs.

For instance, inflammatory IFNy and TNF $\alpha$  are reduced by local injection of aspirin around the stem cell implantation site to markedly improve bone regeneration [311]. The dynamics or outcomes of these inflammatory-active agents could be modulated by the properties of biomaterials. The release of dexamethasone, an anti-inflammatory medication, could be prolonged by microsphere-like materials [312]. The multilayer surface could confer anti-inflammatory properties of material to monocytes [313].

These drugs and their targets of interest could be another avenue to develop Mg-based biomaterials and regulate *in vivo* inflammation. In addition, Mg incorporation could increase the anti-inflammatory potential of a biomaterial.

### **7.2. Therapeutic potential of utilising MSC (HUCPV)-macrophages for bone formation**

Furthermore, current findings regarding the interactions of immune cells and MSC underscore the value of Mg in tissue regeneration. MSC have been widely applied in tissue repair in the field of regenerative medicine given widely available resources, differentiation potential, and immune-modulatory effects on the host microenvironment. In addition, an implant is a crucial carrier to act as biotic and abiotic graft scaffold [314].

Potential cell-based therapy could also be employed for bone regeneration. More attention has focused on either bone-forming MSC or immunoregulatory macrophages. However, minimal research has focused on targeting the interaction between MSC and macrophages to stimulate bone formation. For instance, MSC has been used for bone regenerative therapy *via* differentiating into endothelium of blood vessels, cartilage, and bone at the site of fracture. Regarding macrophages, several methods were optimized to control macrophages for bone regenerative applications, such as delivering induced M1 or M2 macrophages into fracture sites

and manipulating the number or phenotype of macrophages with recombinant molecules and biomaterials [315].

Based on previous and current research, two possible methods to enhance bone regeneration through the crosstalk of MSC and macrophages are outlined:

- To more efficiently attract tissue repair cells (MSC) to into injurious sites, migratory molecules (IL8, MCP-1, and MIP-1 $\alpha/\beta$ ) could be stimulated or coupled with Mg-based materials.
- To induce macrophages towards a tissue regenerative M2 phenotype, Mg-based materials (Mg ions) or agonists/inducing agents of IL4/13 or BMP could be applied.

Some studies have demonstrated the possibility of stimulating bone formation with these bioactive molecules. Wood *et al.* (2014) investigated the function of MCP-1 to promote wound healing in diabetics through restoring the macrophages response [316]. Using a chick chorioallantois membrane assay, MCP-1 mediated TGF $\beta$  activity in the formation of new blood vessels, and this effect could be attenuated by its blocking antibody [317]. MCP-1 and its blocking antibody regulated MSC migration [126]. Inflammatory chemotactic agents (IL8/MCP-1/MIP-1) also attract human MSC in the interface culture of ischemic brain [125]. Engelhardt *et al.* suggested IL8 and MCP-1 contribute to the filtration of leukocytes and thus examined inflammation and reparative activities [318]. The current study on the migratory ability of HUCPV revealed increased levels of migration-related cytokines (GM-CSF, IL8, MCP-1 and MIP-1 $\alpha/\beta$ ) in PBMC induced by Mg in transwell coculture, which was accompanied by enhanced migratory distances of HUCPV (wound healing assay). These findings indicate that Mg could represent a promising strategy to stimulate bone formation.

Several other studies consolidate such integration between inflammation and bone regeneration. For instance, MSC induce the M2 phenotype of macrophage polarization at inflammation sites in the mixture of MSC and macrophages [102, 106]. IL4 and/or IL13 induce M2-like macrophages in an anti-inflammatory environment [319, 320]. Peroxisome proliferator-activated receptor gamma (PPAR $\gamma$ ), an inducer of inflammation, is activated to upregulate M2-like macrophages to produce an anti-inflammatory effect [321].

In addition, materials modulate immunoregulation between tissue healing and inflammation *via* stimulating M2-inducible factors. Therefore, a local anti-inflammation effect could be expected. For instance, Bartneck *et al.* (2015) reported that 3D hydrogel-coated nanofibers induce macrophages with tissue-healing properties [322]. The injection of pro-resolution mediators resulted in increased numbers of M2 macrophages on the crosslinked chitosan (CH) scaffold *in vivo* using a mouse air-pouch model of inflammation [323]. One study indicated the potential for Mg to integrate osteogenesis and macrophage activity *via* the polarizing M2 phenotype and upregulating osteogenic genes, such as BMP2/6 and VEGF, in macrophages [324]. This finding is consistent with the results of the current study on the stimulatory roles of Mg in *BMP6* expression-mediated osteoblastogenesis.

## 8. Summary and conclusion

The dynamic processes of inflammation and bone regeneration in fracture healing are dependent on a close interplay between material-induced immune cell behaviours and bone-forming cell behaviours. Our findings demonstrated that degradable Mg influenced HUCPV-PBMC/macrophage interactions. The interplay of these cells is based on mediators, such as secretory cytokines and microenvironment (Mg concentrations, pH, and osmolality). Mg could affect the cells' behaviour in cooperation with other cell types.

In the early stage (indirect coculture: transwell coculture and conditioned media system; within 7 days) of inflammation:

- Mg collaborated with HUCPV to attenuate inflammation *via* moderate cytokine release accompanied by the induction of the pro-healing M2 macrophage phenotype;
- Mg synergizes with immune cells (PBMC) to stimulate HUCPV migration;
- The pro-osteogenic potential of HUCPV could be influenced by Mg but not PBMC.

Thus, suppressed inflammation and faster bone tissue repair could be expected based on the osteo-immunomodulatory properties of degradable Mg.

In the later stage (direct coculture system; 7-14 days) of inflammation, paracrine secretion from macrophages, such as inflammatory cytokines (OSM, IL6, TNF $\alpha$ , and IL1 $\beta$ ), and growth factors (BMP6) are synergistically involved in Mg- and Mg-10Gd-modulated osteogenic differentiation.

Taken together, the present findings emphasize the osteo-immunomodulatory properties of Mg. Specifically, Mg could create a beneficial immune reaction for pro-osteogenic differentiation of MSC; thus, increased bone regenerative formation and injurious tissue healing can be expected.

# Reference

- [1] T.A. Einhorn, L.C. Gerstenfeld, Fracture healing: mechanisms and interventions, *Nature Reviews Rheumatology* 11(1) (2015) 45-54.  
<https://doi.org/10.1038/nrrheum.2014.164>
- [2] S. Amin, S.J. Achenbach, E.J. Atkinson, S. Khosla, L.J. Melton III, Trends in fracture incidence: a population - based study over 20 years, *Journal of Bone and Mineral Research* 29(3) (2014) 581-589.  
<https://doi.org/10.1002/jbm.2072>
- [3] K.L. Naylor, E. McArthur, W.D. Leslie, L.-A. Fraser, S.A. Jamal, S.M. Cadarette, J.G. Pouget, C.E. Lok, A.B. Hodsman, J.D. Adachi, The three-year incidence of fracture in chronic kidney disease, *Kidney International* 86(4) (2014) 810-818.  
<https://doi.org/10.1038/ki.2013.547>
- [4] T.L. Nickolas, M.B. Leonard, E. Shane, Chronic kidney disease and bone fracture: a growing concern, *Kidney International* 74(6) (2008) 721-731.  
<https://doi.org/10.1038/ki.2008.264>
- [5] J.F. Ludvigsson, K. Michaëlsson, A. Ekbom, S.M. Montgomery, Coeliac disease and the risk of fractures—a general population - based cohort study, *Alimentary Pharmacology & Therapeutics* 25(3) (2007) 273-285.  
<https://doi.org/10.1111/j.1365-2036.2006.03203.x>
- [6] J. Collier, Bone disorders in chronic liver disease, *Hepatology* 46(4) (2007) 1271-1278.  
<https://doi.org/10.1002/hep.21852>
- [7] D.F. Williams, On the nature of biomaterials, *Biomaterials* 30(30) (2009) 5897-5909.  
<https://doi.org/10.1016/j.biomaterials.2009.07.027>
- [8] M. Niinomi, C.J. Boehlert, Titanium alloys for biomedical applications, in: M. Niinomi, T. Narushima, M. Nakai (Eds.), *Advances in Metallic Biomaterials*, Springer2015, pp. 179-213.  
[https://doi.org/10.1007/978-3-662-46836-4\\_8](https://doi.org/10.1007/978-3-662-46836-4_8)
- [9] V. Huynh, N.K. Ngo, T.D. Golden, Surface activation and pretreatments for biocompatible metals and alloys used in biomedical applications, *International Journal of Biomaterials* 2019 (2019) 1-21.  
<https://doi.org/10.1155/2019/3806504>
- [10] R.L. Buly, M.H. Huo, E. Salvati, W. Brien, M. Bansal, Titanium wear debris in failed cemented total hip arthroplasty: an analysis of 71 cases, *The Journal of Arthroplasty* 7(3) (1992) 315-323.  
[https://doi.org/10.1016/0883-5403\(92\)90056-v](https://doi.org/10.1016/0883-5403(92)90056-v)
- [11] H.S. Brar, M.O. Platt, M. Sarntinoranont, P.I. Martin, M.V. Manuel, Magnesium as a biodegradable and bioabsorbable material for medical implants, *JOM* 61(9) (2009) 31-34.  
<https://doi.org/10.1007/s11837-009-0129-0>
- [12] F. Witte, H. Ulrich, M. Rudert, E. Willbold, Biodegradable magnesium scaffolds: part I: appropriate inflammatory response, *Journal of Biomedical Materials Research Part A* 81A(3) (2007) 748-756.  
<https://doi.org/10.1002/jbm.a.31170>

- [13] Q. Peng, K. Li, Z. Han, E. Wang, Z. Xu, R. Liu, Y. Tian, Degradable magnesium - based implant materials with anti - inflammatory activity, *Journal of Biomedical Materials Research Part A* 101A(7) (2013) 1898-1906.  
<https://doi.org/10.1002/jbm.a.34494>
- [14] F. Witte, H. Ulrich, C. Palm, E. Willbold, Biodegradable magnesium scaffolds: part II: peri - implant bone remodeling, *Journal of Biomedical Materials Research Part A* 81A(3) (2007) 757-765.  
<https://doi.org/10.1002/jbm.a.31293>
- [15] A. Stoch, W. Jastrzębski, A. Brożek, J. Stoch, J. Szaraniec, B. Trybalska, G. Kmita, FTIR absorption–reflection study of biomimetic growth of phosphates on titanium implants, *Journal of Molecular Structure* 555(1-3) (2000) 375-382.  
[https://doi.org/10.1016/s0022-2860\(00\)00623-2](https://doi.org/10.1016/s0022-2860(00)00623-2)
- [16] S.K. Nishimoto, M. Nishimoto, S.-W. Park, K.-M. Lee, H.-S. Kim, J.-T. Koh, J.L. Ong, Y. Liu, Y. Yang, The effect of titanium surface roughening on protein absorption, cell attachment, and cell spreading, *International Journal of Oral & Maxillofacial Implants* 23(4) (2008) 675-680.  
<https://www.ncbi.nlm.nih.gov/pubmed/18807564>
- [17] P. Dearnley, A review of metallic, ceramic and surface-treated metals used for bearing surfaces in human joint replacements, *Proceedings of the Institution of Mechanical Engineers, Part H: Journal of Engineering in Medicine* 213(2) (1999) 107-135.  
<https://doi.org/10.1243/0954411991534843>
- [18] M. Vandrovčová, L. Bacakova, Adhesion, growth and differentiation of osteoblasts on surface-modified materials developed for bone implants, *Physiological Research* 60(3) (2011) 403-417.  
<https://doi.org/10.33549/physiolres.932045>
- [19] R. Sridharan, A.R. Cameron, D.J. Kelly, C.J. Kearney, F.J. O'Brien, Biomaterial based modulation of macrophage polarization: a review and suggested design principles, *Materials Today* 18(6) (2015) 313-325.  
<https://doi.org/10.1016/j.mattod.2015.01.019>
- [20] L.M. Burke, Sports nutrition, in: J.W.E. Jr., I.A. Macdonald, S.H. Zeisel (Eds.), *Present Knowledge in Nutrition*, John Wiley & Sons2012, pp. 669-687.  
<https://doi.org/10.1002/9781119946045>
- [21] U. Gröber, J. Schmidt, K. Kisters, Magnesium in prevention and therapy, *Nutrients* 7(9) (2015) 8199-8226.  
<https://doi.org/10.3390/nu7095388>
- [22] A.S. Mildvan, Role of magnesium and other divalent cations in ATP-utilizing enzymes, *Magnesium* 6(1) (1987) 28-33.  
<https://www.ncbi.nlm.nih.gov/pubmed/3029516>
- [23] T. Mert, Y. Gunes, M. Guven, I. Gunay, D. Ozcengiz, Effects of calcium and magnesium on peripheral nerve conduction, *Polish Journal of Pharmacology* 55(1) (2003) 25-30.  
<https://www.ncbi.nlm.nih.gov/pubmed/12856822>
- [24] J.D. Potter, S.P. Robertson, J.D. Johnson, Magnesium and the regulation of muscle contraction, *Federation Proceedings* 40(12) (1981) 2653-2656.  
<https://www.ncbi.nlm.nih.gov/pubmed/7286246>

- [25] L.A. Sonna, C.A. Hirshman, T.L. Croxton, Role of calcium channel blockade in relaxation of tracheal smooth muscle by extracellular Mg<sup>2+</sup>, American Journal of Physiology-Lung Cellular and Molecular Physiology 271(2) (1996) L251-L257.  
<https://doi.org/10.1152/ajplung.1996.271.2.l251>
- [26] H. Chahal, S.W. d'Souza, A.J. Barson, P. Slater, Modulation by magnesium of N-methyl-D-aspartate receptors in developing human brain, Archives of Disease in Childhood-Fetal and Neonatal Edition 78(2) (1998) F116-F120.  
<https://doi.org/10.1136/fn.78.2.f116>
- [27] C.Y. Lin, P.S. Tsai, Y.C. Hung, C.J. Huang, L-type calcium channels are involved in mediating the anti-inflammatory effects of magnesium sulphate, British Journal of Anaesthesia 104(1) (2009) 44-51.  
<https://doi.org/10.1093/bja/aep336>
- [28] Y. Rayssiguier, P. Libako, W. Nowacki, E. Rock, Magnesium deficiency and metabolic syndrome: stress and inflammation may reflect calcium activation, Magnesium Research 23(2) (2010) 73-80.  
<https://doi.org/10.1684/mrh.2010.0208>
- [29] M.I. Tejero-Taldo, J.H. Kramer, I.T. Mak, A.M. Komarov, W.B. Weglicki, The nerve-heart connection in the pro-oxidant response to Mg-deficiency, Heart Failure Reviews 11(1) (2006) 35-44.  
<https://doi.org/10.1007/s10741-006-9191-7>
- [30] W.B. Weglicki, T.M. Phillips, A.M. Freedman, M.M. Cassidy, B.F. Dickens, Magnesium-deficiency elevates circulating levels of inflammatory cytokines and endothelin, Molecular and Cellular Biochemistry 110(2) (1992) 169-173.  
<https://doi.org/10.1007/bf02454195>
- [31] A. Mazur, J.A. Maier, E. Rock, E. Gueux, W. Nowacki, Y. Rayssiguier, Magnesium and the inflammatory response: potential physiopathological implications, Archives of Biochemistry and Biophysics 458(1) (2007) 48-56.  
<https://doi.org/10.1016/j.abb.2006.03.031>
- [32] D.E. King, Inflammation and elevation of C-reactive protein: does magnesium play a key role?, Magnesium Research 22(2) (2009) 57-59.  
<https://doi.org/10.1684/mrh.2009.0161>
- [33] D. Zhu, J. You, N. Zhao, H. Xu, Magnesium Regulates Endothelial Barrier Functions through TRPM7, MagT1, and S1P1, Advanced Science 6(18) (2019) 1901166.  
<https://doi.org/10.1002/advs.201901166>
- [34] J. Sugimoto, A.M. Romani, A.M. Valentin-Torres, A.A. Luciano, C.M.R. Kitchen, N. Funderburg, S. Mesiano, H.B. Bernstein, Magnesium decreases inflammatory cytokine production: a novel innate immunomodulatory mechanism, The Journal of Immunology 188(12) (2012) 6338-6346.  
<https://doi.org/10.4049/jimmunol.1101765>
- [35] N.-Y. Su, T.-C. Peng, P.-S. Tsai, C.-J. Huang, Phosphoinositide 3-kinase/Akt pathway is involved in mediating the anti-inflammation effects of magnesium sulfate, Journal of Surgical Research 185(2) (2013) 726-732.  
<https://doi.org/10.1016/j.jss.2013.06.030>

- [36] B. Rochelson, O. Dowling, N. Schwartz, C.N. Metz, Magnesium sulfate suppresses inflammatory responses by human umbilical vein endothelial cells (HuVECs) through the NF $\kappa$ B pathway, *Journal of Reproductive Immunology* 73(2) (2007) 101-107.  
<https://doi.org/10.1016/j.jri.2006.06.004>
- [37] J. Adams, J. Mitchell, The effect of agents which modify platelet behaviour and of magnesium ions on thrombus formation in vivo, *Thrombosis and Haemostasis* 42(02) (1979) 603-610.  
<https://doi.org/10.1055/s-0038-1666898>
- [38] C. Lin, P. Tsai, Y. Hung, C. Huang, L-type calcium channels are involved in mediating the anti-inflammatory effects of magnesium sulphate, *British Journal of Anaesthesia* 104(1) (2010) 44-51.  
<https://doi.org/10.1093/bja/aep336>
- [39] S. Yoshizawa, A. Brown, A. Barchowsky, C. Sfeir, Magnesium ion stimulation of bone marrow stromal cells enhances osteogenic activity, simulating the effect of magnesium alloy degradation, *Acta Biomaterialia* 10(6) (2014) 2834-2842.  
<https://doi.org/10.1016/j.actbio.2014.02.002>
- [40] C. Wu, Z. Chen, D. Yi, J. Chang, Y. Xiao, Multidirectional effects of Sr-, Mg-, and Si-containing bioceramic coatings with high bonding strength on inflammation, osteoclastogenesis, and osteogenesis, *ACS Applied Materials & Interfaces* 6(6) (2014) 4264-4276.  
<https://doi.org/10.1021/am4060035>
- [41] R.K. Rude, F.R. Singer, H.E. Gruber, Skeletal and hormonal effects of magnesium deficiency, *Journal of the American College of Nutrition* 28(2) (2009) 131-141.  
<https://doi.org/10.1080/07315724.2009.10719764>
- [42] O. Sahota, M. Mundey, P. San, I. Godber, D. Hosking, Vitamin D insufficiency and the blunted PTH response in established osteoporosis: the role of magnesium deficiency, *Osteoporosis International* 17(7) (2006) 1013-1021.  
<https://doi.org/10.1007/s00198-006-0084-3>
- [43] J.E. Sojka, Magnesium supplementation and osteoporosis, *Nutrition Reviews* 53(3) (1995) 71-74.  
<https://doi.org/10.1111/j.1753-4887.1995.tb01505.x>
- [44] B.J. Luthringer, F. Feyerabend, R. Willumeit-Römer, Magnesium-based implants: a mini-review, *Magnesium Research* 27(4) (2014) 142-154.  
<https://doi.org/10.1684/mrh.2015.0375>
- [45] E.C. Huse, A new ligature?, *Chicago Medical Journal Examiner* 37 (1878) 171-172.  
[http://refhub.elsevier.com/S0079-6425\(17\)30050-6/h0095](http://refhub.elsevier.com/S0079-6425(17)30050-6/h0095)
- [46] E. Payr, Contributions to the technique of blood vessel and nerve suture along with information about the use of an resorbable metal in surgery [Beiträge zur Technik der Blutgefäß- und Nervennaht nebst Mittheilungen über die Verwendung eines resorbirbaren Metalles in der Chirurgie], *Archiv für Klinische Chirurgie* 62 (1900) 67-93.  
<https://ci.nii.ac.jp/naid/10007735786/>
- [47] V.D. Lespinasse, G.C. Fisher, J. Eisenstaedt, A practical mechanical method of end-to-end anastomosis of blood-vessels: using absorbable magnesium rings, *Journal of the American Medical Association* 55(21) (1910) 1785-1790.  
<https://doi.org/10.1001/jama.1910.04330210013005>

- [48] E.W. Andrews, Absorbable metal clips as substitutes for ligatures and deep sutures in wound closure, *Journal of the American Medical Association* 69(4) (1917) 278-281.  
<https://doi.org/10.1001/jama.1917.02590310030008>
- [49] P. Stone, J.W. Lord, Jr., An experimental study of the thrombogenic properties of magnesium and magnesium-aluminum wire in the dog's aorta, *Surgery* 30(6) (1951) 987-993.  
<https://www.ncbi.nlm.nih.gov/pubmed/14901224>
- [50] M. Seelig, A study of magnesium wire as an absorbable suture and ligature material, *Archives of Surgery* 8(2) (1924) 669-680.  
<https://doi.org/10.1001/archsurg.1924.01120050210011>
- [51] B. Heublein, R. Rohde, V. Kaese, M. Niemeyer, W. Hartung, A. Haverich, Biocorrosion of magnesium alloys: a new principle in cardiovascular implant technology?, *Heart* 89(6) (2003) 651-656.  
<https://doi.org/10.1136/heart.89.6.651>
- [52] R. Waksman, R. Pakala, P.K. Kuchulakanti, R. Baffour, D. Hellings, R. Seabron, F.O. Tio, E. Wittchow, S. Hartwig, C. Harder, Safety and efficacy of bioabsorbable magnesium alloy stents in porcine coronary arteries, *Catheterization and Cardiovascular Interventions* 68(4) (2006) 607-617.  
<https://doi.org/10.1002/ccd.20727>
- [53] R. Waksman, R. Pakala, T. Okabe, D. Hellings, R. Chan, M.O. Tio, E. Wittchow, S. Hartwig, K.-H. Waldmann, C. Harder, Efficacy and safety of absorbable metallic stents with adjunct intracoronary beta radiation in porcine coronary arteries, *Journal of Interventional Cardiology* 20(5) (2007) 367-372.  
<https://doi.org/10.1111/j.1540-8183.2007.00272.x>
- [54] P. Zartner, R. Cesnjevar, H. Singer, M. Weyand, First successful implantation of a biodegradable metal stent into the left pulmonary artery of a preterm baby, *Catheterization and Cardiovascular Interventions* 66(4) (2005) 590-594.  
<https://doi.org/10.1002/ccd.20520>
- [55] P. Peeters, M. Bosiers, J. Verbist, K. Deloose, B. Heublein, Preliminary results after application of absorbable metal stents in patients with critical limb ischemia, *Journal of Endovascular Therapy* 12(1) (2005) 1-5.  
<https://doi.org/10.1583/04-1349r.1>
- [56] P. Peeters, J. Verbist, K. Deloose, M. Bosiers, Results with heparin bonded polytetrafluoroethylene grafts for femorodistal bypasses, *Journal of Cardiovascular Surgery* 47(4) (2006) 407-413.  
<https://www.ncbi.nlm.nih.gov/pubmed/16953160>
- [57] C.J. McMahon, P. Oslizlok, K.P. Walsh, Early restenosis following biodegradable stent implantation in an aortopulmonary collateral of a patient with pulmonary atresia and hypoplastic pulmonary arteries, *Catheterization and Cardiovascular Interventions* 69(5) (2007) 735-738.  
<https://doi.org/10.1002/ccd.21091>
- [58] P. Barlis, J. Tanigawa, C. Di Mario, Coronary bioabsorbable magnesium stent: 15-month intravascular ultrasound and optical coherence tomography findings, *European Heart Journal* 28(19) (2007) 2319-2319.  
<https://doi.org/10.1093/eurheartj/ehm119>

- [59] R. Erbel, C. Di Mario, J. Bartunek, J. Bonnier, B. de Bruyne, F.R. Eberli, P. Erne, M. Haude, B. Heublein, M. Horrigan, Temporary scaffolding of coronary arteries with bioabsorbable magnesium stents: a prospective, non-randomised multicentre trial, *The Lancet* 369(9576) (2007) 1869-1875.  
[https://doi.org/10.1016/s0140-6736\(07\)60853-8](https://doi.org/10.1016/s0140-6736(07)60853-8)
- [60] R. Waksman, R. Erbel, C. Di Mario, J. Bartunek, B. de Bruyne, F.R. Eberli, P. Erne, M. Haude, M. Horrigan, C. Ilsley, Early- and long-term intravascular ultrasound and angiographic findings after bioabsorbable magnesium stent implantation in human coronary arteries, *JACC: Cardiovascular Interventions* 2(4) (2009) 312-320.  
<https://doi.org/10.1016/j.jcin.2008.09.015>
- [61] M. Haude, R. Erbel, P. Erne, S. Verheyen, H. Degen, D. Böse, P. Vermeersch, I. Wijnbergen, N. Weissman, F. Prati, Safety and performance of the drug-eluting absorbable metal scaffold (DREAMS) in patients with de-novo coronary lesions: 12 month results of the prospective, multicentre, first-in-man BIOSOLVE-I trial, *The Lancet* 381(9869) (2013) 836-844.  
[https://doi.org/10.1016/s0140-6736\(12\)61765-6](https://doi.org/10.1016/s0140-6736(12)61765-6)
- [62] F. Witte, Reprint of: The history of biodegradable magnesium implants: a review, *Acta Biomaterialia* 23 (2015) S28-S40.  
<https://doi.org/10.1016/j.actbio.2015.07.017>
- [63] H. Hermawan, D. Dubé, D. Mantovani, Developments in metallic biodegradable stents, *Acta Biomaterialia* 6(5) (2010) 1693-1697.  
<https://doi.org/10.1016/j.actbio.2009.10.006>
- [64] Y. Zheng, X. Gu, F. Witte, Biodegradable metals, *Materials Science and Engineering: R: Reports* 77 (2014) 1-34.  
<https://doi.org/10.1016/j.mser.2014.01.001>
- [65] T.L.P. Slottow, R. Pakala, T. Okabe, D. Hellinga, R.J. Lovec, F.O. Tio, A.B. Bui, R. Waksman, Optical coherence tomography and intravascular ultrasound imaging of bioabsorbable magnesium stent degradation in porcine coronary arteries, *Cardiovascular Revascularization Medicine* 9(4) (2008) 248-254.  
<https://doi.org/10.1016/j.carrev.2008.04.001>
- [66] M. Maeng, L.O. Jensen, E. Falk, H.R. Andersen, L. Thuesen, Negative vascular remodelling after implantation of bioabsorbable magnesium alloy stents in porcine coronary arteries: a randomised comparison with bare-metal and sirolimus-eluting stents, *Heart* 95(3) (2009) 241-246.  
<https://doi.org/10.1136/heart.2007.139261>
- [67] E.D. McBride, Magnesium screw and nail transfixion in fractures, *Southern Medical Journal* 31(5) (1938) 508-514.  
<https://doi.org/10.1097/00007611-193805000-00010>
- [68] E.D. McBride, Absorbable metal in bone surgery: a further report on the use of magnesium alloys, *Journal of the American Medical Association* 111(27) (1938) 2464-2467.  
<https://doi.org/10.1001/jama.1938.02790530018007>
- [69] H. Waizy, J. Diekmann, A. Weizbauer, J. Reifenrath, I. Bartsch, V. Neubert, R. Schavan, H. Windhagen, In vivo study of a biodegradable orthopedic screw (MgYREZr-alloy) in a rabbit model for up to 12 months, *Journal of Biomaterials Applications* 28(5) (2014) 667-675.  
<https://doi.org/10.1177/0885328212472215>

- [70] Y. Chen, Z. Xu, C. Smith, J. Sankar, Recent advances on the development of magnesium alloys for biodegradable implants, *Acta Biomaterialia* 10(11) (2014) 4561-4573.  
<https://doi.org/10.1016/j.actbio.2014.07.005>
- [71] R. Meier, M. Panzica, Erste Ergebnisse mit einer resorbierbaren MgYREZr-Kompressionsschraube bei der instabilen Kahnbeinfraktur zeigen eine massive Zystenbildung [First results with a resorbable MgYREZr compression screw in unstable scaphoid fractures show extensive bone cysts], *Handchirurgie - Mikrochirurgie - Plastische Chirurgie* 49(1) (2017) 37-41.  
<https://doi.org/10.1055/s-0042-121416>
- [72] R. Setiawati, P. Rahardjo, Bone development and growth, in: H. Yang (Ed.), *Osteogenesis and Bone Regeneration*, IntechOpen2018, pp. 1-20.  
<https://doi.org/10.5772/intechopen.82452>
- [73] Q. Zhao, H. Ren, Z. Han, Mesenchymal stem cells: immunomodulatory capability and clinical potential in immune diseases, *Journal of Cellular Immunotherapy* 2(1) (2016) 3-20.  
<https://doi.org/10.1016/j.jocit.2014.12.001>
- [74] K. Le Blanc, Immunomodulatory effects of fetal and adult mesenchymal stem cells, *Cytotherapy* 5(6) (2003) 485-489.  
<https://doi.org/10.1080/14653240310003611>
- [75] A. Schindeler, M.M. McDonald, P. Bokko, D.G. Little, Bone remodeling during fracture repair: the cellular picture, *Seminars in Cell & Developmental Biology* 19(5) (2008) 459-466.  
<https://doi.org/10.1016/j.semcdb.2008.07.004>
- [76] S.L. Teitelbaum, Bone resorption by osteoclasts, *Science* 289(5484) (2000) 1504-1508.  
<https://doi.org/10.1126/science.289.5484.1504>
- [77] L. Marzona, B. Pavolini, Play and players in bone fracture healing match, *Clinical Cases in Mineral and Bone Metabolism* 6(2) (2009) 159-162.  
<https://www.ncbi.nlm.nih.gov/pubmed/22461167>
- [78] O. Bastian, J. Pillay, J. Alblas, L. Leenen, L. Koenderman, T. Blokhuis, Systemic inflammation and fracture healing, *Journal of Leukocyte Biology* 89(5) (2011) 669-673.  
<https://doi.org/10.1189/jlb.0810446>
- [79] S. Franz, S. Rammelt, D. Scharnweber, J.C. Simon, Immune responses to implants—a review of the implications for the design of immunomodulatory biomaterials, *Biomaterials* 32(28) (2011) 6692-6709.  
<https://doi.org/10.1016/j.biomaterials.2011.05.078>
- [80] M. Wang, Y. Yu, K. Dai, Z. Ma, Y. Liu, J. Wang, C. Liu, Improved osteogenesis and angiogenesis of magnesium-doped calcium phosphate cement via macrophage immunomodulation, *Biomaterials Science* 4(11) (2016) 1574-1583.  
<https://doi.org/10.1039/c6bm00290k>
- [81] M.E. Bolander, Regulation of fracture repair by growth factors, *Proceedings of the Society for Experimental Biology and Medicine* 200(2) (1992) 165-170.  
<https://doi.org/10.3181/00379727-200-43410a>
- [82] Y. Zhou, R. Huang, W. Fan, I. Prasadam, R. Crawford, Y. Xiao, Mesenchymal stromal cells regulate the cell mobility and the immune response during osteogenesis through secretion of vascular endothelial growth factor A, *Journal of Tissue Engineering and Regenerative Medicine* 12(1) (2018) e566-e578.

<https://doi.org/10.1002/term.2327>

[83] E. Seebach, H. Freischmidt, J. Holschbach, J. Fellenberg, W. Richter, Mesenchymal stroma cells trigger early attraction of M1 macrophages and endothelial cells into fibrin hydrogels, stimulating long bone healing without long-term engraftment, *Acta Biomaterialia* 10(11) (2014) 4730-4741.

<https://doi.org/10.1016/j.actbio.2014.07.017>

[84] Q.Z. Zhang, W.R. Su, S.H. Shi, P. Wilder - Smith, A.P. Xiang, A. Wong, A.L. Nguyen, C.W. Kwon, A.D. Le, Human gingiva - derived mesenchymal stem cells elicit polarization of M2 macrophages and enhance cutaneous wound healing, *Stem Cells* 28(10) (2010) 1856-1868.

<https://doi.org/10.1002/stem.503>

[85] R.S. Waterman, S.L. Tomchuck, S.L. Henkle, A.M. Betancourt, A new mesenchymal stem cell (MSC) paradigm: polarization into a pro-inflammatory MSC1 or an immunosuppressive MSC2 phenotype, *PLoS One* 5(4) (2010) e10088.

<https://doi.org/10.1371/journal.pone.0010088>

[86] J. Rojas, J. Salazar, M.S. Martínez, J. Palmar, J. Bautista, M. Chávez-Castillo, A. Gómez, V. Bermúdez, Macrophage heterogeneity and plasticity: impact of macrophage biomarkers on atherosclerosis, *Scientifica* 2015 (2015) 851252.

<https://doi.org/10.1155/2015/851252>

[87] M.H.M. Barros, F. Hauck, J.H. Dreyer, B. Kempkes, G. Niedobitek, Macrophage polarisation: an immunohistochemical approach for identifying M1 and M2 macrophages, *PLoS One* 8(11) (2013) e80908.

<https://doi.org/10.1371/journal.pone.0080908>

[88] B. Chazaud, Macrophages: supportive cells for tissue repair and regeneration, *Immunobiology* 219(3) (2014) 172-178.

<https://doi.org/10.1016/j.imbio.2013.09.001>

[89] M.D. Costantino, A. Schuster, H. Helmholz, A. Meyer-Rachner, R. Willumeit-Romer, B.J.C. Luthringer-Feyerabend, Inflammatory response to magnesium-based biodegradable implant materials, *Acta Biomaterialia* 101 (2020) 598-608.

<https://doi.org/10.1016/j.actbio.2019.10.014>

[90] E. Weagel, C. Smith, P.G. Liu, R. Robison, K. O'Neill, Macrophage polarization and its role in cancer, *Journal of Clinical & Cellular Immunology* 6(4) (2015) 338-345.

<https://doi.org/10.4172/2155-9899.1000338>

[91] P.M. Henson, The immunologic release of constituents from neutrophil leukocytes: I. The role of antibody and complement on nonphagocytosable surfaces or phagocytosable particles, *The Journal of Immunology* 107(6) (1971) 1535-1546.

<https://www.ncbi.nlm.nih.gov/pubmed/5120396>

[92] P.M. Henson, The immunologic release of constituents from neutrophil leukocytes: II. Mechanisms of release during phagocytosis, and adherence to nonphagocytosable surfaces, *The Journal of Immunology* 107(6) (1971) 1547-1557.

<https://www.ncbi.nlm.nih.gov/pubmed/5120397>

[93] P. Nordenfelt, H. Tapper, Phagosome dynamics during phagocytosis by neutrophils, *Journal of Leukocyte Biology* 90(2) (2011) 271-284.

<https://doi.org/10.1189/jlb.0810457>

- [94] Z. Xia, J.T. Triffitt, A review on macrophage responses to biomaterials, *Biomedical Materials* 1(1) (2006) R1-R9.  
<https://doi.org/10.1088/1748-6041/1/1/r01>
- [95] J.M. Anderson, A. Rodriguez, D.T. Chang, Foreign body reaction to biomaterials, *Seminars in Immunology* 20(2) (2008) 86-100.  
<https://doi.org/10.1016/j.smim.2007.11.004>
- [96] M. Zafranskaya, D. Nizheharodava, M. Yurkevich, G. Ivanchik, Y. Demidchik, H. Kozhukh, A. Fedulov, PGE 2 contributes to in vitro MSC - mediated inhibition of non - specific and antigen - specific T cell proliferation in MS patients, *Scandinavian Journal of Immunology* 78(5) (2013) 455-462.  
<https://doi.org/10.1111/sji.12102>
- [97] J. Kim, P. Hematti, Mesenchymal stem cell-educated macrophages: a novel type of alternatively activated macrophages, *Experimental Hematology* 37(12) (2009) 1445-1453.  
<https://doi.org/10.1016/j.exphem.2009.09.004>
- [98] K. Le Blanc, Mesenchymal stromal cells: tissue repair and immune modulation, *Cyotherapy* 8(6) (2006) 559-561.  
<https://doi.org/10.1080/14653240601045399>
- [99] M. François, R. Romieu-Mourez, M. Li, J. Galipeau, Human MSC suppression correlates with cytokine induction of indoleamine 2, 3-dioxygenase and bystander M2 macrophage differentiation, *Molecular Therapy* 20(1) (2012) 187-195.  
<https://doi.org/10.1038/mt.2011.189>
- [100] Y. Li, N. Kong, Z. Li, R. Tian, X. Liu, G. Liu, K. Wang, P. Yang, Bone marrow macrophage M2 polarization and adipose - derived stem cells osteogenic differentiation synergistically promote rehabilitation of bone damage, *Journal of Cellular Biochemistry* 120(12) (2019) 19891-19901.  
<https://doi.org/10.1002/jcb.29297>
- [101] S.M. Melief, S.B. Geutskens, W.E. Fibbe, H. Roelofs, Multipotent stromal cells skew monocytes towards an anti-inflammatory interleukin-10-producing phenotype by production of interleukin-6, *Haematologica* 98(6) (2013) 888-895.  
<https://doi.org/10.3324/haematol.2012.078055>
- [102] S. Selleri, P. Bifsha, S. Civini, C. Pacelli, M.M. Dieng, W. Lemieux, P. Jin, R. Bazin, N. Patey, F.M. Marincola, Human mesenchymal stromal cell-secreted lactate induces M2-macrophage differentiation by metabolic reprogramming, *Oncotarget* 7(21) (2016) 30193-30210.  
<https://doi.org/10.18632/oncotarget.8623>
- [103] M. Heusinkveld, P.J.d.V. van Steenwijk, R. Goedemans, T.H. Ramwadhoebe, A. Gorter, M.J. Welters, T. van Hall, S.H. van der Burg, M2 macrophages induced by prostaglandin E2 and IL-6 from cervical carcinoma are switched to activated M1 macrophages by CD4+ Th1 cells, *The Journal of Immunology* 187(3) (2011) 1157-1165.  
<https://doi.org/10.4049/jimmunol.1100889>
- [104] J. Braune, U. Weyer, C. Hobusch, J. Mauer, J.C. Brüning, I. Bechmann, M. Gericke, IL-6 regulates M2 polarization and local proliferation of adipose tissue macrophages in obesity, *The Journal of Immunology* 198(7) (2017) 2927-2934.  
<https://doi.org/10.4049/jimmunol.1600476>

[105] T. Ohashi, M. Aoki, H. Tomita, T. Akazawa, K. Sato, B. Kuze, K. Mizuta, A. Hara, H. Nagaoka, N. Inoue, M2 - like macrophage polarization in high lactic acid - producing head and neck cancer, *Cancer Science* 108(6) (2017) 1128-1134.

<https://doi.org/10.1111/cas.13244>

[106] S. Gao, F. Mao, B. Zhang, L. Zhang, X. Zhang, M. Wang, Y. Yan, T. Yang, J. Zhang, W. Zhu, Mouse bone marrow-derived mesenchymal stem cells induce macrophage M2 polarization through the nuclear factor- $\kappa$ B and signal transducer and activator of transcription 3 pathways, *Experimental Biology and Medicine* 239(3) (2014) 366-375.

<https://doi.org/10.1177/1535370213518169>

[107] A. Corcione, F. Benvenuto, E. Ferretti, D. Giunti, V. Cappiello, F. Cazzanti, M. Risso, F. Gualandi, G.L. Mancardi, V. Pistoia, A. Uccelli, Human mesenchymal stem cells modulate B-cell functions, *Blood* 107(1) (2006) 367-372.

<https://doi.org/10.1182/blood-2005-07-2657>

[108] G.M. Spaggiari, A. Capobianco, S. Becchetti, M.C. Mingari, L. Moretta, Mesenchymal stem cell-natural killer cell interactions: evidence that activated NK cells are capable of killing MSCs, whereas MSCs can inhibit IL-2-induced NK-cell proliferation, *Blood* 107(4) (2006) 1484-1490.

<https://doi.org/10.1182/blood-2005-07-2775>

[109] Y. Zhou, A. Day, S. Haykal, A. Keating, T.K. Waddell, Mesenchymal stromal cells augment CD4+ and CD8+ T-cell proliferation through a CCL2 pathway, *Cyotherapy* 15(10) (2013) 1195-1207.

<https://doi.org/10.1016/j.jcyt.2013.05.009>

[110] A. Keating, Mesenchymal stromal cells: new directions, *Cell stem cell* 10(6) (2012) 709-716.

<https://doi.org/10.1016/j.stem.2012.05.015>

[111] S.M. Melief, E. Schrama, M.H. Brugman, M.M. Tiemessen, M.J. Hoogduijn, W.E. Fibbe, H. Roelofs, Multipotent stromal cells induce human regulatory T cells through a novel pathway involving skewing of monocytes toward anti - inflammatory macrophages, *Stem Cells* 31(9) (2013) 1980-1991.

<https://doi.org/10.1002/stem.1432>

[112] E. Zappia, S. Casazza, E. Pedemonte, F. Benvenuto, I. Bonanni, E. Gerdoni, D. Giunti, A. Ceravolo, F. Cazzanti, F. Frassoni, Mesenchymal stem cells ameliorate experimental autoimmune encephalomyelitis inducing T-cell anergy, *Blood* 106(5) (2005) 1755-1761.

<https://doi.org/10.1182/blood-2005-04-1496>

[113] J.B. Choi, H. Uchino, K. Azuma, N. Iwashita, Y. Tanaka, H. Mochizuki, M. Migita, T. Shimada, R. Kawamori, H. Watada, Little evidence of transdifferentiation of bone marrow-derived cells into pancreatic beta cells, *Diabetologia* 46(10) (2003) 1366-1374.

<https://doi.org/10.1007/s00125-003-1182-9>

[114] F.E. Ezquer, M.E. Ezquer, D.B. Parrau, D. Carpio, A.J. Yañez, P.A. Conget, Systemic administration of multipotent mesenchymal stromal cells reverts hyperglycemia and prevents nephropathy in type 1 diabetic mice, *Biology of Blood and Marrow Transplantation* 14(6) (2008) 631-640.

<https://doi.org/10.1016/j.bbmt.2008.01.006>

- [115] R. Alves, Osteoblast differentiation and bone: relevant proteins, regulatory processes and the vascular connection, Doctor Degree (2012) 1-163.  
<http://hdl.handle.net/1765/37162>
- [116] A. Bedalov, R. Salvatori, M. Dodig, M. Kronenberg, B. Kapural, Z. Bogdanovic, B.E. Kream, C.O. Woody, S.H. Clark, K. Mack, Regulation of COL1A1 expression in type I collagen producing tissues: identification of a 49 base pair region which is required for transgene expression in bone of transgenic mice, *Journal of Bone and Mineral Research* 10(10) (1995) 1443-1451.  
<https://doi.org/10.1002/jbmr.5650101004>
- [117] S. Gronthos, S. Chen, C.Y. Wang, P.G. Robey, S. Shi, Telomerase accelerates osteogenesis of bone marrow stromal stem cells by upregulation of CBFA1, osterix, and osteocalcin, *Journal of Bone and Mineral Research* 18(4) (2003) 716-722.  
<https://doi.org/10.1359/jbmr.2003.18.4.716>
- [118] M. Wang, F. Chen, J. Wang, X. Chen, J. Liang, X. Yang, X. Zhu, Y. Fan, X. Zhang, Calcium phosphate altered the cytokine secretion of macrophages and influenced the homing of mesenchymal stem cells, *Journal of Materials Chemistry B* 6(29) (2018) 4765-4774.  
<https://doi.org/10.1039/c8tb01201f>
- [119] W. Huang, S. Yang, J. Shao, Y.-P. Li, Signaling and transcriptional regulation in osteoblast commitment and differentiation, *Frontiers in Bioscience* 12 (2007) 3068-3092.  
<https://doi.org/10.2741/2296>
- [120] J.E. Park, A. Barbul, Understanding the role of immune regulation in wound healing, *The American Journal of Surgery* 187(5) (2004) S11-S16.  
[https://doi.org/10.1016/s0002-9610\(03\)00296-4](https://doi.org/10.1016/s0002-9610(03)00296-4)
- [121] J. Lassus, J. Salo, W.A. Jiranek, S. Santavirta, J. Nevalainen, M. Matucci-Cerinic, P. Horák, Y. Konttinen, Macrophage activation results in bone resorption, *Clinical Orthopaedics and Related Research* 352 (1998) 7-15.  
<https://doi.org/10.1097/00003086-199807000-00003>
- [122] E. Song, N. Ouyang, M. Hörbelt, B. Antus, M. Wang, M.S. Exton, Influence of alternatively and classically activated macrophages on fibrogenic activities of human fibroblasts, *Cellular Immunology* 204(1) (2000) 19-28.  
<https://doi.org/10.1006/cimm.2000.1687>
- [123] M.K. Chang, L.-J. Raggatt, K.A. Alexander, J.S. Kuliwaba, N.L. Fazzalari, K. Schroder, E.R. Maylin, V.M. Ripoll, D.A. Hume, A.R. Pettit, Osteal tissue macrophages are intercalated throughout human and mouse bone lining tissues and regulate osteoblast function in vitro and in vivo, *The Journal of Immunology* 181(2) (2008) 1232-1244.  
<https://doi.org/10.4049/jimmunol.181.2.1232>
- [124] Y. Tintut, J. Patel, M. Territo, T. Saini, F. Parhami, L.L. Demer, Monocyte/macrophage regulation of vascular calcification in vitro, *Circulation* 105(5) (2002) 650-655.  
<https://doi.org/10.1161/hc0502.102969>
- [125] L. Wang, Y. Li, X. Chen, J. Chen, S.C. Gautam, Y. Xu, M. Chopp, MCP-1, MIP-1, IL-8 and ischemic cerebral tissue enhance human bone marrow stromal cell migration in interface culture, *Hematology* 7(2) (2002) 113-117.  
<https://doi.org/10.1080/10245330290028588>

- [126] L. Wang, Y. Li, J. Chen, S.C. Gautam, Z. Zhang, M. Lu, M. Chopp, Ischemic cerebral tissue and MCP-1 enhance rat bone marrow stromal cell migration in interface culture, *Experimental Hematology* 30(7) (2002) 831-836.  
[https://doi.org/10.1016/s0301-472x\(02\)00829-9](https://doi.org/10.1016/s0301-472x(02)00829-9)
- [127] W. Zhao, J.-J. Li, D.-Y. Cao, X. Li, L.-Y. Zhang, Y. He, S.-Q. Yue, D.-S. Wang, K.-F. Dou, Intravenous injection of mesenchymal stem cells is effective in treating liver fibrosis, *World Journal of Gastroenterology* 18(10) (2012) 1048-1058.  
<https://doi.org/10.3748/wjg.v18.i10.1048>
- [128] S.J. Prasanna, D. Gopalakrishnan, S.R. Shankar, A.B. Vasandan, Pro-inflammatory cytokines, IFNy and TNF $\alpha$ , influence immune properties of human bone marrow and wharton jelly mesenchymal stem cells differentially, *PLoS One* 5(2) (2010) e9016.  
<https://doi.org/10.1371/journal.pone.0009016>
- [129] S.L. Highfill, P.C. Rodriguez, Q. Zhou, C.A. Goetz, B.H. Koehn, R. Veenstra, P.A. Taylor, A. Panoskaltsis-Mortari, J.S. Serody, D.H. Munn, Bone marrow myeloid-derived suppressor cells (MDSCs) inhibit graft-versus-host disease (GVHD) via an arginase-1-dependent mechanism that is up-regulated by interleukin-13, *Blood* 116(25) (2010) 5738-5747.  
<https://doi.org/10.1182/blood-2010-06-287839>
- [130] A.Y.H. Phua, P. Vijayakumar, M. Choolani, J. Chan, Y.-C. Lim, TNF $\alpha$  antagonizes PDGF-AB chemotactic effects on mesenchymal stem cells (MSC) migration, *The FASEB Journal* 23(1\_supplement) (2009) LB354-LB354.  
[https://www.fasebj.org/doi/abs/10.1096/fasebj.23.1\\_supplement.LB354](https://www.fasebj.org/doi/abs/10.1096/fasebj.23.1_supplement.LB354)
- [131] S.A. Krum, J. Chang, G. Miranda-Carboni, C.-Y. Wang, Novel functions for NF $\kappa$ B: inhibition of bone formation, *Nature Reviews Rheumatology* 6(10) (2010) 607-11.  
<https://doi.org/10.1038/nrrheum.2010.133>
- [132] J. Chang, Z. Wang, E. Tang, Z. Fan, L. McCauley, R. Franceschi, K. Guan, P.H. Krebsbach, C.-Y. Wang, Inhibition of osteoblastic bone formation by nuclear factor- $\kappa$ B, *Nature Medicine* 15(6) (2009) 682-689.  
<https://doi.org/10.1038/nm.1954>
- [133] E. Nishida, Y. Hara, T. Kaneko, Y. Ikeda, T. Ukai, I. Kato, Bone resorption and local interleukin - 1 $\alpha$  and interleukin - 1 $\beta$  synthesis induced by *Actinobacillus actinomycetemcomitans* and *Porphyromonas gingivalis* lipopolysaccharide, *Journal of Periodontal Research* 36(1) (2001) 1-8.  
<https://doi.org/10.1034/j.1600-0765.2001.00637.x>
- [134] N. Kurihara, D. Bertolini, T. Suda, Y. Akiyama, G.D. Roodman, IL-6 stimulates osteoclast-like multinucleated cell formation in long term human marrow cultures by inducing IL-1 release, *The Journal of Immunology* 144(11) (1990) 4226-4230.  
<https://www.ncbi.nlm.nih.gov/pubmed/2341718>
- [135] T. Matsuda, A. Kondo, Y. Tsunashima, A. Togari, Inhibitory effect of vitamin K2 on interleukin-1 $\beta$ -stimulated proliferation of human osteoblasts, *Biological and Pharmaceutical Bulletin* 33(5) (2010) 804-808.  
<https://doi.org/10.1248/bpb.33.804>
- [136] N. Yang, G. Wang, C. Hu, Y. Shi, L. Liao, S. Shi, Y. Cai, S. Cheng, X. Wang, Y. Liu, Tumor necrosis factor  $\alpha$  suppresses the mesenchymal stem cell osteogenesis promoter miR - 21 in

estrogen deficiency-induced osteoporosis, *Journal of Bone and Mineral Research* 28(3) (2013) 559-573.

<https://doi.org/10.1002/jbmr.1798>

[137] H. Hikiji, W.S. Shin, T. Koizumi, T. Takato, T. Susami, Y. Koizumi, Y. Okai-Matsuo, T. Toyo-Oka, Peroxynitrite production by TNF- $\alpha$  and IL-1 $\beta$ : implication for suppression of osteoblastic differentiation, *American Journal of Physiology-Endocrinology and Metabolism* 278(6) (2000) E1031-E1037.

<https://doi.org/10.1152/ajpendo.2000.278.6.e1031>

[138] L.E. Sidney, G.R. Kirkham, L.D. Buttery, Comparison of osteogenic differentiation of embryonic stem cells and primary osteoblasts revealed by responses to IL-1 $\beta$ , TNF- $\alpha$ , and IFN- $\gamma$ , *Stem Cells and Development* 23(6) (2013) 605-617.

<https://doi.org/10.1089/scd.2013.0336>

[139] Z. Chen, L. Chen, R. Liu, Y. Lin, S. Chen, S. Lu, Z. Lin, Z. Chen, C. Wu, Y. Xiao, The osteoimmunomodulatory property of a barrier collagen membrane and its manipulation via coating nanometer-sized bioactive glass to improve guided bone regeneration, *Biomaterials Science* 6(5) (2018) 1007-1019.

<https://doi.org/10.1039/c7bm00869d>

[140] A.J. Celeste, J.A. Iannazzi, R.C. Taylor, R.M. Hewick, V. Rosen, E.A. Wang, J.M. Wozney, Identification of transforming growth factor beta family members present in bone-inductive protein purified from bovine bone, *Proceedings of the National Academy of Sciences* 87(24) (1990) 9843-9847.

<https://doi.org/10.1073/pnas.87.24.9843>

[141] V. Rosen, BMP2 signaling in bone development and repair, *Cytokine & Growth Factor Reviews* 20(5-6) (2009) 475-480.

<https://doi.org/10.1016/j.cytogfr.2009.10.018>

[142] F. Cui, X. Wang, X. Liu, A.S. Dighe, G. Balian, Q. Cui, VEGF and BMP-6 enhance bone formation mediated by cloned mouse osteoprogenitor cells, *Growth Factors* 28(5) (2010) 306-317.

<https://doi.org/10.3109/08977194.2010.484423>

[143] O. Mizrahi, D. Sheyn, W. Tawackoli, I. Kallai, A. Oh, S. Su, X. Da, P. Zarrini, G. Cook-Wiens, D. Gazit, BMP-6 is more efficient in bone formation than BMP-2 when overexpressed in mesenchymal stem cells, *Gene Therapy* 20(4) (2013) 370-377.

<https://doi.org/10.1038/gt.2012.45>

[144] C.H. Heldin, K. Miyazono, P. ten Dijke, TGF-beta signalling from cell membrane to nucleus through SMAD proteins, *Nature* 390(6659) (1997) 465-471.

<https://doi.org/10.1038/37284>

[145] R. Huang, Y. Yuan, J. Tu, G. Zou, Q. Li, Opposing TNF- $\alpha$ /IL-1 $\beta$ -and BMP-2-activated MAPK signalling pathways converge on Runx2 to regulate BMP-2-induced osteoblastic differentiation, *Cell Death & Disease* 5(4) (2014) e1187.

<https://doi.org/10.1038/cddis.2014.101>

[146] H. Liu, Y. Liu, M. Viggeswarapu, Z. Zheng, L. Titus, S.D. Boden, Activation of c - Jun NH2 - terminal kinase 1 increases cellular responsiveness to BMP - 2 and decreases binding of inhibitory Smad6 to the type 1 BMP receptor, *Journal of Bone and Mineral Research* 26(5) (2011) 1122-1132.

<https://doi.org/10.1002/jbmр.296>

[147] X. Guo, X.-F. Wang, Signaling cross-talk between TGF- $\beta$ /BMP and other pathways, *Cell research* 19(1) (2009) 71-88.

<https://doi.org/10.1038/cr.2008.302>

[148] A.B. Core, S. Canali, J.L. Babitt, Hemojuvelin and bone morphogenetic protein (BMP) signaling in iron homeostasis, *Frontiers in Pharmacology* 5 (2014) 104.

<https://doi.org/10.3389/fphar.2014.00104>

[149] N.A. Sims, Cell-specific paracrine actions of IL-6 family cytokines from bone, marrow and muscle that control bone formation and resorption, *The International Journal of Biochemistry & Cell Biology* 79 (2016) 14-23.

<https://doi.org/10.1016/j.biocel.2016.08.003>

[150] P.R. Jay, M. Centrella, J. Lorenzo, A.G. Bruce, M.C. Horowitz, Oncostatin-M: a new bone active cytokine that activates osteoblasts and inhibits bone resorption, *Endocrinology* 137(4) (1996) 1151-1158.

<https://doi.org/10.1210/endo.137.4.8625883>

[151] S. Rose-John, Interleukin-6 family cytokines, *Cold Spring Harbor Perspectives in Biology* 10(2) (2018) a028415.

<https://doi.org/10.1101/cshperspect.a028415>

[152] S.A. Jones, J. Scheller, S. Rose-John, Therapeutic strategies for the clinical blockade of IL-6/gp130 signaling, *The Journal of Clinical Investigation* 121(9) (2011) 3375-3383.

<https://doi.org/10.1172/jci57158>

[153] M. Mihara, M. Hashizume, H. Yoshida, M. Suzuki, M. Shiina, IL-6/IL-6 receptor system and its role in physiological and pathological conditions, *Clinical Science* 122(4) (2011) 143-159.

<https://doi.org/10.1042/cs20110340>

[154] A.J. West, V. Tsui, S.S. Stylli, H.P.T. Nguyen, A.P. Morokoff, A.H. Kaye, R.B. Luwor, The role of interleukin-6-STAT3 signalling in glioblastoma, *Oncology letters* 16(4) (2018) 4095-4104.

<https://doi.org/10.3892/ol.2018.9227>

[155] S. Akira, T. Kishimoto, IL - 6 and NF - IL6 in acute - phase response and viral infection, *Immunological Reviews* 127(1) (1992) 25-50.

<https://doi.org/10.1111/j.1600-065x.1992.tb01407.x>

[156] R. Yang, Q. Lin, H. Gao, P. Zhang, Stress-related hormone norepinephrine induces interleukin-6 expression in GES-1 cells, *Brazilian Journal of Medical and Biological Research* 47(2) (2014) 101-109.

<https://doi.org/10.1590/1414-431x20133346>

[157] T. Taga, T. Kishimoto, gp130 and the interleukin-6 family of cytokines, *Annual Review of Immunology* 15(1) (1997) 797-819.

<https://doi.org/10.1146/annurev.immunol.15.1.797>

[158] X. Yang, B.F. Ricciardi, A. Hernandez-Soria, Y. Shi, N.P. Camacho, M.P. Bostrom, Callus mineralization and maturation are delayed during fracture healing in interleukin-6 knockout mice, *Bone* 41(6) (2007) 928-936.

<https://doi.org/10.1016/j.bone.2007.07.022>

- [159] J.E. Huh, S.Y. Lee, IL-6 is produced by adipose-derived stromal cells and promotes osteogenesis, *Biochimica et Biophysica Acta (BBA)-Molecular Cell Research* 1833(12) (2013) 2608-2616.  
<https://doi.org/10.1016/j.bbamcr.2013.06.025>
- [160] Y. Yeung, K. McDonald, T. Grewal, L. Munoz, Interleukins in glioblastoma pathophysiology: implications for therapy, *British Journal of Pharmacology* 168(3) (2013) 591-606.  
<https://doi.org/10.1111/bph.12008>
- [161] J. Silver, C. Hunter, gp130 at the nexus of inflammation, autoimmunity, and cancer, *Journal of Leukocyte Biology* 88(6) (2010) 1145-1156.  
<https://doi.org/10.1189/jlb.0410217>
- [162] N. Li, S.I. Grivennikov, M. Karin, The unholy trinity: inflammation, cytokines, and STAT3 shape the cancer microenvironment, *Cancer Cell* 19(4) (2011) 429-431.  
<https://doi.org/10.1016/j.ccr.2011.03.018>
- [163] C.D. Richards, The enigmatic cytokine oncostatin m and roles in disease, *ISRN Inflammation* 2013 (2013) 512103.  
<https://doi.org/10.1155/2013/512103>
- [164] H.Y. Song, E.S. Jeon, J.I. Kim, J.S. Jung, J.H. Kim, Oncostatin M promotes osteogenesis and suppresses adipogenic differentiation of human adipose tissue - derived mesenchymal stem cells, *Journal of Cellular Biochemistry* 101(5) (2007) 1238-1251.  
<https://doi.org/10.1002/jcb.21245>
- [165] V. Nicolaïdou, M.M. Wong, A.N. Redpath, A. Ersek, D.F. Baban, L.M. Williams, A.P. Cope, N.J. Horwood, Monocytes induce STAT3 activation in human mesenchymal stem cells to promote osteoblast formation, *PLoS One* 7(7) (2012) e39871.  
<https://doi.org/10.1371/journal.pone.0039871>
- [166] P. Guihard, Y. Danger, B. Brounais, E. David, R. Brion, J. Delecrin, C.D. Richards, S. Chevalier, F. Rédini, D. Heymann, Induction of osteogenesis in mesenchymal stem cells by activated monocytes/macrophages depends on oncostatin M signaling, *Stem Cells* 30(4) (2012) 762-772.  
<https://doi.org/10.1002/stem.1040>
- [167] P. Guihard, M.-A. Boutet, B. Brounais-Le Royer, A.-L. Gamblin, J. Amiaud, A. Renaud, M. Berreur, F. Rédini, D. Heymann, P. Layrolle, Oncostatin m, an inflammatory cytokine produced by macrophages, supports intramembranous bone healing in a mouse model of tibia injury, *The American Journal of Pathology* 185(3) (2015) 765-775.  
<https://doi.org/10.1016/j.ajpath.2014.11.008>
- [168] C.E. Misch, M.L. Perel, H.-L. Wang, G. Sammartino, P. Galindo-Moreno, P. Trisi, M. Steigmann, A. Rebaudi, A. Palti, M.A. Pikos, Implant success, survival, and failure: the International Congress of Oral Implantologists (ICOI) Pisa Consensus Conference, *Implant Dentistry* 17(1) (2008) 5-15.  
<https://doi.org/10.1097/id.0b013e3181676059>
- [169] V. Moraschini, L.d.C. Poubel, V. Ferreira, E. dos Sp Barboza, Evaluation of survival and success rates of dental implants reported in longitudinal studies with a follow-up period of at least 10 years: a systematic review, *International Journal of Oral and Maxillofacial Surgery* 44(3) (2015) 377-388.  
<https://doi.org/10.1016/j.ijom.2014.10.023>

[170] K. Watari, M. Nakaya, M. Nishida, K.-M. Kim, H. Kurose,  $\beta$ -arrestin2 in infiltrated macrophages inhibits excessive inflammation after myocardial infarction, PLoS One 8(7) (2013) e68351.

<https://doi.org/10.1371/journal.pone.0068351>

[171] J.F. Chmiel, M.W. Konstan, J.E. Knesebeck, J.B. Hilliard, T.L. Bonfield, D.V. Dawson, M. Berger, IL-10 attenuates excessive inflammation in chronic *Pseudomonas* infection in mice, American Journal of Respiratory and Critical Care Medicine 160(6) (1999) 2040-2047.

<https://doi.org/10.1164/ajrccm.160.6.9901043>

[172] Y.C. Liu, X.B. Zou, Y.F. Chai, Y.M. Yao, Macrophage polarization in inflammatory diseases, International Journal of Biological Sciences 10(5) (2014) 520-529.

<https://doi.org/10.7150/ijbs.8879>

[173] D.W. Grainger, All charged up about implanted biomaterials, Nature Biotechnology 31(6) (2013) 507-509.

<https://doi.org/10.1038/nbt.2600>

[174] J.M. Anderson, Inflammation, wound healing, and the foreign-body response, in: B.D. Ratner, A.S. Hoffman, F.J. Schoen, J.E. Lemons (Eds.), Biomaterials Science: an introduction to materials in medicine, Elsevier2013, pp. 503-512.

<https://doi.org/10.1016/b978-0-08-087780-8.00044-9>

[175] T. Stieglitz, M. Schuettler, Material-tissue interfaces in implantable systems, in: A. Inmann, D. Hodgins (Eds.), Implantable Sensor Systems for Medical Applications, Woodhead Publishing2013, pp. 39-67.

<https://doi.org/10.1533/9780857096289.1.39>

[176] B.N. Brown, B.D. Ratner, S.B. Goodman, S. Amar, S.F. Badylak, Macrophage polarization: an opportunity for improved outcomes in biomaterials and regenerative medicine, Biomaterials 33(15) (2012) 3792-3802.

<https://doi.org/10.1016/j.biomaterials.2012.02.034>

[177] L. Jahangiri, M. Kesmati, H. Najafzadeh, Evaluation of analgesic and anti-inflammatory effect of nanoparticles of magnesium oxide in mice with and without ketamine, European Review for Medical and Pharmacological Sciences 17(20) (2013) 2706-2710.

<https://www.ncbi.nlm.nih.gov/pubmed/24174350>

[178] T. Kraus, S.F. Fischerauer, A.C. Hänzi, P.J. Uggowitz, J.F. Löffler, A.M. Weinberg, Magnesium alloys for temporary implants in osteosynthesis: in vivo studies of their degradation and interaction with bone, Acta Biomaterialia 8(3) (2012) 1230-1238.

<https://doi.org/10.1016/j.actbio.2011.11.008>

[179] A. Chaya, S. Yoshizawa, K. Verdelis, N. Myers, B.J. Costello, D.-T. Chou, S. Pal, S. Maiti, P.N. Kumta, C. Sfeir, In vivo study of magnesium plate and screw degradation and bone fracture healing, Acta Biomaterialia 18 (2015) 262-269.

<https://doi.org/10.1016/j.actbio.2015.02.010>

[180] L. Baruch, O. Benny, A. Gilert, M. Ukobnik, O.B. Itzhak, M. Machluf, Alginate-PLL cell encapsulation system Co-entrapping PLGA-microspheres for the continuous release of anti-inflammatory drugs, Biomedical Microdevices 11(5) (2009) 1103-1113.

<https://doi.org/10.1007/s10544-009-9327-3>

[181] J.P. Moxham, Oncostatin - M enhances osteoinduction in a rabbit critical calvarial defect model, The Laryngoscope 117(10) (2007) 1790-1797.

<https://doi.org/10.1097/mlg.0b013e3180ed451b>

[182] S.L. Hyzy, R. Olivares-Navarrete, S. Ortman, B.D. Boyan, Z. Schwartz, Bone morphogenetic protein 2 alters osteogenesis and anti-inflammatory profiles of mesenchymal stem cells induced by microtextured titanium in vitro, *Tissue Engineering Part A* 23(19-20) (2017) 1132-1141.

<https://doi.org/10.1089/ten.tea.2017.0003>

[183] E. Vilardi, Tissue-engineered matrix as functional delivery system: controlled release of bioactive pro-angiogenic peptide from degradable PCL scaffold, Ph.D. (2015) 1-100.

<http://doi.org/10.6092/UNINA/FEDOA/10482>

[184] B.D. Boyan, T.W. Hummert, D.D. Dean, Z. Schwartz, Role of material surfaces in regulating bone and cartilage cell response, *Biomaterials* 17(2) (1996) 137-146.

[https://doi.org/10.1016/0142-9612\(96\)85758-9](https://doi.org/10.1016/0142-9612(96)85758-9)

[185] C.M. Stanford, Surface modification of biomedical and dental implants and the processes of inflammation, wound healing and bone formation, *International Journal of Molecular Sciences* 11(1) (2010) 354-369.

<https://doi.org/10.3390/ijms11010354>

[186] E. Birmingham, G. Niebur, P.E. McHugh, Osteogenic differentiation of mesenchymal stem cells is regulated by osteocyte and osteoblast cells in a simplified bone niche, *European Cells and Materials* 23 (2012) 13-27.

<https://doi.org/10.22203/ecm.v023a02>

[187] E. Andreeva, P. Bobyleva, A. Gornostaeva, L. Buravkova, Interaction of multipotent mesenchymal stromal and immune cells: bidirectional effects, *Cytotherapy* 19(10) (2017) 1152-1166.

<https://doi.org/10.1016/j.jcyt.2017.07.001>

[188] A. Kochegarov, L.F. Lemanski, New trends in heart regeneration: a review, *Journal of stem cells & Regenerative medicine* 12(2) (2016) 61-68.

<https://www.ncbi.nlm.nih.gov/pmc/articles/PMC5227105/>

[189] N. Grotenhuis, S.F. De Witte, G.J. van Osch, Y. Bayon, J.F. Lange, Y.M. Bastiaansen-Jenniskens, Biomaterials influence macrophage–mesenchymal stem cell interaction in vitro, *Tissue Engineering Part A* 22(17-18) (2016) 1098-1107.

<https://doi.org/10.1089/ten.tea.2016.0162>

[190] V. Ulivi, R. Tasso, R. Cancedda, F. Descalzi, Mesenchymal stem cell paracrine activity is modulated by platelet lysate: induction of an inflammatory response and secretion of factors maintaining macrophages in a proinflammatory phenotype, *Stem Cells and Development* 23(16) (2014) 1858-1869.

<https://doi.org/10.1089/scd.2013.0567>

[191] N. Hort, Y. Huang, D. Fechner, M. Störmer, C. Blawert, F. Witte, C. Vogt, H. Drücker, R. Willumeit, K. Kainer, Magnesium alloys as implant materials–principles of property design for Mg–RE alloys, *Acta Biomaterialia* 6(5) (2010) 1714-1725.

<https://doi.org/10.1016/j.actbio.2009.09.010>

[192] C. Du, P. Wang, Y. Yu, F. Chen, J. Liu, Y. Li, Gadolinium chloride improves the course of TNBS and DSS-induced colitis through protecting against colonic mucosal inflammation, *Scientific Reports* 4 (2014) 6096.

<https://doi.org/10.1038/srep06096>

- [193] L.C. Adding, G.L. Bannenberg, L.E. Gustafsson, Basic experimental studies and clinical aspects of gadolinium salts and chelates, *Cardiovascular Drug Reviews* 19(1) (2001) 41-56.  
<https://doi.org/10.1111/j.1527-3466.2001.tb00182.x>
- [194] N.A. Agha, R. Willumeit-Römer, D. Laippl, B. Luthringer, F. Feyerabend, The degradation interface of magnesium based alloys in direct contact with human primary osteoblast cells, *PLoS One* 11(6) (2016) e0157874.  
<https://doi.org/10.1371/journal.pone.0157874>
- [195] A.K. Malekshah, A.E. Moghaddam, S.M. Daraka, Comparison of conditioned medium and direct co-culture of human granulosa cells on mouse embryo development, *Indian Journal of Experimental Biology* 44(3) (2006) 189-192.  
<http://nopr.niscair.res.in/handle/123456789/6373>
- [196] Y. Miki, K. Ono, S. Hata, T. Suzuki, H. Kumamoto, H. Sasano, The advantages of co-culture over mono cell culture in simulating in vivo environment, *The Journal of Steroid Biochemistry and Molecular Biology* 131(3-5) (2012) 68-75.  
<https://doi.org/10.1016/j.jsbmb.2011.12.004>
- [197] Z. Chen, T. Klein, R.Z. Murray, R. Crawford, J. Chang, C. Wu, Y. Xiao, Osteoimmunomodulation for the development of advanced bone biomaterials, *Materials Today* 19(6) (2016) 304-321.  
<https://doi.org/10.1016/j.mattod.2015.11.004>
- [198] E. Nidadavolu, F. Feyerabend, T. Ebel, R. Willumeit-Römer, M. Dahms, On the determination of magnesium degradation rates under physiological conditions, *Materials* 9(8) (2016) 627.  
<https://doi.org/10.3390/ma9080627>
- [199] F. Zamani, F.Z. Shahneh, L. Aghebati-Maleki, B. Baradaran, Induction of CD14 expression and differentiation to monocytes or mature macrophages in promyelocytic cell lines: new approach, *Advanced Pharmaceutical Bulletin* 3(2) (2013) 329-332.  
<https://doi.org/10.5681/apb.2013.053>
- [200] D.A. Chistiakov, M.C. Killingsworth, V.A. Myasoedova, A.N. Orekhov, Y.V. Bobryshev, CD68/macrosialin: not just a histochemical marker, *Laboratory Investigation* 97(1) (2017) 4-13.  
<https://doi.org/10.1038/labinvest.2016.116>
- [201] J.M. Hu, K. Liu, J.H. Liu, X.L. Jiang, X.L. Wang, Y.Z. Chen, S.G. Li, H. Zou, L.J. Pang, C.X. Liu, X.B. Cui, L. Yang, J. Zhao, X.H. Shen, J.F. Jiang, W.H. Liang, X.L. Yuan, F. Li, CD163 as a marker of M2 macrophage, contribute to predict aggressiveness and prognosis of Kazakh esophageal squamous cell carcinoma, *Oncotarget* 8(13) (2017) 21526-21538.  
<https://doi.org/10.18632/oncotarget.15630>
- [202] G. Szalóki, K. Goda, Compensation in multicolor flow cytometry, *Cytometry Part A* 87(11) (2015) 982-985.  
<https://doi.org/10.1002/cyto.a.22736>
- [203] R. Sarugaser, D. Lickorish, D. Baksh, M.M. Hosseini, J.E. Davies, Human umbilical cord perivascular (HUCPV) cells: a source of mesenchymal progenitors, *Stem Cells* 23(2) (2005) 220-229.  
<https://doi.org/10.1634/stemcells.2004-0166>

- [204] A. Grada, M. Otero-Vinas, F. Prieto-Castrillo, Z. Obagi, V. Falanga, Research techniques made simple: analysis of collective cell migration using the wound healing assay, *Journal of Investigative Dermatology* 137(2) (2017) e11-e16.  
<https://doi.org/10.1016/j.jid.2016.11.020>
- [205] S. Kinoshita, K. Uzu, K. Nakano, M. Shimizu, T. Takahashi, M. Matsui, Mitomycin derivatives. 1. preparation of mitosane and mitosene compounds and their biological activities, *Journal of Medicinal Chemistry* 14(2) (1971) 103-109.  
<https://doi.org/10.1021/jm00284a005>
- [206] M.M. Cohen, M.W. Shaw, Effects of mitomycin C on human chromosomes, *The Journal of Cell Biology* 23(2) (1964) 386-395.  
<https://doi.org/10.1083/jcb.23.2.386>
- [207] M. Weiss, Y. López, K. McIntosh, Wharton's jelly-derived mesenchymal stromal cells as immunoregulatory cells, in: N. Bhattacharya, P. Stubblefield (Eds.), *Human Fetal Tissue Transplantation*, Springer2013, pp. 87-105.  
[https://doi.org/10.1007/978-1-4471-4171-6\\_7](https://doi.org/10.1007/978-1-4471-4171-6_7)
- [208] S. Jyothi Prasanna, V. Sowmya Jahnavi, Wharton's jelly mesenchymal stem cells as off-the-shelf cellular therapeutics: a closer look into their regenerative and immunomodulatory properties, *The Open Tissue Engineering and Regenerative Medicine Journal* 4(1) (2011) 28-38.  
<https://doi.org/10.2174/1875043501104010028>
- [209] M.N. Walter, K.T. Wright, H.R. Fuller, S. MacNeil, W.E.B. Johnson, Mesenchymal stem cell-conditioned medium accelerates skin wound healing: an in vitro study of fibroblast and keratinocyte scratch assays, *Experimental Cell Research* 316(7) (2010) 1271-1281.  
<https://doi.org/10.1016/j.yexcr.2010.02.026>
- [210] S.A. Park, C.H. Ryu, S.M. Kim, J.Y. Lim, S.I. Park, C.H. Jeong, J. Jun, J.H. Oh, S.H. Park, W. Oh, CXCR4-transfected human umbilical cord blood-derived mesenchymal stem cells exhibit enhanced migratory capacity toward gliomas, *International Journal of Oncology* 38(1) (2011) 97-103.  
[https://doi.org/10.3892/ijo\\_00000828](https://doi.org/10.3892/ijo_00000828)
- [211] D.E.H. Heinemann, H. Siggelkow, L.M. Ponce, V. Viereck, K.G. Wiese, J.H. Peters, Alkaline phosphatase expression during monocyte differentiation overlapping markers as a link between monocytic cells, dendritic cells, osteoclasts and osteoblasts, *Immunobiology* 202(1) (2000) 68-81.  
[https://doi.org/10.1016/S0171-2985\(00\)80054-6](https://doi.org/10.1016/S0171-2985(00)80054-6)
- [212] L. Claes, S. Recknagel, A. Ignatius, Fracture healing under healthy and inflammatory conditions, *Nature Reviews Rheumatology* 8(3) (2012) 133-143.  
<https://doi.org/10.1038/nrrheum.2012.1>
- [213] D.J. Prockop, Concise review: two negative feedback loops place mesenchymal stem/stromal cells at the center of early regulators of inflammation, *Stem Cells* 31(10) (2013) 2042-2046.  
<https://doi.org/10.1002/stem.1400>
- [214] S. Franz, S. Rammelt, D. Scharnweber, J.C. Simon, Immune responses to implants - a review of the implications for the design of immunomodulatory biomaterials, *Biomaterials* 32(28) (2011) 6692-6709.

<https://doi.org/10.1016/j.biomaterials.2011.05.078>

[215] P.M. Chen, M.L. Yen, K.J. Liu, H.K. Sytwu, B.L. Yen, Immunomodulatory properties of human adult and fetal multipotent mesenchymal stem cells, *Journal of Biomedical Science* 18(1) (2011) 49.

<https://doi.org/10.1186/1423-0127-18-49>

[216] D. Baksh, R. Yao, R.S. Tuan, Comparison of proliferative and multilineage differentiation potential of human mesenchymal stem cells derived from umbilical cord and bone marrow, *Stem Cells* 25(6) (2007) 1384-1392.

<https://doi.org/10.1634/stemcells.2006-0709>

[217] L. Penolazzi, E. Lambertini, E. Tavanti, E. Torreggiani, F. Vesce, R. Gambari, R. Piva, Evaluation of chemokine and cytokine profiles in osteoblast progenitors from umbilical cord blood stem cells by BIO - PLEX technology, *Cell Biology International* 32(2) (2008) 320-325.

<https://doi.org/10.1016/j.cellbi.2007.08.030>

[218] R.B. Naqvi, Y.F. Joya, M.R.A. Karim, Next-generation biomaterials for bone-tissue regeneration: Mg-alloys on the move, *Key Engineering Materials* 778 (2018) 306-315.

<https://doi.org/10.4028/www.scientific.net/kem.778.306>

[219] Y.C. Li, M.H. Li, W.Y. Hu, P.D. Hodgson, C.E. Wen, Biodegradable Mg-Ca and Mg-Ca-Y alloys for regenerative medicine, *Materials Science Forum* 654-656 (2010) 2192-2195.

<https://doi.org/10.4028/www.scientific.net/msf.654-656.2192>

[220] S. Agarwal, J. Curtin, B. Duffy, S. Jaiswal, Biodegradable magnesium alloys for orthopaedic applications: a review on corrosion, biocompatibility and surface modifications, *Materials Science and Engineering: C* 68 (2016) 948-963.

<https://doi.org/10.1016/j.msec.2016.06.020>

[221] Z. Zhen, T.F. Xi, Y.F. Zheng, A review on in vitro corrosion performance test of biodegradable metallic materials, *Transactions of Nonferrous Metals Society of China* 23(8) (2013) 2283-2293.

[https://doi.org/10.1016/s1003-6326\(13\)62730-2](https://doi.org/10.1016/s1003-6326(13)62730-2)

[222] R. Willumeit, A. Möhring, F. Feyerabend, Optimization of cell adhesion on mg based implant materials by pre-incubation under cell culture conditions, *International Journal of Molecular Sciences* 15(5) (2014) 7639-7650.

<https://doi.org/10.3390/ijms15057639>

[223] A. Lock, J. Cornish, D.S. Musson, The role of in vitro immune response assessment for biomaterials, *Journal of Functional Biomaterials* 10(3) (2019) 31.

<https://doi.org/10.3390/ifb10030031>

[224] A.M. Romani, Cellular magnesium homeostasis, *Archives of Biochemistry and Biophysics* 512(1) (2011) 1-23.

<https://doi.org/10.1016/j.abb.2011.05.010>

[225] W. Jähnen-Decent, M. Ketteler, Magnesium basics, *Clinical Kidney Journal* 5(Suppl\_1) (2012) i3-i14.

<https://doi.org/10.1093/ndtplus/sfr163>

[226] C. Sissi, M. Palumbo, Effects of magnesium and related divalent metal ions in topoisomerase structure and function, *Nucleic Acids Research* 37(3) (2009) 702-711.

<https://doi.org/10.1093/nar/gkp024>

- [227] C.W. Bock, A.K. Katz, G.D. Markham, J.P. Glusker, Manganese as a replacement for magnesium and zinc: functional comparison of the divalent ions, *Journal of the American Chemical Society* 121(32) (1999) 7360-7372.  
<https://doi.org/10.1021/ja9906960>
- [228] C. Sissi, A. Chemello, E. Vazquez, L.A. Mitchenall, A. Maxwell, M. Palumbo, DNA gyrase requires DNA for effective two-site coordination of divalent metal ions: further insight into the mechanism of enzyme action, *Biochemistry* 47(33) (2008) 8538-8545.  
<https://doi.org/10.1021/bi800480j>
- [229] J.E. Deweese, A.B. Burgin, N. Osheroff, Human topoisomerase II $\alpha$  uses a two-metal-ion mechanism for DNA cleavage, *Nucleic Acids Research* 36(15) (2008) 4883-4893.  
<https://doi.org/10.1093/nar/gkn466>
- [230] A. Drynda, N. Deinet, N. Braun, M. Peuster, Rare earth metals used in biodegradable magnesium - based stents do not interfere with proliferation of smooth muscle cells but do induce the upregulation of inflammatory genes, *Journal of Biomedical Materials Research Part A* 91A(2) (2009) 360-369.  
<https://doi.org/10.1002/jbm.a.32235>
- [231] K.L. West, E.L. Meczes, R. Thorn, R.M. Turnbull, R. Marshall, C.A. Austin, Mutagenesis of E477 or K505 in the B' domain of human topoisomerase II $\beta$  increases the requirement for magnesium ions during strand passage, *Biochemistry* 39(6) (2000) 1223-1233.  
<https://doi.org/10.1021/bi991328b>
- [232] S.S. Ozturk, B.O. Palsson, Effect of medium osmolarity on hybridoma growth, metabolism, and antibody production, *Biotechnology and Bioengineering* 37(10) (1991) 989-993.  
<https://doi.org/10.1002/bit.260371015>
- [233] F. Cecchinato, N.A. Agha, A.H. Martinez-Sanchez, B.J.C. Luthringer, F. Feyerabend, R. Jimbo, R. Willumeit-Römer, A. Wennerberg, Influence of magnesium alloy degradation on undifferentiated human cells, *PloS One* 10(11) (2015) e0142117.  
<https://doi.org/10.1371/journal.pone.0142117>
- [234] F. Seuss, S. Seuss, M. Turhan, B. Fabry, S. Virtanen, Corrosion of Mg alloy AZ91D in the presence of living cells, *Journal of Biomedical Materials Research Part B: Applied Biomaterials* 99B(2) (2011) 276-281.  
<https://doi.org/10.1002/jbm.b.31896>
- [235] Y. Wang, X. Xie, H. Li, X. Wang, M. Zhao, E. Zhang, Y. Bai, Y. Zheng, L. Qin, Biodegradable CaMgZn bulk metallic glass for potential skeletal application, *Acta Biomaterialia* 7(8) (2011) 3196-3208.  
<https://doi.org/10.1016/j.actbio.2011.04.027>
- [236] D.A. Bushinsky, Metabolic alkalosis decreases bone calcium efflux by suppressing osteoclasts and stimulating osteoblasts, *American Journal of Physiology-Renal Physiology* 271(1) (1996) F216-F222.  
<https://doi.org/10.1152/ajprenal.1996.271.1.F216>
- [237] J. Wang, F. Witte, T. Xi, Y. Zheng, K. Yang, Y. Yang, D. Zhao, J. Meng, Y. Li, W. Li, Recommendation for modifying current cytotoxicity testing standards for biodegradable magnesium-based materials, *Acta Biomaterialia* 21 (2015) 237-249.  
<https://doi.org/10.1016/j.actbio.2015.04.011>

[238] D. Bushinsky, N. Krieger, D. Geisser, E. Grossman, F. Coe, Effects of pH on bone calcium and proton fluxes in vitro, American Journal of Physiology-Renal Physiology 245(2) (1983) F204-F209.

<https://doi.org/10.1152/ajprenal.1983.245.2.f204>

[239] W. Liu, T. Wang, C. Yang, B.W. Darvell, J. Wu, K. Lin, J. Chang, H. Pan, W.W. Lu, Alkaline biodegradable implants for osteoporotic bone defects—importance of microenvironment pH, Osteoporosis International 27(1) (2016) 93-104.

<https://doi.org/10.1007/s00198-015-3217-8>

[240] L. Chung, D.R. Maestas Jr, F. Housseau, J.H. Elisseeff, Key players in the immune response to biomaterial scaffolds for regenerative medicine, Advanced Drug Delivery Reviews 114 (2017) 184-192.

<https://doi.org/10.1016/j.addr.2017.07.006>

[241] B.D. Ratner, A.S. Hoffman, F.J. Schoen, J.E. Lemons, Biomaterials science: an introduction to materials in medicine, 2nd ed., Elsevier2004.

<https://doi.org/10.1016/C2009-0-02433-7>

[242] R. Chen, J. Curran, F. Pu, Z. Zhuola, Y. Bayon, J.A. Hunt, In vitro response of human peripheral blood mononuclear cells (PBMC) to collagen films treated with cold plasma, Polymers 9(7) (2017) 254.

<https://doi.org/10.3390/polym9070254>

[243] A. Hammerl, C.E. Diaz Cano, E.M. De-Juan-Pardo, M. van Griensven, P.S. Poh, A growth factor-free co-culture system of osteoblasts and peripheral blood mononuclear cells for the evaluation of the osteogenesis potential of melt-electrowritten polycaprolactone scaffolds, International Journal of Molecular Sciences 20(5) (2019) 1068.

<https://doi.org/10.3390/ijms20051068>

[244] D. Friberg, J. Bryant, W. Shannon, T. Whiteside, In vitro cytokine production by normal human peripheral blood mononuclear cells as a measure of immunocompetence or the state of activation, Clinical and Diagnostic Laboratory Immunology 1(3) (1994) 261-268.

<https://www.ncbi.nlm.nih.gov/pmc/articles/PMC368246/>

[245] M. Seitz, M. Zwicker, B. Wider, Enhanced in vitro induced production of interleukin 10 by peripheral blood mononuclear cells in rheumatoid arthritis is associated with clinical response to methotrexate treatment, The Journal of Rheumatology 28(3) (2001) 496-501.

<https://www.ncbi.nlm.nih.gov/pubmed/11296948>

[246] B.N. Brown, J.E. Valentin, A.M. Stewart-Akers, G.P. McCabe, S.F. Badylak, Macrophage phenotype and remodeling outcomes in response to biologic scaffolds with and without a cellular component, Biomaterials 30(8) (2009) 1482-1491.

<https://doi.org/10.1016/j.biomaterials.2008.11.040>

[247] B.N. Brown, R. Londono, S. Tottey, L. Zhang, K.A. Kukla, M.T. Wolf, K.A. Daly, J.E. Reing, S.F. Badylak, Macrophage phenotype as a predictor of constructive remodeling following the implantation of biologically derived surgical mesh materials, Acta Biomaterialia 8(3) (2012) 978-987.

<https://doi.org/10.1016/j.actbio.2011.11.031>

[248] S. Gordon, The macrophage: past, present and future, European Journal of Immunology 37(S1) (2007) S9-S17.

<https://doi.org/10.1002/eji.200737638>

- [249] A. Mantovani, S.K. Biswas, M.R. Galdiero, A. Sica, M. Locati, Macrophage plasticity and polarization in tissue repair and remodelling, *The Journal of Pathology* 229(2) (2013) 176-185.  
<https://doi.org/10.1002/path.4133>
- [250] F. Porcheray, S. Viaud, A.C. Rimaniol, C. Leone, B. Samah, N. Dereuddre - Bosquet, D. Dormont, G. Gras, Macrophage activation switching: an asset for the resolution of inflammation, *Clinical and Experimental Immunology* 142(3) (2005) 481-489.  
<https://doi.org/10.1111/j.1365-2249.2005.02934.x>
- [251] T. Lawrence, C. Fong, The resolution of inflammation: anti-inflammatory roles for NF- $\kappa$ B, *The International Journal of Biochemistry & Cell Biology* 42(4) (2010) 519-523.  
<https://doi.org/10.1016/j.biocel.2009.12.016>
- [252] F.J. Van Dalen, M.H. Van Stevendaal, F.L. Fennemann, M. Verdoes, O. Ilina, Molecular repolarisation of tumour-associated macrophages, *Molecules* 24(1) (2019) 9.  
<https://doi.org/10.3390/molecules24010009>
- [253] X. Zheng, K. Turkowski, J. Mora, B. Brüne, W. Seeger, A. Weigert, R. Savai, Redirecting tumor-associated macrophages to become tumoricidal effectors as a novel strategy for cancer therapy, *Oncotarget* 8(29) (2017) 48436-48452.  
<https://doi.org/10.18632/oncotarget.17061>
- [254] C. Mills, M1 and M2 macrophages: oracles of health and disease, *Critical Reviews™ in Immunology* 32(6) (2012) 463-488.  
<https://doi.org/10.1615/critrevimmunol.v32.i6.10>
- [255] J.D. Bryers, C.M. Giachelli, B.D. Ratner, Engineering biomaterials to integrate and heal: the biocompatibility paradigm shifts, *Biotechnology and Bioengineering* 109(8) (2012) 1898-1911.  
<https://doi.org/10.1002/bit.24559>
- [256] J.M. Anderson, A.K. McNally, Biocompatibility of implants: lymphocyte/macrophage interactions, *Seminars in Immunopathology* 33(3) (2011) 221-233.  
<https://doi.org/10.1007/s00281-011-0244-1>
- [257] E.M. Sussman, M.C. Halpin, J. Muster, R.T. Moon, B.D. Ratner, Porous implants modulate healing and induce shifts in local macrophage polarization in the foreign body reaction, *Annals of Biomedical Engineering* 42(7) (2014) 1508-1516.  
<https://doi.org/10.1007/s10439-013-0933-0>
- [258] K.L. Spiller, R.R. Anfang, K.J. Spiller, J. Ng, K.R. Nakazawa, J.W. Daulton, G. Vunjak-Novakovic, The role of macrophage phenotype in vascularization of tissue engineering scaffolds, *Biomaterials* 35(15) (2014) 4477-4488.  
<https://doi.org/10.1016/j.biomaterials.2014.02.012>
- [259] P. Batten, P. Sarathchandra, J.W. Antoniw, S.S. Tay, M.W. Lowdell, P.M. Taylor, M.H. Yacoub, Human mesenchymal stem cells induce T cell anergy and downregulate T cell allo-responses via the TH2 pathway: relevance to tissue engineering human heart valves, *Tissue Engineering* 12(8) (2006) 2263-2273.  
<https://doi.org/10.1089/ten.2006.12.2263>
- [260] A. Bertolo, D. Pavlicek, A. Gemperli, M. Baur, T. Pötzl, J. Stoyanov, Increased motility of mesenchymal stem cells is correlated with inhibition of stimulated peripheral blood mononuclear cells in vitro, *Journal of Stem Cells & Regenerative Medicine* 13(2) (2017) 62-74.  
<https://www.ncbi.nlm.nih.gov/pubmed/29391751>

- [261] W. Bonner, H. Hulett, R. Sweet, L. Herzenberg, Fluorescence activated cell sorting, Review of Scientific Instruments 43(3) (1972) 404-409.  
<https://doi.org/10.1063/1.1685647>
- [262] T. Hu, H. Xu, C. Wang, H. Qin, Z. An, Magnesium enhances the chondrogenic differentiation of mesenchymal stem cells by inhibiting activated macrophage-induced inflammation, Scientific Reports 8(1) (2018) 3406.  
<https://doi.org/10.1038/s41598-018-21783-2>
- [263] B. Li, H. Cao, Y. Zhao, M. Cheng, H. Qin, T. Cheng, Y. Hu, X. Zhang, X. Liu, In vitro and in vivo responses of macrophages to magnesium-doped titanium, Scientific Reports 7 (2017) 42707.  
<https://doi.org/10.1038/srep42707>
- [264] C. Manferdini, F. Paolella, E. Gabusi, L. Gambari, A. Piacentini, G. Filardo, S. Fleury-Cappellessi, A. Barbero, M. Murphy, G. Lisignoli, Adipose stromal cells mediated switching of the pro-inflammatory profile of M1-like macrophages is facilitated by PGE2: in vitro evaluation, Osteoarthritis and Cartilage 25(7) (2017) 1161-1171.  
<https://doi.org/10.1016/j.joca.2017.01.011>
- [265] L.Y. Lu, F. Loi, K. Nathan, T.h. Lin, J. Pajarinen, E. Gibon, A. Nabeshima, L. Cordova, E. Jämsen, Z. Yao, Pro - inflammatory M1 macrophages promote osteogenesis by mesenchymal stem cells via the COX - 2 - prostaglandin E2 pathway, Journal of Orthopaedic Research 35(11) (2017) 2378-2385.  
<https://doi.org/10.1002/jor.23553>
- [266] J. Frasor, A.E. Weaver, M. Pradhan, K. Mehta, Synergistic up-regulation of prostaglandin E synthase expression in breast cancer cells by 17 $\beta$ -estradiol and proinflammatory cytokines, Endocrinology 149(12) (2008) 6272-6279.  
<https://doi.org/10.1210/en.2008-0352>
- [267] M.B. Al - Shaibani, X.N. Wang, P.E. Lovat, A.M. Dickinson, Cellular therapy for wounds: applications of mesenchymal stem cells in wound healing, in: V.A. Alexandrescu (Ed.), Wound Healing-New insights into Ancient Challenges, InTechOpen2016, pp. 99-131.  
<https://doi.org/10.5772/63963>
- [268] A. Gebler, O. Zabel, B. Seliger, The immunomodulatory capacity of mesenchymal stem cells, Trends in Molecular Medicine 18(2) (2012) 128-134.  
<https://doi.org/10.1016/j.molmed.2011.10.004>
- [269] K. Kumagai, A. Vasanji, J.A. Drazba, R.S. Butler, G.F. Muschler, Circulating cells with osteogenic potential are physiologically mobilized into the fracture healing site in the parabiotic mice model, Journal of Orthopaedic Research 26(2) (2008) 165-175.  
<https://doi.org/10.1002/jor.20477>
- [270] C. Colnot, S. Huang, J. Helms, Analyzing the cellular contribution of bone marrow to fracture healing using bone marrow transplantation in mice, Biochemical and Biophysical Research Communications 350(3) (2006) 557-561.  
<https://doi.org/10.1016/j.bbrc.2006.09.079>
- [271] L. da Silva Meirelles, A.M. Fontes, D.T. Covas, A.I. Caplan, Mechanisms involved in the therapeutic properties of mesenchymal stem cells, Cytokine & Growth Factor Reviews 20(5-6) (2009) 419-427.  
<https://doi.org/10.1016/j.cytogfr.2009.10.002>

- [272] J.J. El-Jawhari, E. Jones, P.V. Giannoudis, The roles of immune cells in bone healing; what we know, do not know and future perspectives, *Injury* 47(11) (2016) 2399-2406.  
<https://doi.org/10.1016/j.injury.2016.10.008>
- [273] A. Yadav, V. Saini, S. Arora, MCP-1: chemoattractant with a role beyond immunity: a review, *Clinica Chimica Acta* 411(21-22) (2010) 1570-1579.  
<https://doi.org/10.1016/j.cca.2010.07.006>
- [274] H. Wei, X. Zhao, R. Yuan, X. Dai, Y. Li, L. Liu, Effects of PB-EPCs on homing ability of rabbit BMSCs via endogenous SDF-1 and MCP-1, *PloS One* 10(12) (2015) e0145044.  
<https://doi.org/10.1371/journal.pone.0145044>
- [275] T. Furuta, S. Miyaki, H. Ishitobi, T. Ogura, Y. Kato, N. Kamei, K. Miyado, Y. Higashi, M. Ochi, Mesenchymal stem cell - derived exosomes promote fracture healing in a mouse model, *Stem Cells Translational Medicine* 5(12) (2016) 1620-1630.  
<https://doi.org/10.5966/sctm.2015-0285>
- [276] S.S. Jakobsen, A. Larsen, M. Stoltenberg, J.M. Bruun, K. Soballe, Effects of as-cast and wrought cobalt-chrome-molybdenum and titanium-aluminium-vanadium alloys on cytokine gene expression and protein secretion in J774A. 1 macrophages, *European Cells & Materials* 14 (2007) 45-55.  
<https://doi.org/10.22203/ecm.v014a05>
- [277] S. Vallet, S. Pozzi, K. Patel, N. Vaghela, M. Fulciniti, P. Veiby, T. Hidemitsu, L. Santo, D. Cirstea, D.T. Scadden, A novel role for CCL3 (MIP-1 $\alpha$ ) in myeloma-induced bone disease via osteocalcin downregulation and inhibition of osteoblast function, *Leukemia* 25(7) (2011) 1174-1181.  
<https://doi.org/10.1038/leu.2011.43>
- [278] M. Maurer, E. Von Stebut, Macrophage inflammatory protein-1, *The International Journal of Biochemistry & Cell Biology* 36(10) (2004) 1882-1886.  
<https://doi.org/10.1016/j.biocel.2003.10.019>
- [279] A. Yang, Y. Lu, J. Xing, Z. Li, X. Yin, C. Dou, S. Dong, F. Luo, Z. Xie, T. Hou, IL-8 enhances therapeutic effects of BMSCs on bone regeneration via CXCR2-mediated PI3k/Akt signaling pathway, *Cellular Physiology and Biochemistry* 48(1) (2018) 361-370.  
<https://doi.org/10.1159/000491742>
- [280] Y.S. Hwang, S.K. Lee, K.K. Park, W.Y. Chung, Secretion of IL-6 and IL-8 from lysophosphatidic acid-stimulated oral squamous cell carcinoma promotes osteoclastogenesis and bone resorption, *Oral Oncology* 48(1) (2012) 40-48.  
<https://doi.org/10.1016/j.oraloncology.2011.08.022>
- [281] J. Kim, N.K. Kim, S.R. Park, B.H. Choi, GM-CSF enhances mobilization of bone marrow mesenchymal stem cells via a CXCR4-mediated mechanism, *Tissue Eng Regen Med* 16(1) (2018) 59-68.  
<https://doi.org/10.1007/s13770-018-0163-5>
- [282] J.J. Grzesiak, M.D. Pierschbacher, Shifts in the concentrations of magnesium and calcium in early porcine and rat wound fluids activate the cell migratory response, *The Journal of Clinical Investigation* 95(1) (1995) 227-233.  
<https://doi.org/10.1172/jci117644>
- [283] A. Hussain, K. Bessho, K. Takahashi, Y. Tabata, Magnesium calcium phosphate as a novel component enhances mechanical/physical properties of gelatin scaffold and osteogenic

differentiation of bone marrow mesenchymal stem cells, *Tissue Engineering Part A* 18(7-8) (2011) 768-774.

<https://doi.org/10.1089/ten.tea.2011.0310>

[284] J.M. Díaz-Tocados, C. Herencia, J.M. Martínez-Moreno, A.M. De Oca, M.E. Rodríguez-Ortiz, N. Vergara, A. Blanco, S. Steppan, Y. Almadén, M. Rodríguez, Magnesium chloride promotes osteogenesis through notch signaling activation and expansion of mesenchymal stem cells, *Scientific Reports* 7(1) (2017) 7839.

<https://doi.org/10.1038/s41598-017-08379-y>

[285] K. Ekström, O. Omar, C. Granéli, X. Wang, F. Vazirisani, P. Thomsen, Monocyte exosomes stimulate the osteogenic gene expression of mesenchymal stem cells, *PloS One* 8(9) (2013) e75227.

<https://doi.org/10.1371/journal.pone.0075227>

[286] Z. Sheikh, P.J. Brooks, O. Barzilay, N. Fine, M. Glogauer, Macrophages, foreign body giant cells and their response to implantable biomaterials, *Materials* 8(9) (2015) 5671-5701.

<https://doi.org/10.3390/ma8095269>

[287] C.A. Heid, J. Stevens, K.J. Livak, P.M. Williams, Real time quantitative PCR, *Genome Research* 6(10) (1996) 986-994.

<https://doi.org/10.1101/gr.6.10.986>

[288] T.J. Cho, J.A. Kim, C.Y. Chung, W.J. Yoo, L.C. Gerstenfeld, T.A. Einhorn, I.H. Choi, Expression and role of interleukin-6 in distraction osteogenesis, *Calcified Tissue International* 80(3) (2007) 192-200.

<https://doi.org/10.1007/s00223-006-0240-y>

[289] R.-L. Huang, Y. Yuan, G.-M. Zou, G. Liu, J. Tu, Q. Li, LPS-stimulated inflammatory environment inhibits BMP-2-induced osteoblastic differentiation through crosstalk between TLR4/MyD88/NF-κB and BMP/Smad signaling, *Stem Cells and Development* 23(3) (2013) 277-289.

<https://doi.org/10.1089/scd.2013.0345>

[290] H. Liu, H. Peng, Y. Wu, C. Zhang, Y. Cai, G. Xu, Q. Li, X. Chen, J. Ji, Y. Zhang, The promotion of bone regeneration by nanofibrous hydroxyapatite/chitosan scaffolds by effects on integrin-BMP/Smad signaling pathway in BMSCs, *Biomaterials* 34(18) (2013) 4404-4417.

<https://doi.org/10.1016/j.biomaterials.2013.02.048>

[291] B. Huang, Y. Yuan, T. Li, S. Ding, W. Zhang, Y. Gu, C. Liu, Facilitated receptor-recognition and enhanced bioactivity of bone morphogenetic protein-2 on magnesium-substituted hydroxyapatite surface, *Scientific Reports* 6 (2016) 24323.

<https://doi.org/10.1038/srep24323>

[292] S. Ding, J. Zhang, Y. Tian, B. Huang, Y. Yuan, C. Liu, Magnesium modification up-regulates the bioactivity of bone morphogenetic protein-2 upon calcium phosphate cement via enhanced BMP receptor recognition and Smad signaling pathway, *Colloids and Surfaces B: Biointerfaces* 145 (2016) 140-151.

<https://doi.org/10.1016/j.colsurfb.2016.04.045>

[293] L. Deng, D. Li, Z. Yang, X. Xie, P. Kang, Repair of the calvarial defect in goat model using magnesium-doped porous hydroxyapatite combined with recombinant human bone morphogenetic protein-2, *Bio-Medical Materials and Engineering* 28(4) (2017) 361-377.

<https://doi.org/10.3233/bme-171678>

- [294] S.C. Cifuentes, F. Bensiamar, A.M. Gallardo - Moreno, T.A. Osswald, J.L. González - Carrasco, R. Benavente, M.L. González - Martín, E. García - Rey, N. Vilaboa, L. Saldaña, Incorporation of Mg particles into PDLLA regulates mesenchymal stem cell and macrophage responses, *Journal of Biomedical Materials Research Part A* 104(4) (2016) 866-878.  
<https://doi.org/10.1002/jbm.a.35625>
- [295] Z. Chen, X. Mao, L. Tan, T. Friis, C. Wu, R. Crawford, Y. Xiao, Osteoimmunomodulatory properties of magnesium scaffolds coated with  $\beta$ -tricalcium phosphate, *Biomaterials* 35(30) (2014) 8553-8565.  
<https://doi.org/10.1016/j.biomaterials.2014.06.038>
- [296] B. Li, P. Gao, H. Zhang, Z. Guo, Y. Zheng, Y. Han, Osteoimmunomodulation, osseointegration, and in vivo mechanical integrity of pure Mg coated with HA nanorod/pore-sealed MgO bilayer, *Biomaterials Science* 6(12) (2018) 3202-3218.  
<https://doi.org/10.1039/c8bm00901e>
- [297] D. Lacey, P. Simmons, S. Graves, J. Hamilton, Proinflammatory cytokines inhibit osteogenic differentiation from stem cells: implications for bone repair during inflammation, *Osteoarthritis and Cartilage* 17(6) (2009) 735-742.  
<https://doi.org/10.1016/j.joca.2008.11.011>
- [298] Y. Li, A. Li, K. Strait, H. Zhang, M.S. Nanes, M.N. Weitzmann, Endogenous TNF $\alpha$  lowers maximum peak bone mass and inhibits osteoblastic Smad activation through NF -  $\kappa$ B, *Journal of Bone and Mineral Research* 22(5) (2007) 646-655.  
<https://doi.org/10.1359/jbmr.070121>
- [299] C.B. Sullivan, R.M. Porter, C.H. Evans, T. Ritter, G. Shaw, F. Barry, J.M. Murphy, TNF $\alpha$  and IL-1 $\beta$  influence the differentiation and migration of murine MSCs independently of the NF- $\kappa$ B pathway, *Stem Cell Research & Therapy* 5(4) (2014) 104.  
<https://doi.org/10.1186/scrt492>
- [300] P. Tian, X. Liu, Surface modification of biodegradable magnesium and its alloys for biomedical applications, *Regenerative Biomaterials* 2(2) (2015) 135-151.  
<https://doi.org/10.1093/rb/rbu013>
- [301] X. Xu, Y. Li, L. Wang, Y. Li, J. Pan, X. Fu, Z. Luo, Y. Sui, S. Zhang, L. Wang, Triple-functional polyetheretherketone surface with enhanced bacteriostasis and anti-inflammatory and osseointegrative properties for implant application, *Biomaterials* 212 (2019) 98-114.  
<https://doi.org/10.1016/j.biomaterials.2019.05.014>
- [302] H. Sun, Y. Zhang, L. Dou, X. Song, C. Sun, Surface modification of pure titanium to improve its anti-inflammatory function, *European Journal of Inflammation* 13(3) (2015) 204-208.  
<https://doi.org/10.1177/1721727x15610336>
- [303] W. Wang, K.W. Yeung, Bone grafts and biomaterials substitutes for bone defect repair: a review, *Bioactive Materials* 2(4) (2017) 224-247.  
<https://doi.org/10.1016/j.bioactmat.2017.05.007>
- [304] Z. Chen, D. Yi, X. Zheng, J. Chang, C. Wu, Y. Xiao, Nutrient element-based bioceramic coatings on titanium alloy stimulating osteogenesis by inducing beneficial osteoimmunomodulation, *Journal of Materials Chemistry B* 2(36) (2014) 6030-6043.  
<https://doi.org/10.1039/c4tb00837e>

- [305] X. Lu, K. Li, Y. Xie, S. Qi, Q. Shen, J. Yu, L. Huang, X. Zheng, Improved osteogenesis of boron incorporated calcium silicate coatings via immunomodulatory effects, *Journal of Biomedical Materials Research Part A* 107(1) (2019) 12-24.  
<https://doi.org/10.1002/jbm.a.36456>
- [306] J. Pajarinen, Y. Tamaki, J.K. Antonios, T.H. Lin, T. Sato, Z. Yao, M. Takagi, Y.T. Konttinen, S.B. Goodman, Modulation of mouse macrophage polarization in vitro using IL - 4 delivery by osmotic pumps, *Journal of Biomedical Materials Research Part A* 103(4) (2015) 1339-1345.  
<https://doi.org/10.1002/jbm.a.35278>
- [307] A.J. Spencer, S.A. Wilson, J. Batchelor, A. Reid, J. Pees, E. Harpur, Gadolinium chloride toxicity in the rat, *Toxicologic Pathology* 25(3) (1997) 245-255.  
<https://doi.org/10.1177/019262339702500301>
- [308] O.P. Gautschi, S.P. Frey, R. Zellweger, Bone morphogenetic proteins in clinical applications, *ANZ Journal of Surgery* 77(8) (2007) 626-631.  
<https://doi.org/10.1111/j.1445-2197.2007.04175.x>
- [309] B. Tabisz, W. Schmitz, M. Schmitz, T. Luehmann, E. Heusler, J.C. Rybak, L. Meinel, J.E. Fiebig, T.D. Mueller, J. Nickel, Site directed immobilization of BMP-2: two approaches for the production of osteoinductive scaffolds, *Biomacromolecules* 18(3) (2017) 695-708.  
<https://doi.org/10.1021/acs.biomac.6b01407>
- [310] G. Wu, Y. Liu, T. Iizuka, E.B. Hunziker, The effect of a slow mode of BMP-2 delivery on the inflammatory response provoked by bone-defect-filling polymeric scaffolds, *Biomaterials* 31(29) (2010) 7485-7493.  
<https://doi.org/10.1016/j.biomaterials.2010.06.037>
- [311] Y. Liu, L. Wang, T. Kikuchi, K. Akiyama, C. Chen, X. Xu, R. Yang, W. Chen, S. Wang, S. Shi, Mesenchymal stem cell-based tissue regeneration is governed by recipient T lymphocytes via IFN- $\gamma$  and TNF- $\alpha$ , *Nature Medicine* 17(12) (2011) 1594-1601.  
<https://doi.org/10.1038/nm.2542>
- [312] T. Hickey, D. Kreutzer, D. Burgess, F. Moussy, Dexamethasone/PLGA microspheres for continuous delivery of an anti-inflammatory drug for implantable medical devices, *Biomaterials* 23(7) (2002) 1649-1656.  
[https://doi.org/10.1016/s0142-9612\(01\)00291-5](https://doi.org/10.1016/s0142-9612(01)00291-5)
- [313] N. Benkirane - Jessel, P. Lavalle, F. Meyer, F. Audouin, B. Frisch, P. Schaaf, J. Ogier, G. Decher, J.C. Voegel, Control of monocyte morphology on and response to model surfaces for implants equipped with anti - inflammatory agent, *Advanced Materials* 16(17) (2004) 1507-1511.  
<https://doi.org/10.1002/adma.200306613>
- [314] X. Wang, Y. Wang, W. Gou, Q. Lu, J. Peng, S. Lu, Role of mesenchymal stem cells in bone regeneration and fracture repair: a review, *International Orthopaedics* 37(12) (2013) 2491-2498.  
<https://doi.org/10.1007/s00264-013-2059-2>
- [315] K.L. Spiller, T.J. Koh, Macrophage-based therapeutic strategies in regenerative medicine, *Advanced Drug Delivery Reviews* 122 (2017) 74-83.  
<https://doi.org/10.1016/j.addr.2017.05.010>
- [316] S. Wood, V. Jayaraman, E.J. Huelsmann, B. Bonish, D. Burgad, G. Sivaramakrishnan, S. Qin, L.A. DiPietro, A. Zloza, C. Zhang, Pro-inflammatory chemokine CCL2 (MCP-1) promotes

healing in diabetic wounds by restoring the macrophage response, PloS One 9(3) (2014) e91574.

<https://doi.org/10.1371/journal.pone.0091574>

[317] J. Ma, Q. Wang, T. Fei, J.-D.J. Han, Y.-G. Chen, MCP-1 mediates TGF- $\beta$ -induced angiogenesis by stimulating vascular smooth muscle cell migration, Blood 109(3) (2007) 987-994.

<https://doi.org/10.1182/blood-2006-07-036400>

[318] E. Engelhardt, A. Toksoy, M. Goebeler, S. Debus, E.-B. Bröcker, R. Gillitzer, Chemokines IL-8, GRO $\alpha$ , MCP-1, IP-10, and Mig are sequentially and differentially expressed during phase-specific infiltration of leukocyte subsets in human wound healing, The American Journal of Pathology 153(6) (1998) 1849-1860.

[https://doi.org/10.1016/s0002-9440\(10\)65699-4](https://doi.org/10.1016/s0002-9440(10)65699-4)

[319] S. Gao, J. Zhou, N. Liu, L. Wang, Q. Gao, Y. Wu, Q. Zhao, P. Liu, S. Wang, Y. Liu, Curcumin induces M2 macrophage polarization by secretion IL-4 and/or IL-13, Journal of Molecular and Cellular Cardiology 85 (2015) 131-139.

<https://doi.org/10.1016/j.yjmcc.2015.04.025>

[320] T. Veremeyko, S. Siddiqui, I. Sotnikov, A. Yung, E.D. Ponomarev, IL-4/IL-13-dependent and independent expression of miR-124 and its contribution to M2 phenotype of monocytic cells in normal conditions and during allergic inflammation, PloS One 8(12) (2013) e81774.

<https://doi.org/10.1371/journal.pone.0081774>

[321] M.A. Bouhlel, B. Derudas, E. Rigamonti, R. Dièvert, J. Brozek, S. Haulon, C. Zawadzki, B. Jude, G. Torpier, N. Marx, PPAR $\gamma$  activation primes human monocytes into alternative M2 macrophages with anti-inflammatory properties, Cell Metabolism 6(2) (2007) 137-143.

<https://doi.org/10.1016/j.cmet.2007.06.010>

[322] M. Bartneck, K.-H. Heffels, Y. Pan, M. Bovi, G. Zwadlo-Klarwasser, J. Groll, Inducing healing-like human primary macrophage phenotypes by 3D hydrogel coated nanofibres, Biomaterials 33(16) (2012) 4136-4146.

<https://doi.org/10.1016/j.biomaterials.2012.02.050>

[323] D.P. Vasconcelos, M. Costa, I.F. Amaral, M.A. Barbosa, A.P. Águas, J.N. Barbosa, Modulation of the inflammatory response to chitosan through M2 macrophage polarization using pro-resolution mediators, Biomaterials 37 (2015) 116-123.

<https://doi.org/10.1016/j.biomaterials.2014.10.035>

[324] X. Li, Q. Huang, L. Liu, W. Zhu, T.A. Elkhooly, Y. Liu, Q. Feng, Q. Li, S. Zhou, Y. Liu, Reduced inflammatory response by incorporating magnesium into porous TiO<sub>2</sub> coating on titanium substrate, Colloids and Surfaces B: Biointerfaces 171 (2018) 276-284.

<https://doi.org/10.1016/j.colsurfb.2018.07.032>

## Acknowledgements

I would like to express my sincere appreciation to Prof. Dr. Regine Willumeit-Römer and Dr. Bérengère J.C. Luthringer-Feyerabend for giving me opportunity to work in such a great research team. Your broad perspective and full enthusiasm in scientific work helped and encouraged me to fulfill a wonderful doctoral career.

I will be forever thankful to all my colleagues in our warm-hearted team for their work support and communication. Sincerely grateful to Dr. Heike Helmholtz for AAS analysis and scientific writing. Sincerely grateful to Lei Xu, for help of flow cytometry analysis. Sincerely thanks to Steven Behr, for their full support of delivery of donated fresh blood. Sincerely thanks to Anke Schuster, Monika Luczak and Nils Holländer, for all the technical supports. I sincerely thank all my colleagues for the professional work supports and stimulating discussions. No words could express my gratitude.

Thanks are due for fresh blood donations from the University Medical Center Hamburg-Eppendorf. You are all do greatest effort in my doctoral scientific work.

Special thanks to my beloved family. Love you from the depths of my soul.

I appreciate the China Scholarship Council (CSC) for sponsoring my research in Germany.

# Appendix

## Supplementary data

Table S1 Levels of secreted cytokines (normalised by total DNA) in supernatants in transwell coculture system at day 1, 4 and 7. Data were acquired: Cytokine level (pg/mL)/Total DNA contents (µg/mL), and obtained from biological duplicate of three independent experiments came from at least two donors of HUCPV (H) and PBMC (P), resulting in n≥12 (samples size). <<OOR represents “out of calibration range” in multiplex immunoassay.

Day 1	H		H+Mg		P		P+Mg		H+P		H+P+Mg	
	Mean	SD	Mean	SD	Mean	SD	Mean	SD	Mean	SD	Mean	SD
<b>IL6</b>	12988.1017107.7715894.1120299.56	2.79	1.92	329.72	450.86	867.51	1127.60	947.88	1045.25			
<b>IL7</b>	34.02	55.46	133.85	148.98	1.70	2.61	19.72	12.97	2.33	4.36	10.44	13.28
<b>IL9</b>	37.32	87.54	69.60	103.62	1.97	3.62	55.78	31.96	2.62	4.09	4.43	8.24
<b>IL12</b>	16.45	26.38	138.26	194.68	0.29	0.43	4.40	4.12	0.31	0.37	2.77	4.78
<b>IL15</b>	1198.93	1729.66	985.20	1188.27	2.65	4.31	114.44	81.06	64.03	88.69	60.58	79.56
<b>IL17</b>	132.51	146.55	257.37	88.61	1.21	2.09	73.45	44.10	9.17	7.17	12.66	13.09
<b>Eotaxin</b>	100.78	151.06	78.77	116.45	<< OOR	<< OOR	6.79	6.22	6.70	10.09	6.23	9.43
<b>FGFb</b>	182.53	202.45	3164.98	2819.42	0.38	1.00	26.21	12.71	22.18	18.36	296.49	372.40
<b>IP10</b>	288.33	475.68	679.66	631.23	3313.47	4184.98	41227.4929702.55	176.26	280.25	5936.37	9986.01	
<b>VEGF</b>	1070.22	1425.64	7686.98	9930.55	12.04	28.43	257.26	218.41	38.11	62.21	188.44	242.98
<b>PDGF-</b>	<< OOR	<< OOR	<< OOR	<< OOR	<< OOR	<< OOR	<< OOR	<< OOR	<< OOR	<< OOR	<< OOR	<< OOR
<b>RANTES</b>	<< OOR	<< OOR	<< OOR	<< OOR	<< OOR	<< OOR	<< OOR	<< OOR	<< OOR	<< OOR	<< OOR	<< OOR

Table S1 (*Continued*)

<b>Day 4</b>	<b>H</b>		<b>H+Mg</b>		<b>P</b>		<b>P+Mg</b>		<b>H+P</b>		<b>H+P+Mg</b>	
	<b>Mean</b>	<b>SD</b>	<b>Mean</b>	<b>SD</b>	<b>Mean</b>	<b>SD</b>	<b>Mean</b>	<b>SD</b>	<b>Mean</b>	<b>SD</b>	<b>Mean</b>	<b>SD</b>
<b>IL6</b>	18299.47	23981.42	5367.18	6086.13	2.48	1.34	13.55	13.40	1511.72	1870.99	482.20	480.92
<b>IL7</b>	25.66	49.62	22.58	56.90	2.67	7.30	5.07	13.10	1.82	3.49	5.40	9.34
<b>IL9</b>	1.89	6.56	<< OOR	<< OOR	6.30	11.32	7.53	17.52	<< OOR	<< OOR	1.92	3.57
<b>IL12</b>	8.47	13.77	26.79	60.95	0.08	0.16	0.62	1.96	0.58	0.90	2.60	6.10
<b>IL15</b>	1257.32	1599.77	346.15	516.98	3.94	6.24	30.24	72.60	129.38	149.73	31.99	55.33
<b>IL17</b>	187.04	147.88	120.41	112.86	0.37	0.86	4.38	9.65	22.08	17.12	2.37	2.37
<b>Eotaxin</b>	100.44	148.60	14.40	39.36	<< OOR	<< OOR	<< OOR	<< OOR	9.85	14.55	2.10	4.12
<b>FGFb</b>	131.61	55.24	251.70	356.09	0.14	0.47	1.51	4.13	11.45	8.98	42.93	72.81
<b>IP10</b>	204.03	248.55	<< OOR	<< OOR	6921.19	5811.16	10623.43	19495.79	917.48	1059.92	2836.29	5855.56
<b>VEGF</b>	619.42	822.55	2969.12	3231.06	3.71	12.86	45.32	82.75	57.03	55.21	171.34	314.94
<b>PDGF-</b>	<< OOR											
<b>RANTES</b>	<< OOR											

Table S1 (*Continued*)

Day 7	H		H+Mg		P		P+Mg		H+P		H+P+Mg	
	Mean	SD	Mean	SD	Mean	SD	Mean	SD	Mean	SD	Mean	SD
<b>IL6</b>	3635.70	4525.99	8243.39	9506.49	<< OOR << OOR	16.85	13.39	596.68	776.61	970.99	1174.95	
<b>IL7</b>	10.23	25.30	86.02	139.22	0.28	0.97	13.12	19.09	2.38	4.96	12.49	18.64
<b>IL9</b>	42.22	68.07	11.60	40.17	<< OOR << OOR	10.57	16.33	0.33	1.15	8.63	15.51	
<b>IL12</b>	0.14	0.33	110.49	165.18	0.10	0.31	0.69	0.64	0.37	0.65	13.81	19.92
<b>IL15</b>	365.40	548.62	531.48	773.04	0.28	0.96	109.22	104.12	42.95	73.40	92.92	104.09
<b>IL17</b>	34.81	34.65	30.48	40.58	<< OOR << OOR	38.61	20.23	5.07	6.22	13.04	8.45	
<b>Eotaxin</b>	39.07	59.06	35.37	63.19	<< OOR << OOR	1.00	1.00	6.04	9.16	7.10	10.54	
<b>FGFb</b>	22.62	25.13	27.66	80.01	<< OOR << OOR	11.22	9.43	3.74	4.50	23.25	22.82	
<b>IP10</b>	115.94	143.80	<< OOR << OOR	1570.82	1528.60	5394.64	3832.94	273.88	248.67	6234.32	9852.31	
<b>VEGF</b>	1.00	1.00	7298.08	10419.56	2.35	8.13	215.95	178.25	1.54	5.33	934.35	1193.39
<b>PDGF-</b>	<< OOR											
<b>RANTES</b>	<< OOR											

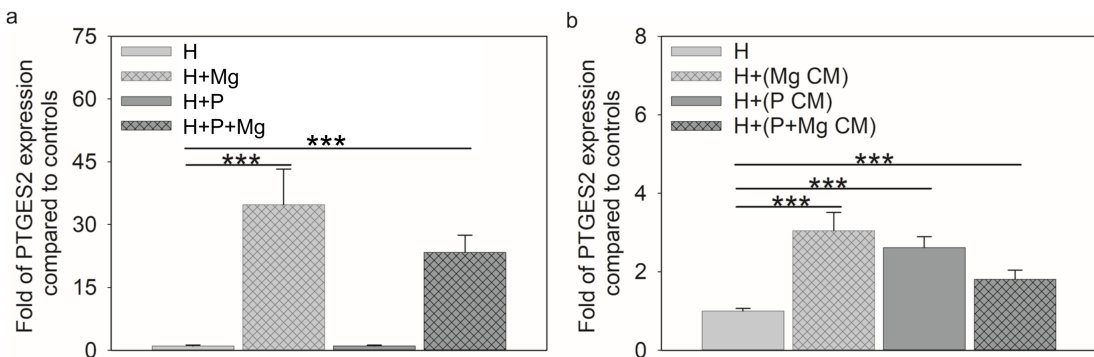


Fig. S1 Fold levels of *PTGES2* expression of HUCPV in transwell coculture (a) and conditioned media system (b) on day 7. The primer sequences for the *PTGES2* gene were (upper), 5'-CTTCCTTTCTGGGCTTCG-3' and (lower), 5'-GAAGACCAGGAAGTGCATCCA-3'. Bars represent mean  $\pm$  SD ( $n \geq 12$ ). The significances are represented by asterisks and were obtained from post hoc multiple comparisons between each group or to controls in ANOVA ( $\alpha=0.05$ , \*\*\* $P \leq 0.001$ ). H: HUCPV; P: PBMC; CM: conditioned media.

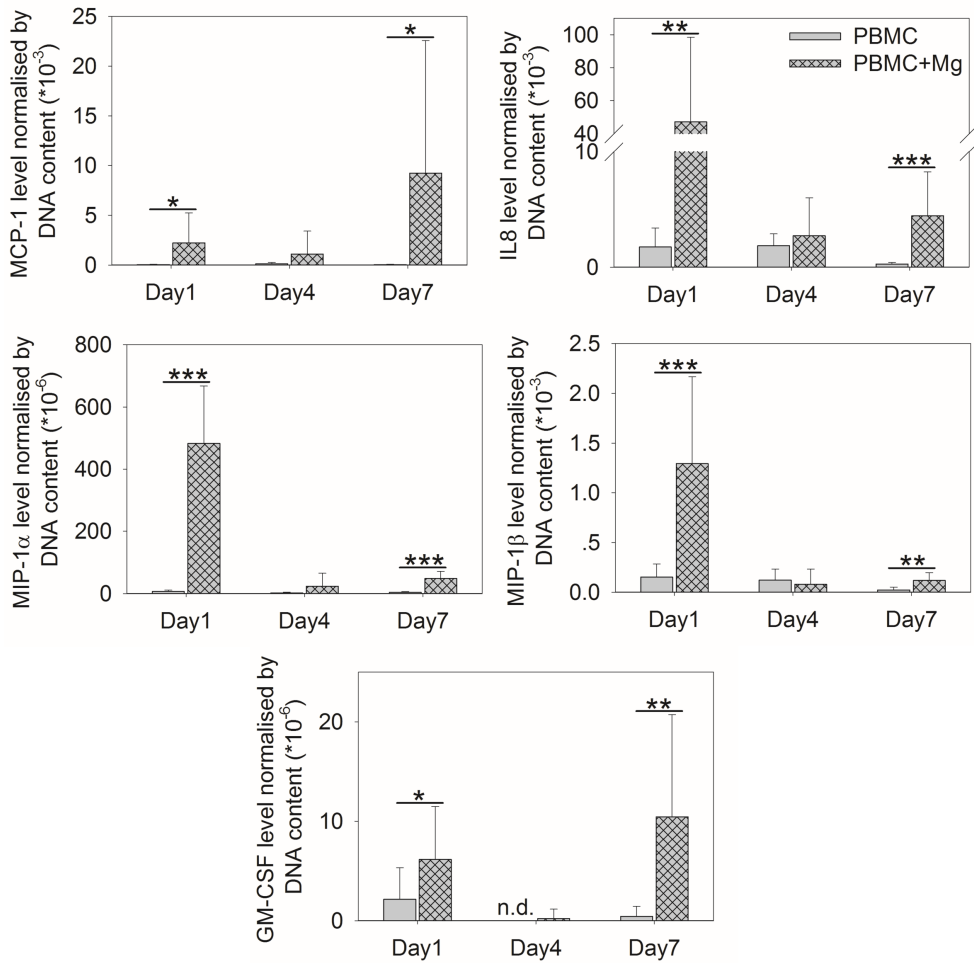


Fig. S2 Production of selected cytokines (IL8, GM-CSF, MIP-1 $\alpha$ / $\beta$ , and MCP-1) in P and P+Mg at each time point in a transwell coculture system. Bars represent mean  $\pm$  SD (n≥12). The significances between two conditions are represented by asterisks and were obtained from t-test ( $\alpha=0.05$ , \* $P \leq 0.05$ , \*\* $P \leq 0.01$  and \*\*\* $P \leq 0.001$ ). Here, "n.d." represents "not detected".

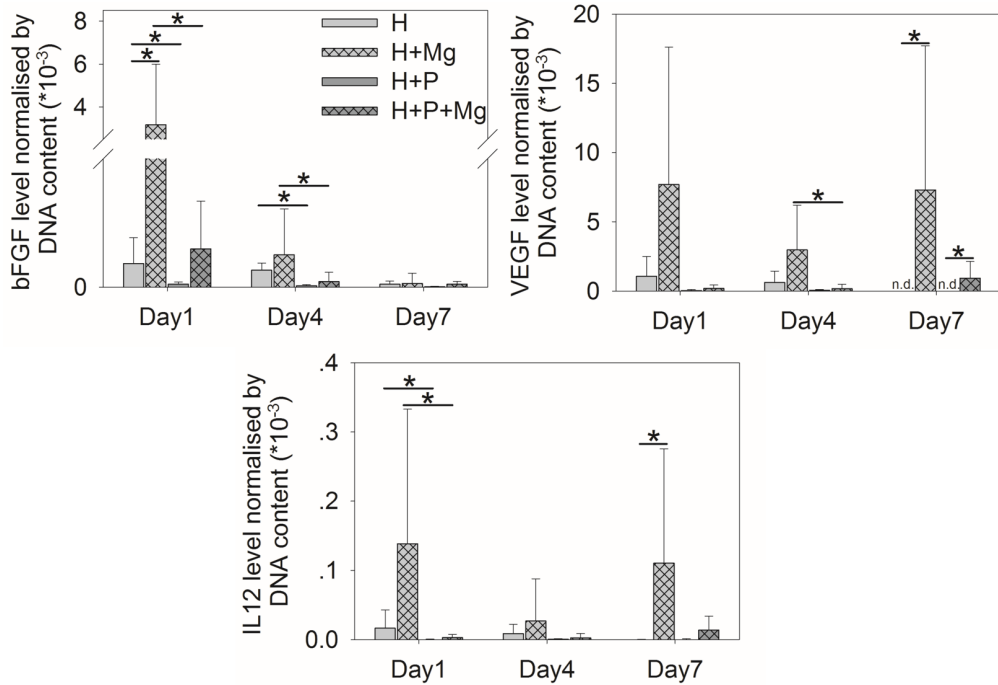


Fig. S3 Selected cytokines (bFGF, VEGF, and IL12) production in H/H+P with and without Mg at each time point in the transwell coculture system. Bars represent mean  $\pm$  SD (n $\geq$ 12). The significances are represented by asterisks and were obtained from post hoc multiple comparisons between each group or to controls in ANOVA ( $\alpha=0.05$ , \* $P\leq 0.05$ ). Here, "n.d." represents "not detected". H: HUCPV; P: PBMC.

## Symbols and abbreviations

Acronym	Definition
<b>AAS</b>	Atomic absorption spectroscopy
<b>ALP</b>	Alkaline phosphatase
<b>AMS</b>	Absorbable metal stents
<b>ANOVA</b>	Analysis of variance
<b>ATP</b>	Adenosine triphosphate
<b>bFGF</b>	Basic fibroblast growth factor
<b>BMP</b>	Bone morphogenetic protein
<b>BMPR</b>	Bone morphogenetic protein receptor
<b>BMMSC</b>	Bone marrow mesenchymal stem cells
<b>BSA</b>	Bovine serum albumin
<b>B2M</b>	B2 microglobulin
<b>CBF</b>	Core-binding factor
<b>COL1A1</b>	Collagen type I alpha 1
<b>CLC</b>	Cardiotrophin-like cytokine
<b>CNTF</b>	Ciliary neurotrophic factor
<b>CSC</b>	China scholarship council
<b>M-CSF</b>	Macrophage colony-stimulating factor
<b>G-CSF</b>	Granulocyte-colony stimulating factor
<b>GM-CSF</b>	Granulocyte-macrophage colony-stimulating factor
<b>DBM</b>	Demineralized bone matrix
<b>DNA</b>	Deoxyribonucleic acid
<b>ECM</b>	Extracellular matrix
<b>EDTA</b>	Ethylenediaminetetraacetic acid
<b>ELISA</b>	Enzyme-linked immunosorbent assay
<b>FBGC</b>	Foreign body giant cells
<b>FBR</b>	Foreign body reaction
<b>FBS</b>	Foetal bovine serum
<b>FITC</b>	Fluorescein isothiocyanate
<b>FSC</b>	Forward scatter
<b>GAPDH</b>	Glyceraldehyde 3-phosphate dehydrogenase
<b>GPI</b>	Glycophosphatidylinositol
<b>HAS</b>	Hydroxyapatite scaffolds
<b>HEPES</b>	4-(2-hydroxyethyl)-1-piperazineethanesulfonic acid
<b>HGF</b>	Hepatocyte growth factor
<b>HLA-DR</b>	Human leukocyte antigen-DR isotype
<b>HRP</b>	Horseradish peroxidase
<b>HUCPV</b>	Human umbilical cord perivascular
<b>IDO</b>	Indolamin-2,3-dioxygenase
<b>IFNy</b>	Interferon gamma
<b>IL</b>	Interleukin

<b>IP10</b>	Interferon gamma-induced protein 10
<b>JAK</b>	Janus kinase
<b>JNK</b>	C-Jun N-terminal kinase
<b>LIFR</b>	Leukaemia inhibitory factor receptor
<b>LPS</b>	Lipopolysaccharides
<b>MCP</b>	Monocyte chemoattractant protein
<b>MCPC</b>	Magnesium–calcium phosphate cement
<b>MEM</b>	Minimum essential medium
<b>MIP</b>	Macrophage inflammatory protein
<b>MSC</b>	Mesenchymal stem cell
<b>NF<math>\kappa</math>B</b>	Nuclear factor kappa-light-chain-enhancer of activated B cells
<b>NMDA</b>	N-methyl-d-aspartate
<b>NTC</b>	No template control
<b>OC</b>	Osteocalcin
<b>OOR</b>	Out of range
<b>OPN</b>	Osteopontin
<b>OSM</b>	Oncostatin M
<b>OSMR</b>	Oncostatin M receptor
<b>PBMC</b>	Peripheral blood mononuclear cells
<b>PBS</b>	Phosphate-buffered saline
<b>PCR</b>	Polymerase chain reaction
<b>PDGF-BB</b>	Platelet-derived growth factor-BB
<b>PGE2</b>	Prostaglandin E2
<b>PMN</b>	Polymorphonuclear leukocytes
<b>PPAR<math>\gamma</math></b>	Peroxisome proliferator-activated receptor gamma
<b>PTGES2</b>	Prostaglandin E synthase 2
<b>PTH</b>	Parathyroid hormone
<b>RANK</b>	Receptor activator of nuclear factor kappa-B
<b>RANKL</b>	Receptor activator of nuclear factor kappa-B ligand
<b>RANTES</b>	Regulated upon activation, normal T cell expressed and presumably secreted
<b>RFU</b>	Relative fluorescence unit
<b>RNA</b>	Ribonucleic acid
<b>ROS</b>	Reactive oxygen species
<b>RPL10</b>	Ribosomal protein L10
<b>RPMI 1640</b>	Roswell Park Memorial Institute 1640
<b>SFCA</b>	Surfactant-free cellulose acetate
<b>SMAD</b>	Mothers against decapentaplegic homolog
<b>SMS</b>	$\text{Sr}_2\text{MgSi}_2\text{O}_7$
<b>SSC</b>	Side scatter
<b>STAT</b>	Signal transducer and activator of transcription
<b>SZS</b>	$\text{Sr}_2\text{ZnSi}_2\text{O}_7$
<b>TGF</b>	Tumour growth factor

<b>TH1/2</b>	T helper type 1/2
<b>TLR</b>	Toll-like receptor
<b>TMB</b>	Tetramethylbenzidine
<b>TNF</b>	Tumour necrosis factor
<b>TRAP</b>	Tartrate-resistant acid phosphatase
<b>Treg</b>	Regulatory T cell
<b>VEGF</b>	Vascular endothelial growth factor
<b>Wnt5A</b>	Wnt family member 5A

## List of figures and tables

Fig. 1 Biological responses following biomaterial implantation.....	2
Fig. 2 The basic composition of bone.....	7
Fig. 3 Fracture healing.....	8
Fig. 4 Specific markers in different stages of osteogenic differentiation of MSC.....	10
Fig. 5 BMP signalling pathway.....	12
Fig. 6 IL6 signalling pathway.....	13
Fig. 7 OSM signalling pathway.....	13
Fig. 8 An excessive immune reaction resulting in encapsulation of an implant.....	14
Fig. 9 Forms of chemical signalling and models for investigating the interactions of MSC (HUCPV)-immune cells (PBMC/macrophages).....	16
Fig. 10 Hypothesis in the present study (indirect and direct coculture system).....	18
Fig. 11 PBMC isolation.....	20
Fig. 12 The isolation of CD 14 <sup>+</sup> monocytes from PBMC.....	22
Fig. 13 Indirect <i>in vitro</i> coculture systems: transwell coculture of HUCPV and PBMC.....	22
Fig. 14 Indirect <i>in vitro</i> coculture systems: HUCPV/PBMC-conditioned media.....	23
Fig. 15 Direct <i>in vitro</i> coculture systems.....	24
Fig. 16 The scheme of multiplex immunoassay.....	32
Fig. 17 Procedures of ELISA.....	34
Fig. 18 The wound healing assay of HUCPV.....	35
Fig. 19 Cell viability and proliferation of HUCPV in the transwell coculture system.....	40
Fig. 20 Cell viability and proliferation of PBMC in the transwell coculture system.....	41
Fig. 21 Cell viability and proliferation of HUCPV in the conditioned media system.....	42
Fig. 22 Cell viability and proliferation of PBMC in the conditioned media system.....	43
Fig. 23 The cytokine levels in the supernatant of HUCPV, PBMC and HUCPV-PBMC coculture in the presence and absence of Mg discs.....	45
Fig. 24 Subpopulations (%) of PBMC.....	49
Fig. 25 Flow cytometric analysis of the M2 subpopulation.....	50
Fig. 26 The percentage of M2 cells in the total macrophage population in the transwell coculture and conditioned media systems.....	51
Fig. 27 The migration distance of HUCPV when cultured in the supernatant from the transwell coculture system.....	52
Fig. 28 The migration distance of HUCPV when cultured in the supernatant from the conditioned media system.....	53

Fig. 29 The osteogenic potential of HUCPV indicated by ALP activity in the transwell coculture and conditioned media systems at day 7.....	54
Fig. 30 Osteogenesis-related gene expression in transwell coculture and conditioned media system at day 7 in HUCPV was measured by RT-qPCR.....	55
Fig. 31 Live/dead staining of HUCPV alone or cocultured with macrophages at days 7 and 14. ....	57
Fig. 32 The DNA content of HUCPV alone and in coculture with macrophages at days 7 and 14.....	58
Fig. 33 The cell distribution in the direct coculture groups at days 7 and 14.....	58
Fig. 34 Cell subpopulations (%) in the direct coculture groups at days 7 and 14. ....	59
Fig. 35 The ALP activity in HUCPV and cocultures.....	59
Fig. 36 Selected gene expression in HUCPV alone or in cocultures at days 7 and 14.....	60
Fig. 37 The OSM and IL6 levels in the supernatant of cocultured HUCPV and macrophages in a direct culture on metallic biomaterial. ....	61
Fig. 38 ALP activity after OSM and gp130 neutralisation in the cocultures at days 7 and 14. 62	62
Fig. 39 <i>BMP6</i> expression in macrophages under stimulation by Mg and Mg-10Gd. ....	62
Fig. 40 <i>BMPR1A</i> and <i>BMPR2</i> expression in HUCPV and cocultures under stimulation of Mg and Mg-10Gd. ....	63
Fig. 41 <i>Smad 1/4/5</i> expression in HUCPV and cocultures under stimulation by Mg and Mg-10Gd. ....	64
Fig. 42 TNF $\alpha$ and IL1 $\beta$ levels in the monoculture and cocultures.....	65
Fig. 43 Possible roles of degradable Mg on the interactions between immune cells and HUCPV in a transwell coculture and conditioned media system. ....	70
Fig. 44 Mechanisms of Mg-based material-induced secretion of signalling factors by macrophages promoting the osteogenic differentiation of HUCPV in a direct coculture system. ....	75
Fig. 45 Common specific targets of relevant metallic ions and their therapeutic roles in the human body.....	79
Fig. S1 Fold levels of PTGES2 expression of HUCPV in transwell coculture (a) and conditioned media system (b) on day 7.....	116
Fig. S2 Production of selected cytokines (IL8, GM-CSF, MIP-1 $\alpha$ / $\beta$ , and MCP-1) in P and P+Mg at each time point in a transwell coculture system. ....	116
Fig. S3 Selected cytokines (bFGF, VEGF, and IL12) production in H/H+P with and without Mg at each time point in the transwell coculture system. ....	117

Table 1 The roles of Mg and its deficiency/supplementation in biology.....	4
Table 2 The history of Mg and its alloys in cardiovascular applications. ....	5
Table 3 The history of Mg and its alloys in orthopaedic applications.....	6
Table 4 Summary of different coculture systems.....	17
Table 5 Compositions of Mg and Mg-10Gd.....	19
Table 6 Experimental conditions of the indirect <i>in vitro</i> coculture systems.....	24
Table 7 Direct <i>in vitro</i> coculture system.....	25
Table 8 Chemicals of DNA assay. ....	26
Table 9 Primers sequences.....	28
Table 10 Protocol of the thermal cycling. ....	29
Table 11 Cytokines and functions investigated by multiplex immunoassay.....	33
Table 12 Materials and kits for ELISA.....	35
Table 13 The Mg concentration under different conditions in the transwell coculture system.	38
Table 14 The Mg concentration, pH and osmolality under different conditions in the conditioned media system. ....	39
Table 15 The levels of secreted cytokines (normalised by the total DNA content) in the supernatants in the transwell coculture system at days 1, 4 and 7.....	46
Table 16 The Mg concentration, pH, osmolality and corrosion rate characterisation of the solutions for all experimental conditions in the direct coculture system. ....	56
Table S1 Levels of secreted cytokines (normalised by total DNA) in supernatants in transwell coculture system at day 1, 4 and 7.....	113

## **Curriculum Vitae**

**Qian Wang**

[nicoyo.wang@gmail.com](mailto:nicoyo.wang@gmail.com)

### **Education**

Sep 2009 – Jun 2013	Bachelor of Bioengineering
Department of Life Science and Technology, China Pharmaceutical University, Nanjing, China	
Sep 2013 – Jun 2016	Master of Pharmacy
College of Pharmacy, Dalian Medical University, Dalian, China	
Sep 2016 – Feb 2020	PhD candidate
Helmholtz-Zentrum Geesthacht (Faculty of Engineering, Christian-Albrecht-University (CAU) Kiel), Germany	

### **Research experience**

Feb 2013 – May 2013	State Key Laboratory of Biotherapy, Sichuan University
May 2014 – Jun 2016	Institute of Materia Medica, Chinese Academy of Science, Shanghai, China
Sep 2016 – Feb 2020	Helmholtz-Zentrum Geesthacht (HZG), Germany

## List of publications and conferences

### Peer-reviewed articles:

- Q. Wang**, L. Xu, H. Helmholz, R. Willumeit-Römer, B. Luthringer-Feyerabend. Effects of degradable magnesium on paracrine signaling between human umbilical cord perivascular cells and peripheral blood mononuclear cells. *Biomaterials Science*, 2020. DOI: 10.1039/D0BM00834F
- Q. Wang**, L. Xu, R. Willumeit-Römer, B. Luthringer-Feyerabend. Macrophages expression of oncostatin M/bone morphogenetic protein 6 in response to Mg-based materials influences pro-osteogenic activity of human mesenchymal stem cells. (Submitted)
- Q. Wang**, R. Willumeit-Römer, B. Luthringer-Feyerabend. Secretion of soluble factors mediated by Mg-based materials induces osteoclastogenesis. (In preparation)

### Conference contribution:

- Q. Wang**, R. Willumeit-Römer, B. Luthringer-Feyerabend. Effect of magnesium on the crosstalk between human umbilical cord perivascular cells and monocytes. **9th Symposium on Biodegradable Metals**, Bertinoro, Italy, 2017 (Poster)
- Q. Wang**, R. Willumeit-Römer, B. Luthringer-Feyerabend. Effect of biodegradable magnesium on the immune response *in vitro*. **10th Symposium on Biodegradable Metals**, Oxford, UK, 2018 (Poster)